The role of mechanical hysteresis source in mechanical and mechanobiological performances of load-bearing biomaterials

Thèse N° 9401

Présentée le 28 mars 2019

à la Faculté des sciences et techniques de l'ingénieur
Laboratoire de biomécanique en orthopédie
Programme doctoral en mécanique

pour l'obtention du grade de Docteur ès Sciences

par

Naser NASROLLAHZADEH MAMAGHANI

Acceptée sur proposition du jury

Prof. J. M. Kolinski, président du jury
Prof. D. Pioletti, directeur de thèse
Prof. F. Guilak, rapporteur
Prof. J. Snedeker, rapporteur
Prof. V. Michaud, rapporteuse

2019

ÉCOLE POLYTECHNIQUE
FÉDÉRALE DE LAUSANNE

Acknowledgments

I am very grateful to my thesis director, Prof. Dominique P. Pioletti, who supported me throughout my PhD study and respective research. In particular, I am thankful for his patience, motivation and guidance to accomplish this dissertation.

I would like to appreciate the valuable participation of the jury members, Prof. Farshid Guilak, Prof. Jess Gerrit Snedeker, Prof. Veronique Michaud and Prof. John Martin Kolinski in the evaluation of my thesis. In particular, I am grateful for their precious comments to improve this work.

I would like to thank all the members of the Laboratory of Biomechanical Orthopedics (LBO) for their invaluable help and support during my PhD period. Special thanks to Dr. Philippe Abdel Sayed, Dr. Mohammad Reza Nassajian Moghadam, Sandra Jaccoud and Peyman Karami for their advice and technical supports. I am also grateful to the rest of the LBO family, Virginie Kokocinski, Dr. Alexandre Terrier, Dr. Ulrike Kettenberger, Dr. Tanja Hausherr, Dr. Valérie Malfroy Camine, Dr. Adeliya Latypova, Dr. Jens Antons, Yasmine Boulanaache, Oriane Poupart, Jorge Solana Munoz, Céline Samira Wyss, Dr. Ehsan Sarshari, Josiane Smith-Clerc, Dr. Vogel Arne Christian, Zahra Saghaei Nooshabadi and all other members with whom I shared great moments in LBO.

I would like to thank the Regenerative Therapy Unit of University Hospital of Lausanne (CHUV) and in particular Prof. Lee Ann Laurent-Applegate for providing the human chondro-progenitor cells. Likewise, I would like to thank the Laboratory of Polymer in EPFL, especially Prof. Harm Anton Klok and Jian Wang for their collaboration in the functionalization process of synthetic hydrogels. My special thanks to Marc Jeanneret and the team of the mechanics workshop, for their technical help in designing and manufacturing the required set-ups.

I would like to appreciate my parents and siblings who were physically far from me, but metaphysically supported and encouraged me during this work. I am also grateful to all my friends with whom I shared unforgettable moments.

Last but not least, I am extremely thankful to my wife, Lida Bagheri, for her patience, consideration, kindness and constant backing throughout my PhD period.

Abstract

Tissue engineering is a promising approach for articular cartilage regeneration as no satisfactory treatment is actually available for cartilage, partly due to the very limited self-healing capability of this tissue. To successfully induce a cartilaginous tissue formation, however, a variety of contributing factors either from a biological or engineering standpoint should be optimized. In particular, sufficient biophysical signals should be provided to promote the response of the spatially distributed cells in a biomimetic three dimensional (3D) scaffold. Given the significance of cartilage dissipative properties when it is submitted to loading, we hypothesized that hydrogels presenting adequate viscoelastic properties could provide a mechano-mimetic niche that would support proliferation and differentiation of cells with chondrogenic lineage. In addition, a preserved hysteresis source is an essential feature for a tough biomaterial with robust mechanical behavior. As a consequence, a carefully designed dissipative hydrogel might simultaneously enhance its mechanical and mechanobiological performances. Therefore, the development of mechanically and biologically functional hydrogels as model systems to study the mechanobiology of cartilage is the central aim of this thesis. Indeed, elucidating the aspects of cartilage mechanobiology can facilitate the clinical translation of engineered constructs as the mechanical cues significantly influence the cells response. In parallel, temperature evolution due to the conversion of the dissipated energy to heat following cyclic loading brings new insights to interpret the effects of mechanical forces on the cells behavior. In this context, identifying the optimal thermo-mechanical stimulation of cell-laden hydrogels can positively contribute to the development of engineered cartilage.

Given hydrogel as a biphasic material, it can dissipate the input mechanical energy via interstitial fluid frictional drag and macromolecular network resistance to deformation. These two fundamentally different physical mechanisms, which induce a mechanical hysteresis, can be controlled by the biphasic material's permeability and by the composition of its network, respectively. Accordingly, we firstly developed an experimental method to directly measure the strain-dependent permeability of visco-porous hydrogels. Based on the correlation between the permeability-composition pair and the hydrogel dissipation, an original combination of flow-dependent and flow-independent dissipation source was proposed for the design of biomechanically functional hydrogels. In particular, a heteroporous yet low permeable, fatigue-resistant hydrogel was developed via a hybrid crosslinking strategy presenting weak physical bonds and strong covalent bonds. We showed that hydrogels with the same level of stiffness

and energy dissipation respond to fatigue loading in a significant different way, depending on their preserved or shrank hysteresis curves during cyclic loading. By developing a semi-inverse poro-viscoelastic model, we also showed that the load is partly carried by the solid phase in hybridly crosslinked hydrogels with low permeability thanks to the support of the pressurized fluid.

Before evaluating the role of the dissipation mechanisms in chondrogenesis, we developed a reproducible cell seeding technique via a combination of computational and experimental approaches. In particular, the optimized compression release-induced suction (CRIS) cell-seeding regime was supplemented with slow rotation after seeding treatment to enhance the cells distribution in the scaffold. Then, a systematic experimental analysis was performed demonstrating that permeability has a higher impact on the seeding outcome compared to scaffold coating and thickness. In the next step, two cell-penetrable hydrogels with significantly different contributions of the fluidic and intrinsic dissipation sources under cyclic compression were employed to study the cells behavior. We found that chondrogenesis is favored in the cell-laden hydrogels preserving the mechanical hysteresis through an effective contribution of the frictional drag mechanism compared to hydrogels having destructive sources of dissipation.

To further gain insight on a possible synergetic influence of the temperature and the loading in the framework of studying cartilage thermo-mechanobiology (as the self-heating phenomenon links the temperature increase to cyclic deformation), we developed a customized *in vitro* platform in the final part of this thesis. For this purpose, RGD ligands were covalently conjugated to the mechano-mimetic heteroporous hydrogels while maintaining the desired mechanical properties. In parallel, a modular bioreactor was designed to apply compressive load and desired temperature scheme during culture of cell-laden hydrogels while CO_2/O_2 and humidity levels could be regulated. It was shown that cell adhesion was improved and cells-hydrogel interaction following biophysical stimulus was better preserved within the RGD functionalized hydrogels. By coupling mechanical and thermal stimuli, the expression of the transcription factor Sox9, an early chondrogenic marker, was increased and complementarily the expression of Twist1, an inhibitor of chondrogenesis, was reduced compared to thermal and mechanical stimulation alone. Compared to the knee cartilage temperature at rest corresponding to 32°C, by increasing culture temperature to 37°C, the chondrogenic differentiation of the cells was improved, whereas their metabolism was reduced. Nevertheless,

the metabolic activity of cell-laden hydrogels submitted to intermittent thermo-mechanical stimulation was similar to free–swelling samples at 32°C. It was thus concluded that intermittent thermo-mechanical stimulus could support cells metabolism while promoting chondrogenesis.

Collectively, the development of hydrogels with incorporation of proper dissipation sources could open new opportunities to enhance biomechanical functionality for load-bearing applications while promoting chondrocytes differentiation. As permeability directly influences cells distribution and infusion depth, the design of a cell-penetrable scaffold with dominant flow-dependent dissipation source requires a careful consideration. While cells-scaffold constructs are conventionally cultured at a temperature corresponding to the core body (37°C), applying an optimal thermo-mechanical environment might enhance the engineered cartilage products.

Keywords: Hydrogel, intrinsic dissipation, frictional drag, fatigue performance, hybrid crosslinking, permeability, cartilage, thermo-mechanobiology, bioreactor, cell seeding.

Résume

L'ingénierie tissulaire est une approche prometteuse pour la régénération de cartilage articulaire puisque aucun traitement satisfaisant est actuellement disponible pour le cartilage, en partie à cause de la très faible capacité d'auto-guérison de ce tissu. Pour induire une formation de tissu cartilagineux de manière efficace, plusieurs paramètres contribuant d'un point de vue biologique ou d'ingénierie doivent être optimisés. En particulier, des signaux biophysiques suffisants doivent être fournis pour promouvoir une réponse des cellules distribuées spatialement dans une matrice biomimétique tridimensionnelle (3D). Etant donné l'importance des propriétés dissipatives du cartilage quand il est soumis à un chargement, nous avons fait l'hypothèse que les hydrogels présentant des propriétés viscoélastiques adéquates peuvent fournir une niche mécano-mimétique qui pourrait favoriser la prolifération et la différenciation des précurseurs chondrocytaires. De plus, une source d'hystérèse conservée est une caractéristique essentielle pour un biomatériau dur avec un comportement mécanique robuste. De ce fait, des hydrogels dissipatifs soigneusement conçus pourraient améliorer simultanément ses performances mécaniques et mécanobiologiques. Par conséquent, le développement d'hydrogels mécaniquement et biologiquement fonctionnels en tant que modèle pour étudier la mécanobiologie du cartilage est le but principal de cette thèse. En effet, élucider les aspects de la mécanobiologie du cartilage peut faciliter l'application clinique du dispositif conçu car les signaux mécaniques influencent de façon significative la réponse cellulaire. En parallèle, l'évolution de la température due à la conversion de l'énergie dissipée en chaleur après les chargements cycliques apporte de nouvelles connaissances pour interpréter les effets des forces mécaniques sur le comportement des cellules. Dans ce contexte, identifier la stimulation thermomécanique optimale des cellules ensemencées dans les hydrogels peut contribuer positivement au développement d'un cartilage artificiel.

Etant donné que l'hydrogel est un matériau biphasique, il peut dissiper l'énergie mécanique donnée par friction fluidique interstitielle et par résistance à la déformation du réseau macromoléculaire. Ces deux mécanismes fondamentalement différents induisant une hystérèse mécanique peuvent être contrôlés par la perméabilité du matériau biphasique et par la composition du réseau, respectivement. Par conséquent, nous avons développé, dans un premier temps, une méthode expérimentale pour mesurer de manière directe la perméabilité des hydrogels porovisqueux en fonction de la contrainte. Basée sur la corrélation entre la paire perméabilité-composition et la dissipation de l'hydrogel, une combinaison originale d'une

source de dissipation dépendante et indépendante du flux a été proposée pour la conception des hydrogels biomécaniquement fonctionnels. En particulier, un hydrogel hétéroporeux mais peu perméable et résistant à la fatigue a été développé par une stratégie de réticulation hybride présentant des faibles liaisons physiques et des fortes liaisons covalentes. Nous avons montré que les hydrogels avec le même niveau de rigidité et d'énergie de dissipation répondent au chargement en fatigue de manière significativement différente en fonction de leur courbe d'hystérèse conservée ou réduite durant les chargements cycliques. En développant un modèle poroviscoélastique semi-inverse, nous avons aussi montré que la charge est en partie supportée par la phase solide de l'hydrogel réticulé de manière hybride avec une faible perméabilité grâce au fluide pressurisé.

Avant d'évaluer le rôle des mécanismes de dissipation dans la chondrogenèse, nous avons développé une technique d'ensemencement reproductible par combinaison d'approches computationnelles et expérimentales. En particulier, le régime d'ensemencement cellulaire par succion optimisée induite par le relâchement d'une compression a été complété par une lente rotation après le traitement d'ensemencement pour améliorer la distribution des cellules dans la matrice. Puis, une analyse expérimentale systématique a été effectuée prouvant que la perméabilité a un plus grand impact sur l'ensemencement résultant comparé au revêtement et à l'épaisseur de la matrice. Dans l'étape suivante, deux hydrogels perméables aux cellules avec une contribution significativement différente des sources de dissipation fluidique et intrinsèque sous compression cyclique ont été utilisés pour étudier le comportement cellulaire. Nous avons constaté que la chondrogenèse est favorisée dans les hydrogels ensemencés qui conservent l'hystérèse mécanique à travers une contribution efficace du mécanisme de friction comparé aux hydrogels ayant des sources de dissipation destructives.

Pour mieux comprendre la possible influence synergétique de la température et du chargement dans le cadre de l'étude de la thermomécanobiologie du cartilage (puisque le phénomène d'auto-réchauffement lie l'augmentation de la température à la déformation cyclique), nous avons développé une plateforme *in vitro* sur mesure dans la dernière partie de cette thèse. A cet effet, des ligands RGD ont été conjugués de manière covalente aux hydrogels hétéroporeux mécano-mimétiques tout en maintenant les propriétés mécaniques souhaitées. En parallèle, un bioréacteur modulaire a été conçu afin d'appliquer une charge en compression et un profil de température souhaités pendant la culture des hydrogels ensemencés tout en pouvant contrôler les niveaux de CO_2/O_2 et d'humidité. Il a été montré que l'adhésion cellulaire a été

améliorée et que l'interaction hydrogels-cellules après le stimulus biophysique était mieux conservée dans les hydrogels fonctionnalisés avec RGD. L'expression du facteur de transcription Sox9, un marqueur de la chondrogenèse précoce, était augmentée et de manière complémentaire l'expression de Twist1, un inhibiteur de la chondrogenèse, était réduite par le couplage des stimuli mécaniques et thermiques comparé à la stimulation thermique et mécanique seule. Comparée à la condition de la température du cartilage du genou au repos correspondant à 32°C, en augmentant la température de culture à 37°C, la différenciation chondrogénique a été améliorée, alors que le métabolisme a été diminué. Cependant, l'activité métabolique des cellules dans les hydrogels soumis' à la stimulation thermomécanique était similaire aux échantillons en gonflement libre à 32°C. Il a donc été conclu que des courtes périodes de stimulations thermomécaniques favorisent le métabolisme des cellules tout en promouvant la chondrogenèse.

Le développement des hydrogels intégrant des sources de dissipation appropriées peut ouvrir des nouvelles opportunités pour améliorer la fonctionnalité biomécanique pour des applications où des charges sont présentes tout en promouvant la différenciation des chondrocytes. Puisque la perméabilité des matrices influence directement sur la distribution des cellules et la profondeur d'infusion, la conception du biomatériau perméable aux cellules avec une source de dissipation dépendante du flux demande une attention particulière. Alors que les dispositifs de matrice cellulaire sont conventionnellement cultivés *in vivo* à une température correspondant à celle du corps (37°C), appliquer un environnement thermomécanique optimal peut améliorer les cartilages issus de l'ingénierie tissulaire.

Mots-clés : Hydrogel, dissipation intrinsèque, traînée de friction, performance de fatigue, réticulation hybride, perméabilité, cartilage, thermomécanobiologie, bioréacteur, ensemencement cellulaire.

Table of Contents

Chapter 1: Introduction

From a mechanical standpoint, articular cartilage can be considered as a viscoelastic porous material. Its dissipation capabilities are therefore central to its functional behavior. In this thesis, we will focus on the study of dissipative aspects in cartilage either from a mechanical or mechanobiological point of view. We will then capitalize on the newly obtained insight to develop functional biomaterials for cartilage tissue engineering.

1-1 Articular Cartilage

Articular cartilage (hyaline cartilage) is an avascular load-bearing tissue covering the surface of bones in synovial joints. Hip and knee are the largest articulating joints of the lower extremity (Figure 1-a) similar to shoulder and elbow in the upper extremity. These synovial joints support crucial mechanical forces and moments during daily life activities (Figure 1-b) [1]. From a biomechanical point of view, articular cartilage can experience different load types including compression, hydrostatic pressure, shear and tension. Cartilage tissue not only distributes and damps the transmitted contact loads in joints, but also provides a lubricating interface for articulation allowing bones to smoothly glide over each other. Articular cartilage is a mechanically durable, low friction ($\mu<0.1$), poorly permeable ($k<10^{-16}$ m^2) and tough ($\Gamma<1.5$ kJ m^{-2}) material with relatively high stiffness ($E_{eq}\approx1$ MPa) and moderate deformability ($\varepsilon < 50\%$) [1-5].

From a biological perspective, sparsely populated chondrocytes (Figure 1-c) within the extracellular matrix (ECM) control the hemostasis of cartilage tissue by anabolic and catabolic processes. The ECM is a biphasic material mainly composed of water (65-80% w), collagen type II fibers (15-22% w) and proteoglycan (PG) aggregates (4-7% w) [1]. In particular, ECM is a viscoelastic and composite network with porous structure, in which complex interactions take place between solid phase and interstitial fluid upon an applied loading [6]. Moreover,

cartilage has anisotropic and inhomogeneous mechanical properties in which a gradient of elastic modulus has been observed from articulating surface to the interface of subchondral bone [7]. This is mainly due to its stratified structure presenting different features of ECM components in successive regions designated as superficial, transitional/middle and deep zones (Figure 1-c) on top of a calcified layer on the interface with subchondral bone. As shown in Figure 1-c, morphology of chondrocytes and organization of the collagen network vary in different zones.

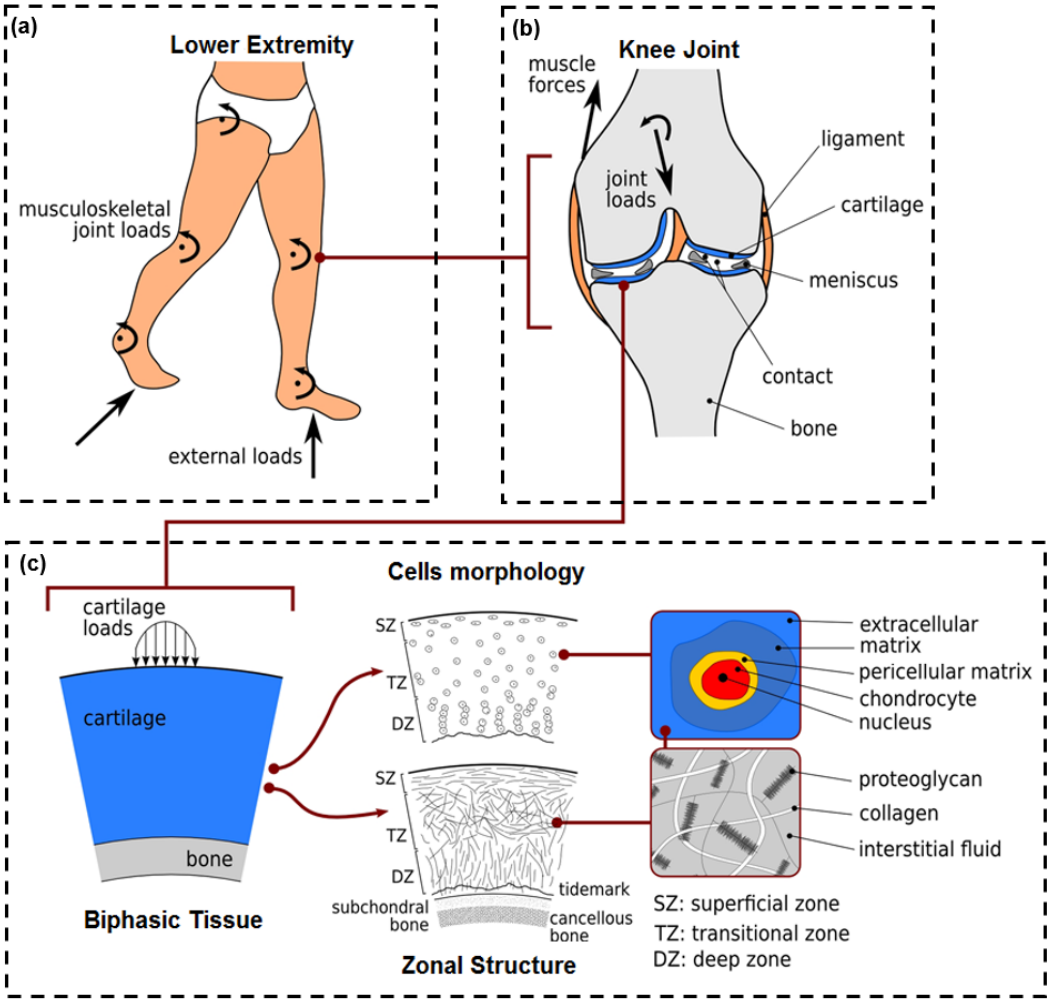

Figure 1. Biomechanical function, structure and composition of articular cartilage in synovial joints. (a) Articulating joints of the lower extremity and external reaction forces to body weight. (b) Musculoskeletal elements of knee joints sustain demanding mechanical forces and moments. (c) Articular cartilage is a biphasic tissue covering the end extremity of the bones in joints. This viscoelastic tissue has a depth dependent zonal structure with specific collagen fibers orientation and chondrocytes distribution and shape. Collagen type II, proteoglycan aggregates and intestinal fluid are the main components of the cartilage tissue's ECM (reproduced with permission from [6]).

1-1-1 Cartilage lesion and regeneration

Articular cartilage is prone to damage, loss of mechanical function and pathological cascades by aging and in case of severe loading. Due to limited progenitor cells source, avascular

composition, slow dynamics of ECM turnover and lack of blood supply, the regeneration of articular cartilage is very limited [8, 9]. Even a minor injury can, therefore, induce a tissue degeneration (even for young people) and finally lead to osteoarthritis with acute pain and disability. Arthroplasty is the gold standard clinical treatment for the extensive joint damage seen in osteoarthritis. Nevertheless, some treatments are proposed to recover lesion before its progression to osteoarthritis such as micro-fracture and cells implantation [10, 11]. The neo-tissue formed as a result of these treatments, however, lacks the functional properties of hyaline cartilage; hence, further improvements are still required for effective clinical solutions [12]. Tissue engineering is an emerging approach, which combines biological and engineering approaches to repair degenerated tissues via cell-scaffold constructs. Cartilage tissue engineering is, therefore, a promising strategy to enhance the outcome of therapies for cartilage lesions.

1-1-2 Cartilage tissue engineering

Cells, three dimensional (3D) support, and signaling are generally the main pillars for classical tissue engineering framework (Figure 2). To successfully induce a cartilaginous tissue formation, the culture microenvironment should provide sufficient physical and biochemical regulatory signals to promote differentiation of embedded-cells in the 3D construct. In the following sections we briefly summarize key contributing factors for this purpose.

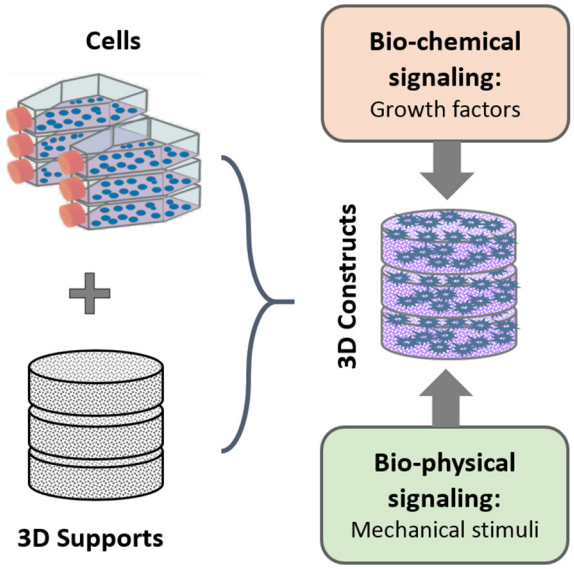

Figure 2. Main contributing factors to classical tissue engineering strategy. Proper cell type should be efficiently infused into a mechanically stable biomaterial for 3D culture. Chondrogenesis is then controlled via chemical and biophysical stimuli to induce optimal tissue formation.

1-1-2-1 Cell sources and delivery

The first step in the tissue engineering approach is incorporation of a regenerative cell source into the 3D support [13]. Autologous chondrocytes and mesenchymal stem cells (MSCs) are the mainly studied cell sources for cartilage regeneration [14]. The restricted availability of autologous chondrocytes, high cost and two-step surgical process of this strategy have made MSC a potential candidate for tissue engineering [9]. However, a specific protocol is required to push MSCs toward chondrogenic phenotype and maintain their linage in the artificial culture condition [15]. Lack of control on MSCs maturation, early hypertrophy and ossification after the induced differentiation process are still major issues of MSCs for their use in cartilage repair [14, 16]. To address these limitations, human epiphyseal chondro-progenitor (ECP) cells have recently been proposed as an allogeneic, responsive and stable therapeutic cell type for cartilage regeneration [17, 18]. Given ECP predictable proliferation capability, their single donor source and established cell bank, these cells of fetal origin could be a reliable option for cartilage tissue engineering studies and therapy. Other potentially interesting cell type candidates under investigation for cartilage cell-based therapies include nasal chondrocytes , embryonic stem cells, allogeneic chondrocytes, adipose and induced pluripotent stem cells (see reference [12] for pros and cons of various cell sources for cartilage tissue engineering).

Efficient cell seeding into the scaffolds helps to modulate tissue formation and insures reproducible initial conditions to establish clinical procedures. Indeed, there is no chance to modify cells distribution and density following an ineffective cell seeding [19]. However, cell seeding is not yet a standard and straightforward process for a pre-formed scaffold presenting small pore sizes and complex tortuosity. There is a growing evidence that sophisticated seeding methods for different biomaterials should be employed to optimize the seeding process effectiveness and reproducibility. In this regard, several static or dynamic methods have been developed and some of them are shown in Figure 3. Despite the simplicity of the surface pipetting in static technique and the high viability of the attached cells, an inhomogeneous cells distribution in the scaffold has been observed in general for this technique [20]. While gravity is the driving force for the cells infusion with the static method, an external force is applied to facilitate the cells infiltration in the dynamic seeding methods. Spinner flask [21], flow perfusion [22], vacuum-aided infusion [19] and the compression forced-induced suction [23] are reported as promising systems for dynamic cell seeding in cartilage tissue engineering applications. These studies have shown that active infiltration can improve cells distribution

inside the scaffold in comparison to static methods. Currently, the challenge for the dynamic approach is to find the least complex setups and protocols for cell seeding, which can be performed in a limited amount of time while increasing seeding efficiency and uniformity.

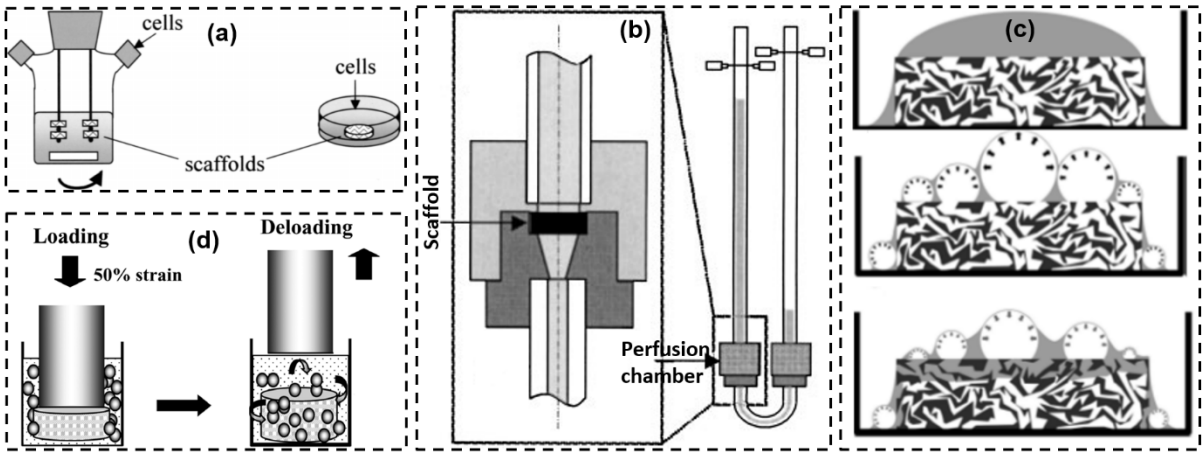

Figure 3. Promising dynamic cell-seeding techniques for cartilage tissue engineering. (a) The hydrodynamic forces assist cells penetration in spinner flask contrary to static seeding (adapted from [21]). (b) The medium containing cells traverses through the perfusion chamber containing scaffold to improve cells infiltration (adapted from [22]). (c) As the chamber containing cells suspension and scaffold is evacuated and released in vacuum seeding method, the cells suspension penetrates inside the air-free voids (adapted from [19]). (d) The cells suspension is infiltrated into the scaffold following compressive loading and unloading (adapted from [23]).

1-1-2-2 Biomaterial

Structural support of cells is provided by using a 3D scaffold to promote cells spatial distribution, viability and differentiation. The employed biomaterial should be at minimum biocompatible, present some bioactivity, and be mechanically stable under loading while allowing required solutes transport (see reference [24]: a recent review for different biomaterials in the field of cartilage regeneration). Hydrogels as hydrated polymeric structures are promising biomaterials for this purpose. In particular, hydrogels inherent analogy with soft tissues (water-swollen solid network) has made them unique candidate as tissues substitute. The main limitation of commonly used hydrogels is their nano-scale pore size which restricts neo-tissue formation [25]. Macro-porous polymeric biomaterials are also widely employed as 3D structures for tissue engineering owing to their capability for tissue growth and nutrients transport. A variety of techniques can be utilized for the development of porous scaffolds including, particle leaching, phase separation, weaving, electrospinning and 3D printing (see reference [26]: a review for different methods of 3D scaffold fabrication).

From a material standpoint, intrinsic bioactivity of natural biomaterials such as collagen or decellularized tissues let them to properly interact with cells [27]. The main drawback of natural biomaterials is, however, their insufficient mechanical properties which restricts their application when load support is required. Apart from biological key features in the development of a scaffold, a demanding set of mechanical properties including stiffness, damping, permeability, toughness and durability is required to sustain load in case of cartilage equivalents [3, 28]. Indeed, the mechanical properties of synthetic biomaterials can be enhanced by smart design of the material composition [29]. Yet, the ECM mimicking cell–surface interface would be an extra demand in this case. In this context, functionalization of synthetic biomaterials by ECM proteins (mostly fibronectin) and anchoring ligands (mainly RGD) are common yet debatable approaches [30, 31]. Despite many advances in biomaterials development, fabricating a chondro-inductive biomaterial with enhanced mechanical properties to support consistent tissue formation still remains a significant challenge [32].

1-1-2-3 Signaling

The chondrocytes functions within the articular cartilage is controlled through a set of biomechanical, electrical, and chemical cues [33]. Several growth and transcription factors were employed (e.g., in culture medium, or by gene and drug delivery systems) to directly introduce biochemical mediators for inducing chondrogenesis [12, 34]. In particular, individual or synergitical use of transforming growth factors family (TGF-β) and insulin-like growth factor (IGF-1) were shown to be influential for inducing cartilaginous ECM formation [34]. In parallel, chondrocytes can sense multi-faceted physical signals from their surrounding microenvironment and transduce them to control ECM anabolic and catabolic turnovers [35]. In this context, fluid exchange following an applied mechanical force enhances solutes transport within the poorly diffusive and avascular tissue to maintain cells metabolic activity. Likewise, interstitial fluid exudation can cause tissue osmolarity following ions transport and streaming potentials due to negatively charged proteoglycans [33, 36]. Moreover, mechanical loading influences the contribution of the TGF-β growth factor family by either activating their corresponding cell receptor or enhancing TGF-β expression [37-39]. Accordingly, there is a complex interaction between different signaling pathways/cascades within the cartilage tissue and limited fundamental mechanisms were elaborated so far. Indeed, mechanotransduction within the 3D mechanical environment surrounding cells is a significant signaling pathway for ECM homeostasis [36, 40-43]. The cartilage degradation, similar to bone resorption, in lack of

required mechanical loadings following joint immobilization is a known phenomenon since many years [44, 45]. In parallel, it is widely reported that proper mechanical stimulus can generate necessary signals for cartilage biosynthesis [43].

1-2 Mechanobiology of articular cartilage

Conversion of mechanical inputs at the cellular level to biochemical signals is called mechanotransduction. Accordingly, studying the role of mechanical environment such as substrate stiffness and transmitted force in cells function and tissue hemostasis would define the framework of mechanobiology. There is a surge of interest in elucidating mechanobiology of articular cartilage to enhance the outcome of tissue engineering products [46, 47]. However, it still remains to fully understand the role of different physical cues and governing coupling phenomena to decipher their translation from tissue level to intracellular transcriptions. Total collagen and glycosaminoglycan productions are the common tissue level markers for ECM development in engineered cartilage [43, 48]. Likewise, collagen type II (Col2a1), aggrecan (Acan/Agc1) and SRY-related HMG-box gene 9 (Sox9) genes are the most utilized chondrogenic references at the molecular level for mechanobiological studies [49]. While Col2a1 is the main collagen marker of articular cartilage, the type I collagen (Col1a1, marker for bone), is also expressed in primary chondrocytes. Following differentiation process, the ratio of Col2a1 to Col1a1 expression is increased resulting in a larger differentiation index for chondrogenic phenotype [50, 51]. The transcription factor Sox9 is an early marker for chondrogenic differentiation and its successive contribution is also critical in matrix synthesis in synergy with Col2a1 and Acan genes as shown in Figure 4 during chondrocytes maturation [35, 52]. In addition, Sox9 negatively regulates collagen X (Col10a1) expression which is a strong hypertrophic indicator, and therefore, Sox9 inhibits chondrocyte terminal differentiation/ossification [53]. In parallel, Twist-related protein 1 (Twist1) is known to hinder chondrogenesis by direct inhibition of Sox9 as the master regulator of chondrogenic differentiation process [54]. Accordingly, the expression behavior of these chondrogenic genes following a mechanical intervention could determine how the external signal is regulating intracellular transcriptions.

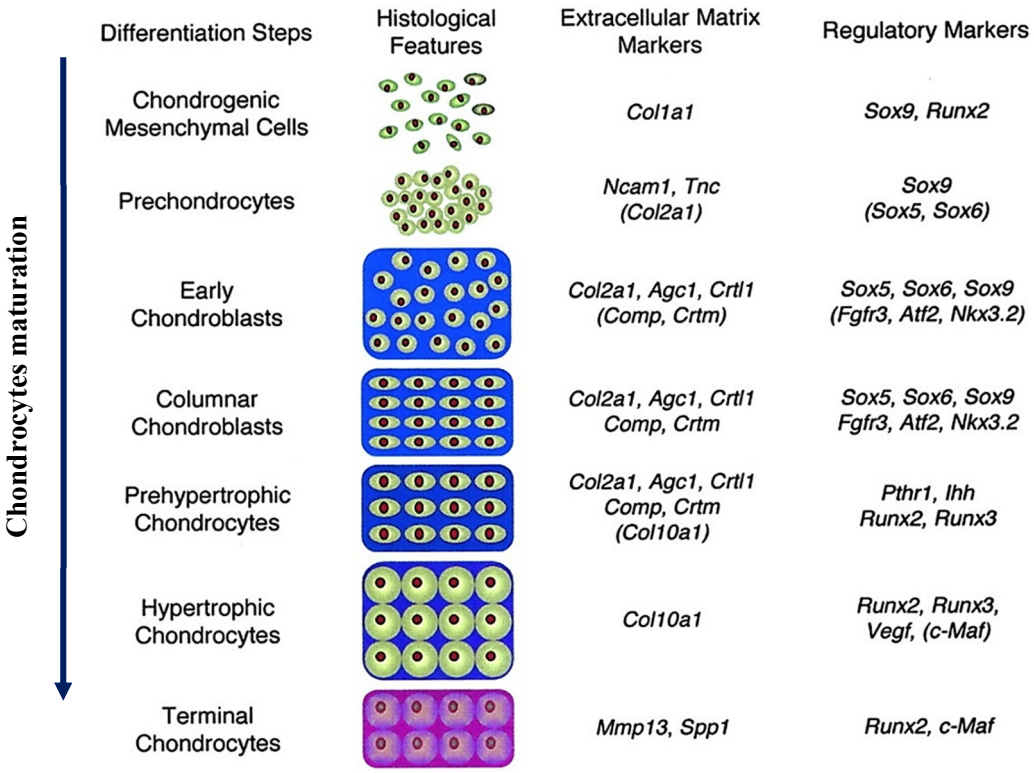

Figure 4. Schematic model representing different stages of differentiation during chondrocyte maturation and corresponding histological features, extracellular matrix markers and regulatory genes (reproduced with permission from [52]).

1-2-1 *In vitro* models for mechanobiological study

Given the complexity of *in vivo* studies and the limitation to accurately link chondrocytes biological response to a specific mechanical signal, conceptual *in vitro* models are required to recapitulate target cues of cartilage tissue. It is well established that cells behavior in 3D systems could be fundamentally different from 2D culture due to spatial distribution of cells adhesion, morphology and force transmission [13, 40]. Therefore, 3D *in vitro* models are generally preferred for mechanobiological study to better mimic the native environment. Various materials such as alginate [55], agarose [56], pHEMA [57] with different 3D features (network, porosity, water content, stiffness) have been employed to study chondrogenesis. Recently, it has been shown that viscoelastic hydrogels with a faster stress relaxation promote cartilage formation indicating the importance of cells mechanical confinement in 3D systems as a physical input [55]. In parallel, a broad range of external mechanical stimuli including compression [58], shear [59] and tension [60] as well as hydrostatic pressure [61] has been investigated for cartilage mechanobiology (see reference [43]: a recent review for mechanical stimulation). Even with tension stimulation which is not the typical loading condition for

cartilage tissue, matrix organization and tensile properties of self-assembling neo-cartilage constructs were shown to be enhanced [60].

To facilitate clinical translation of *in vitro* engineered constructs, biomimetic platforms should be employed to optimize cells response with respect to biological or biomechanical manipulations [13]. Apart from the influence of biological mediators like growth factors, both the scaffold intrinsic characteristics (e.g. surface chemistry) and the material properties (e.g. permeability) act in synergy with external physical cues (e.g. mechanical stimulation) to orchestrate chondrogenesis [62, 63]. In particular, the mechanobiological regulators such as strain and pressure fields are generated by the applied loading based on the mechanical properties of the biomaterials (Figure 5). Accordingly, careful combination of 3D scaffolds and loadings is necessary to develop a mechano-mimetic microenvironment like cartilage. Despite successful implementation of specific loading regimens such as compression and shear *in vitro*, rational matching of 3D scaffolds mechanical properties to cartilage has been overlooked. Many mechanobiological studies have been performed on very soft hydrogels with a stiffness that barely reaches 100 kPa [55, 64, 65], which is insufficient to model cartilage tissue mechanical behavior. Indeed, only competent and recapitulating systems might provide pertinent *in vitro* models for mechanobiological studies.

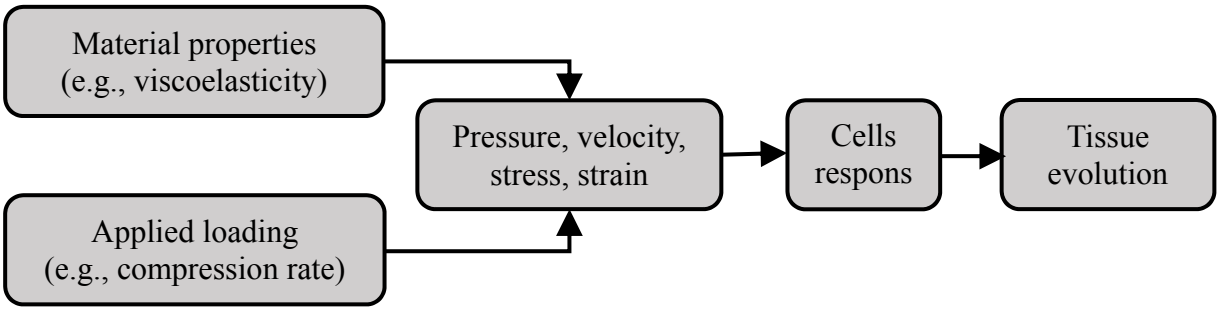

Figure 5. Interstitial fluid pressure, velocity, strain and stress fields can be important biophysical mediators to modulate chondrogenic differentiation process and ECM turnover. These mechanical regulators are varied by applied loading condition and biomaterial characteristics.

1-2-2 Cyclic compression: a classic mechanical stimulus

Articular cartilage usually experiences compressive stress following joint loading and a strain range of 7 to 23% has been measured *in vivo* in the tibiofemoral contact region during walking [66]. Cyclic compression is, therefore, the most relevant simulating loading regime and is widely employed to study the effect of the mechanical forces in cartilage mechanobiology [43, 46, 67, 68]. Dynamic compression leads to spatiotemporal chondrocytes deformation as well

as fluid flow in the local mechanical micro-environment surrounding the cells. As shown in Figure 6, these direct and indirect effects can trigger different signaling transductions over nucleus, ion channels, primary cilium and cytoskeleton [46]. For instance, transient receptor potential vanilloid 4, as a mechano or osmo-sensitive calcium channel, was associated to transduction of dynamic compression in chondrocytes-agarose constructs [56].

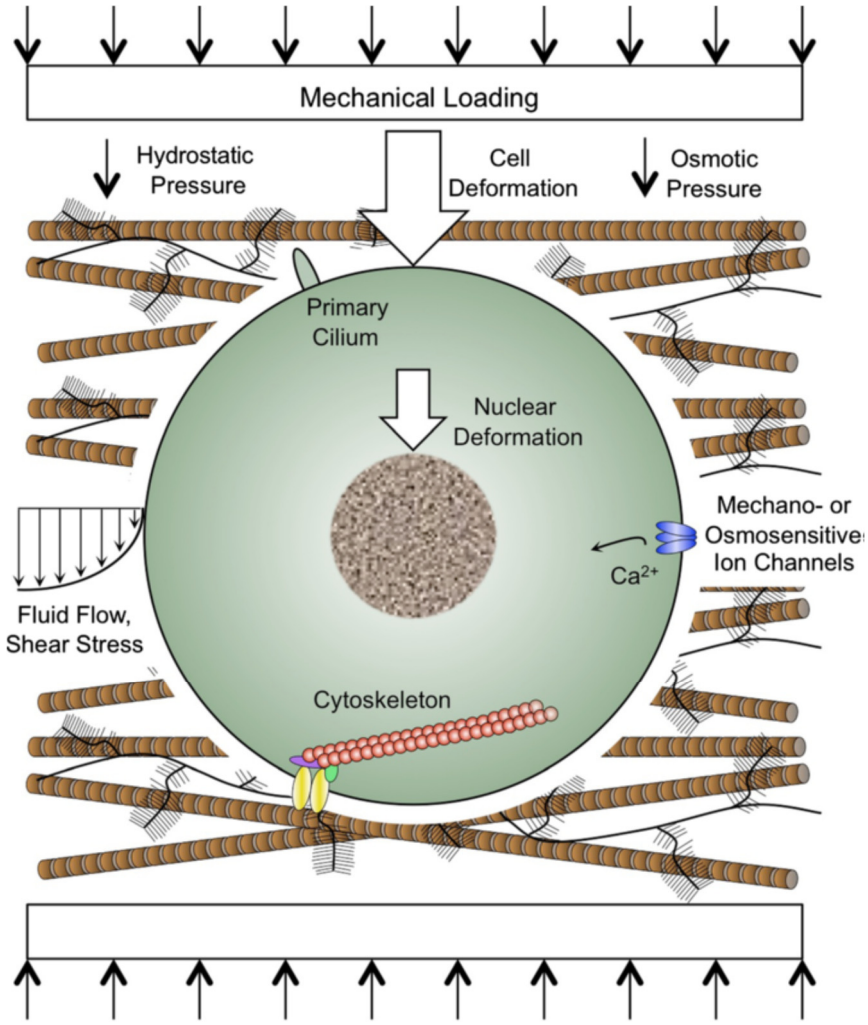

Figure 6. Direct (e.g., nucleus deformation) and indirect (e.g., fluid pressure) mechanical signals can be generated following cyclic compression of cartilage tissue. These physical cues can trigger signal transduction through mechano-sensitive elements embedded on or inside the cell membrane (reproduced from [46]).

The effect of cyclic compression on chondrocytes function can be varied with material properties, structure of the biomaterial, loading amplitude or frequency of stimulation as shown in Figure 7 [45]. While dynamic compression is in general stimulatory for chondrogenesis and ECM production [67, 69, 70], inhibitory effect of cyclic compression was also observed [71, 72]. Indeed, the combination of a variety of loading parameters and scaffold properties can lead to diversely different mechanical cues for chondrocytes. In view of the complex interplay of

all these parameters, various *in vitro* models might not necessarily lead to a conductive mechanical environment for chondrogenesis. Therefore, large discrepancies in the cells response and synthesis of cartilage tissue component could be expected.

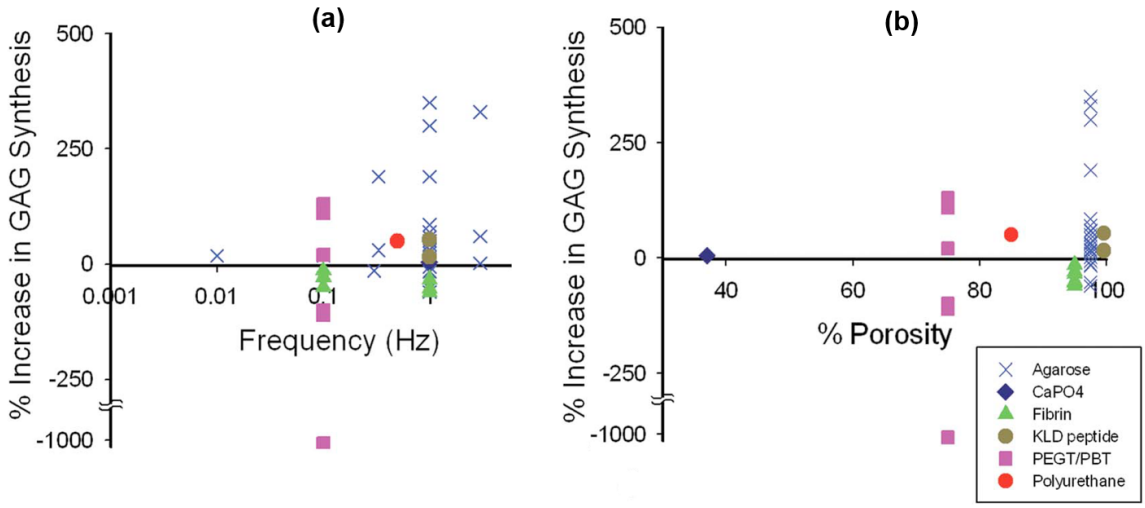

Figure 7. Substantial variation of glycosaminoglycan (GAG) biosynthesis following cyclic compression in different biomaterials. (a) Effect of frequency of loading. (b) Effect of biomaterials porosity (Reproduced from [45]).

In order to simplify this situation and to allow for a more straightforward correlation between an applied mechanical stimulus and an observed tissue differentiation, an overarching mechanobiological variable covering all contributing parameters would be of great help. Mechanical hysteresis has been recently proposed to be such a mechanobiological determinant to encompass the influence of key physical cues [57]. Abdel-Sayed *et al* have shown that chondro-progenitor cells seeded in polymeric scaffolds are sensitive to the level of energy dissipation under cyclic compression. As shown in Figure 8, chondrogenic expression was at its highest level for scaffold dissipation close to the dissipation of healthy cartilage. Despite the acquired knowledge about the correlation between dissipation level and chondrogenesis, it still remains to be demonstrated whether only the level of energy dissipation is the sufficient condition to promote chondrogenesis or if the mechanism of dissipation could also have an influence.

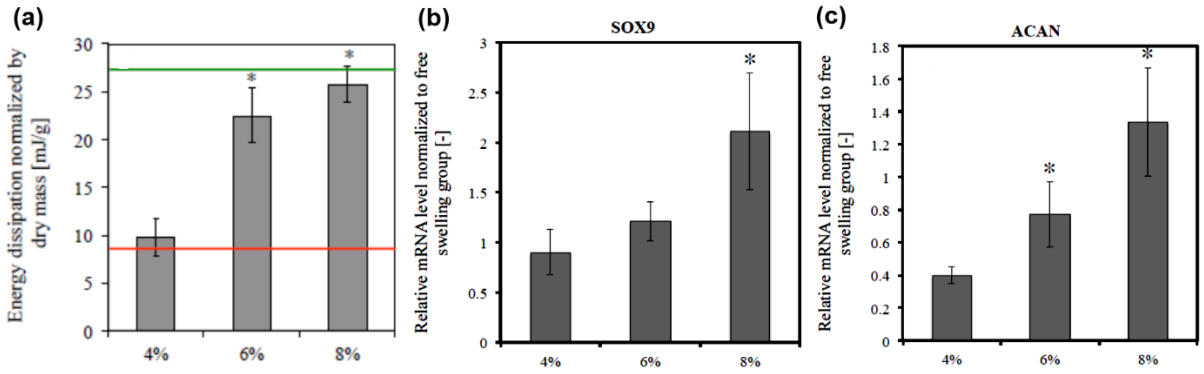

Figure 8. Energy dissipation as a mechanobiological variable for chondrogenesis. (a) The level of energy dissipation for different pHEMA based scaffolds submitted to identical compression regimen and corresponding values for healthy (green) and degenerated (red) human cartilage (the % in the horizontal axis represents the molar ratio of crosslinker to monomer of the polymeric network to modulate the dissipative capacity). (b-c) Direct correlation was reported for expression of chondrogenic genes (ACAN and SOX9) and the level of energy dissipation in scaffolds (reproduced with permission from [57]).

1-2-3 Biomechanically functional and recapitulating biomaterial

Knowing that cartilage is a poro-viscoelastic tissue with non-linear, anisotropic and inhomogeneous properties [3], development of a perfectly biomimetic material is very unlikely and probably not necessary for specific models. In this regard, different priorities have been considered in the literature for matching featured mechanical properties such as compressive and tensile moduli and toughness [3, 8, 73]. Indeed, compressive stiffness of biomaterial is of great importance in case of cartilage to withstand the demanding joints loading condition after implantation [29, 47]. Given the inverse correlation between porosity and the stiffness of biomaterial [74], physiological water content close to that of cartilage (65-80%) can serve as a constraining parameter for its design. For the mechanical performances, dissipation is indeed a key attribute for defect growth resistance and toughness of biomaterials under mechanical loading [75, 76]. In parallel, a new paradigm is emerging on the role of dissipative phenomena in mechanobiology of load-bearing tissues as quoted recently in an editorial of Nature Materials [77]: “The role of time-dependent properties of biomaterials such as viscoelasticity on cell response is becoming increasingly important”. Therefore, there exists a strong incentive to further elaborate on the concept of energy dissipation in the development of load-bearing biomaterial for two important and complementary goals which are mechanical and mechanobiological performances.

Interestingly, cartilage as a load-bearing soft tissue can efficiently dissipate the input energy following an applied loading thanks to its poro-viscoelastic properties [1, 57, 78]. Being a tough

material with unique tribology, articular cartilage can also sustain innumerous cycles of physiological loading over the lifetime [1, 8]. A biomaterial with similar degree of porosity, dissipation and stiffness to articular cartilage could, therefore, be a biomechanically mimetic and functional platform for mechanobiological study. However, a merely stiff and hysteretic biomaterial is not necessarily fatigue resistance. Indeed, the different sources of dissipation must be carefully designed for a robust mechanical performance under cyclic loading.

1-3 Mechanical hysteresis

The mechanical dissipation is generally described as a global variable and is usually quantified by the area of the hysteresis loop for viscoelastic materials under dynamic loadings (Figure 9-a). This loop is generated due to the difference of the given and the retrieved mechanical energy during loading and unloading steps. Indeed, the energy dissipation of visco-porous biomaterials under cyclic loading could be either due to intrinsic solid matrix dissipation or frictional drag mechanisms (i.e. flow-independent or flow-dependent viscoelasticity) [1, 78]. While resistance to flow of interstitial fluid within the solid matrix is the dominant mechanism for the latter, the former is influenced by interaction and rearrangement of the polymeric network upon loading. Therefore, not only parameters of external stimulus can modulate the hysteresis loop area, but also the material composition and internal structure contribute to dissipative phenomena during cyclic loading (Fig. 9-b).

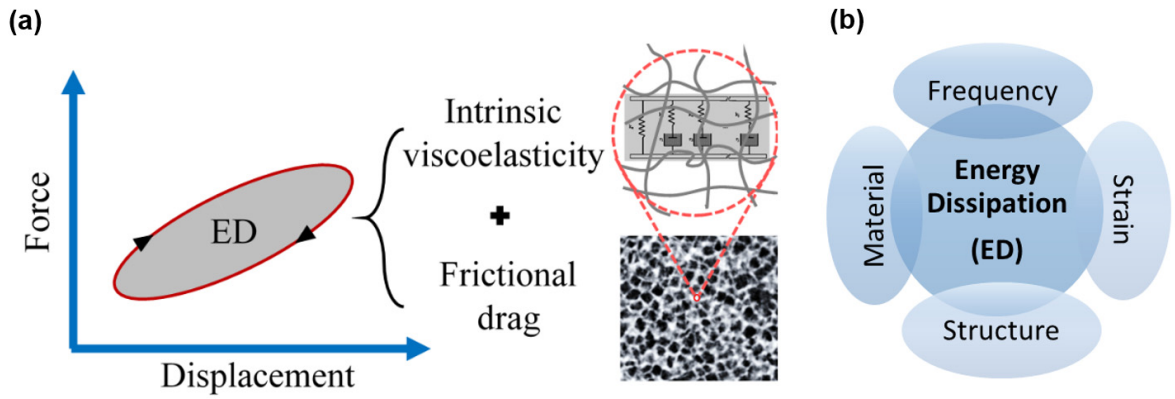

Figure 9. Energy dissipation in viscoelastic material. (a) Hysteresis curve is generated due to intrinsic (solid network attributes) and fluidic (solid-fluid interaction in porous media) dissipative phenomena and the load-displacement values do not follow the same path during loading and unloading. (b) Energy dissipation is associated with applied loading frequency and amplitude as well as mechanical and structural properties of material.

1-3-1 Dissipative biomaterials

Toughness as the amount of energy to fracture is a key mechanical property for a load-bearing material to avoid failure. Damping of input energy via mechanical hysteresis in dissipation zone protects the loaded material by shielding the crack tip and improves its toughness [76]. Since insufficient dissipative capacity is the main reason for low toughness, various dissipative hydrogels have been developed with the aim of achieving high toughness similar to biological tissues to sustain physiological loads [73]. In this intensive research context, innovative strategies were proposed including double network (DN) [79], hydrophobic modification [80], block copolymers [81], opposite polyelectrolytes [28] as well as hybrid [82] and composite [83] systems. Although these strategies all follow the same principle of dissipating imposed input energy by incorporating different sacrificial elements into the polymeric network, the nature of the intrinsic dissipative blocks and their working mechanisms are quite different (See reference [75]: a recent review for designing intrinsic mechanisms of dissipation). Collectively, significant results have been obtained in the development of dissipative hydrogels with reported toughness values even outperforming the cartilage one [73, 84]. However, insufficient load support capability in moderate strain range limits the application of these tough hydrogels for cartilage tissue regeneration. In addition, only recently the preserved sources of dissipation have been considered for a robust fatigue behavior under cyclic loading [84-86].

Gong and colleagues pioneered the idea of employing sacrificial elements in covalently crosslinked DN hydrogels (Figure 10-a) via a two-step process [79, 87], in which the second soft and ductile network supplements the firstly formed stiff and brittle network. Despite superior mechanical properties of the interpenetrating networks over their single-component hydrogels, the conventional covalent DN systems show weak fatigue performance [75]. In this system, the rigid and brittle network is fractured to dissipate energy while flexibility of the second network keeps its configuration. However, due to permanent bonds rupture after the initial loading, the source of dissipation is vanished for subsequent cycles of loading. To address this limitation, semi-physical DN hydrogels (Figure 10-b) were developed by employing reversible ionic bonds as sacrificial elements to dissipate energy [88]. A major limitation for ionic bonds is the lack of chemical stability in presence of mobile ions which is a common situation in a biological environment [82]. In addition, the uncontrollable water uptake after immersion in aqueous environments is another issue in hydrophilic DN hydrogels [89] and can deteriorate the mechanical performance of these hydrogels for biomedical

applications. To reduce the high swelling and simultaneously increase mechanical dissipation, reinforcing nano-fibers were incorporated into the polymeric structure of semi-physical DN hydrogels [83].

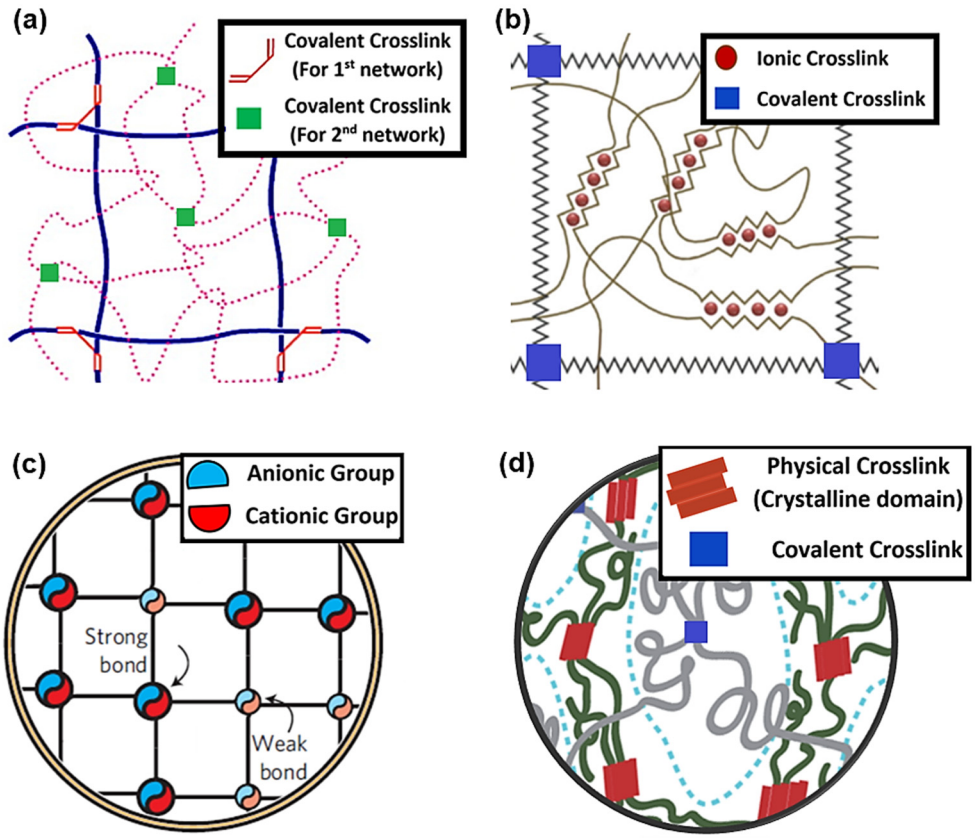

Figure 10. Schematic representation of different strategies for enhancing intrinsic dissipation of hydrogels. (a) Classical double network approach with two covalently crosslinked interpenetrating network (adapted with permission from [87]). (b) Semi-physical double network approach with ionic crosslinking in one network and covalent crosslinking in another network (adapted with permission from [73]). (c) Single network structure of polyions with different bonds strength (adapted with permission from [28]). (d) Hybrid double network with covalent bonds and crystalline domains (adapted with permission from [82]).

Recently, fully physical DN hydrogels with partial fatigue resistance and self-healing capability have been designed by using hydrophobic associations [84, 85]. Despite being dissipative upon large deformations and having high water content (80-90%), these physical hydrogels usually have poor stiffness in moderate strain range (<50%), and therefore, their load support capability is limited. The principle of sacrificial bonds has also been employed in single network (SN) systems by tri-block copolymers [81] and opposite charge polyions (Figure 10-c) [28]. By developing a dually crosslinked structure with different bonds strength, these SN hydrogels can dissipate energy via weak bonds and maintain system configuration by strong

bonds (Figure 10-c). Despite showing attractive mechanical performance in 50-70% water content range, the pH sensitivity due to ionic bonds as source of dissipation is still a significant limitation for these hydrogels [82]. To fabricate chemically stable, stiff and tough hydrogels, successive steps of polymerization, drying, annealing and re-hydration were designed to form a hybrid DN system with crystalline domains and covalent crosslinkers (Figure 10-d). The main advantage of this system is using crystallites as a stable dissipation source under deformation instead of ionic bonds with degraded dissipative capacity in electrolyte solutions [82]. Long recovery time for reassociation of unzipped domains and relatively low compressive stiffness are, however, the main weaknesses of these hybrid hydrogels. Collectively, despite development of many dissipative hydrogels, designing biomechanically functional biomaterials presenting preserved mechanical hysteresis still remains a significant challenge.

In addition, non-physiological fabrication methods for developing stiff and dissipative hydrogel are generally incompatible with cells encapsulation approach [73]. Development of porous structure using these hydrogels composition by bio-fabrication methods and subsequently infusion of cells into their pre-formed scaffolds could potentially help to utilize them in tissue engineering applications. Architecture of porous structures can be varied by porosity, pore size, pores interconnectivity and orientation. However, the effect of all morphological attributes can be described by the permeability as a robust quantitative parameter. Permeability directly influences transport phenomenon (important for nutrients, growth factors and cell delivery) and indirectly regulates fluid pressure and velocity in porous scaffolds [51, 90]. Indeed, permeability of a porous material can contribute to its time-dependent behavior under loading through frictional drag mechanism. Therefore, an interesting potential also exists to employ permeability for supplementing intrinsic material dissipation with fluidic dissipation in the development of dissipative biomaterials.

1-3-2 Temperature increase due to energy dissipation

Temperature increase due to dissipated energy following cyclic loading is an established concept for viscoelastic materials [91, 92]. Since articular cartilage is a viscoelastic tissue with high dissipative capacity, temperature increase following joint loading could occur. Normal knee temperature at rest is about 32-33°C [93, 94] which is 4-5°C lower than the core body temperature and standard culture condition *in vitro* (37°C). By using finite element modeling, it has been numerically shown [95] that the power of heat generation in normal cartilage may increase the internal tissue temperature around 1-2°C following a 10 minutes cyclic

compression (15% amplitude at 1.5 Hz) [95]. As measured inside intra-articular region of the knee by implanted probes, the temperature can be increased to 38°C after 60 minutes of jogging [94]. A temperature increase of about 4°C after 1 hour of walking was also predicted by employing a simplified lumped model with experimentally determined heat transfer parameters from normal knee cartilage [96]. Accordingly, the self-heating phenomenon due to viscoelastic behavior of articular cartilage has been introduced as a new mechanobiological cue for chondrogenesis [96, 97].

While *in vitro* mechanobiological models typically consider a constant culture temperature of 37°C, there are only a few studies regarding the effect of culture temperature on chondrocytes biological response. In a recent study by Ito *et al* in this context, behavior of human chondrocytes in monolayer and pellet formats were analyzed at 32, 37 and 41°C culture conditions [98]. It was observed that culture at 41°C significantly decrease the cells metabolic activity and chondrogenesis compared to both other culture temperatures at 32 and 37°C. In addition, a higher metabolic activity for the 32°C condition was observed contrary to a better chondrogenic differentiation at 37°C. Similar conclusions were also drawn for human chondro-progenitor cells cultured at 33 and 37°C in 2D condition [97]. Collectively, it has been shown that proper heat stimulation (temperature increase) can enhance chondrocytes viability and chondrogenic differentiation [99-101]. Over-stimulation by heat, however, reduces the cells viability and inhibits cartilage matrix synthesis [98, 99].

1-4 Bioreactors

Bioreactors are devices designed to maintain culture environment for cells or cells-scaffold constructs to grow, while applying physicochemical cues in a controllable manner. In the simplest case, a standard incubator is a static bioreactor for a culture dish with the ability to control constant CO_2, temperature and humidity level inside the chamber. However, careful modulation of the *in vitro* culture conditions, as an attempt to simulate certain cues of *in vivo* environment, is accomplished via more refined bioreactors. In this context, various types of dynamic bioreactors have been developed for regulating nutrient transport, oxygen tension and biophysical stimulation [13, 43, 102]. Rotating wall vessels, spinner flasks and perfusion chambers are widely employed systems in tissue engineering framework to overcome the diffusion–based mass transfer limitations. They all improve nutrient supply and oxygen infiltration depth into and complementarily waste removal from the engineered construct.

Applied shear stress on cells due to fluid flow can also be controlled to some extent by the flow rate of the perfusion system and rotation speed of the vessel [43].

In parallel, bioreactors capable to apply hydrostatic pressure, compression, shear and tension are sophisticated loading platforms for cartilage tissue engineering and mechanobiology [43, 68]. Additionally, multi-functional bioreactors that combine compression, shear, rolling and sliding have been designed to simulate complex physiological loading condition in articulating joints [68, 103]. It has been shown that synergetic physical stimulation could be more effective than a single loading mode for specific chondrogenic markers [59, 68]. Despite the existing evidence that chondrocytes can experience a varied thermal environment subsequent to joint loading, *in vitro* mechanobiological models usually consider a constant culture temperature during mechanical stimulation. Therefore, developing a bioreactor to allow the control of temperature evolution during dynamic loading is required to better simulate the *in vivo* cartilage environment and investigate the synergetic effect of temperature and loading.

1-5 Thesis overview

The central theme of this thesis is to study the function of dissipation mechanisms in the development of load-bearing biomaterials. Given the critical role of dissipative phenomena on the toughness and the emerging evidence for viscoelasticity as a key feature to regulate cells behavior, an interesting potential exists to capitalize biomaterials dissipation for enhancing mechanical and mechanobiological performances simultaneously. To study these two different but complementary goals, pHEMA based hydrogels were employed as a biocompatible 3D support with tunable mechanical properties. To develop a mechanically functional biomaterial as a recapitulating platform for cartilage mechanobiology, stiffness, water content and dissipative capacity were considered as primary design parameters. The fatigue performance of dissipative hydrogels was carefully designed by controlling different sources of dissipation. Permeability of the visco-porous hydrogel was introduced as the design variable for flow-dependent dissipation and hydrogel's material composition for the network intrinsic dissipation. In parallel, a systematic analysis was performed to decipher the relative importance of influential factors on the effectiveness of cell seeding into the scaffolds. To evaluate the role of dissipation mechanisms in chondrogenesis, two cell-penetrable hydrogels with significantly different contribution of the fluidic and intrinsic dissipation sources under cyclic compression were developed. With the aim of enhancing cell-scaffold interaction, a method was developed to bio-conjugate RGD motifs onto the exposed surfaces of the porous hydrogel. A modular

bioreactor was also developed to independently control the applied stress/strain, temperature and CO_2/O_2 levels during culture of cell seeded-hydrogels. This device was then employed to study the synergetic and decomposed effects of cyclic compression and temperature evolution on chondrogenic differentiation of cells.

Based on the overview for the thesis, we divided the research to four specific studies each of them presented in a chapter as briefly presented here.

Chapter 2. Permeability of the 3D biomaterial has considerable effect on solutes transport (affects also cell seeding), developed pressure/velocity fields inside pores and fluid-solid interactions. Direct characterization of permeability in tissue engineering scaffolds under deformation is also a critical step for evaluating the flow-dependent viscoelasticity and therefore is the first goal of this research.

Chapter 3. An efficient and uniform distribution of cells in a scaffold is essential to obtain a normalized initial condition either for the fundamental *in vitro* experiments or for clinical applications. Since there is no chance to modify the cells distribution and density following an ineffective cell seeding, the second objective of the work is developing a practical seeding protocol leading to uniform distribution of cells inside 3D scaffolds.

Chapter 4. Dissipation is a key attribute for performance of viscoelastic biomaterials under mechanical loading. A new paradigm is also emerging in the role of dissipative phenomena on mechanobiology of load-bearing tissues. Therefore, an interesting potential exists to employ dissipation for these two different but complementary goals in the development of biomaterials. Determining the role of the different dissipation sources on the mechanical and mechanobiological behaviors of the load-bearing hydrogels is the third yet primary objective of this research.

Chapter 5. Careful design of biomaterials properties, cell-scaffold interaction and *in vivo* like stimulation is required to guide chondrocytes differentiation and facilitate clinical translation of engineered cartilage. Considering the self-heating phenomenon in cartilage upon cyclic loading, developing a customized *in vitro* platform to study the synergetic effect of temperature increase and mechanical stimulation is the last objective of this thesis.

A final chapter closes the thesis by summarizing and discussing the major obtained results.

1-6 References

[1] Mow VC, Ratcliffe A, Poole AR. Cartilage and diarthrodial joints as paradigms for hierarchical materials and structures. Biomaterials 1992;13:67-97.

[2] Stok K, Oloyede A. Conceptual fracture parameters for articular cartilage. Clin Biomech 2007;22:725-35.

[3] Moutos FT, Freed LE, Guilak F. A biomimetic three-dimensional woven composite scaffold for functional tissue engineering of cartilage. Nat Mater 2007;6:162.

[4] Ateshian G, Warden W, Kim J, Grelsamer R, Mow V. Finite deformation biphasic material properties of bovine articular cartilage from confined compression experiments. J Biomech 1997;30:1157-64.

[5] Simha N, Carlson C, Lewis J. Evaluation of fracture toughness of cartilage by micropenetration. J Mater Sci Mater Med 2004;15:631-9.

[6] Halloran J, Sibole S, Van Donkelaar C, Van Turnhout M, Oomens C, Weiss J, et al. Multiscale mechanics of articular cartilage: potentials and challenges of coupling musculoskeletal, joint, and microscale computational models. Ann Biomed Eng 2012;40:2456-74.

[7] Antons J, Marascio MGM, Nohava J, Martin R, Applegate L, Bourban P, et al. Zone-dependent mechanical properties of human articular cartilage obtained by indentation measurements. J Mater Sci Mater Med 2018;29:57.

[8] Guilak F, Butler DL, Goldstein SA. Functional tissue engineering: the role of biomechanics in articular cartilage repair. Clinical Orthopaedics and Related Research® 2001;391:S295-S305.

[9] Seda Tığlı R, Ghosh S, Laha MM, Shevde NK, Daheron L, Gimble J, et al. Comparative chondrogenesis of human cell sources in 3D scaffolds. Journal of tissue engineering and regenerative medicine 2009;3:348-60.

[10] Hunziker E. Articular cartilage repair: basic science and clinical progress. A review of the current status and prospects. Osteoarthritis and cartilage 2002;10:432-63.

[11] Kon E, Filardo G, Di Martino A, Marcacci M. ACI and MACI. Journal of Knee Surgery 2012;25:017.

[12] Johnstone B, Alini M, Cucchiarini M, Dodge GR, Eglin D, Guilak F, et al. Tissue engineering for articular cartilage repair–the state of the art. Eur Cell Mater 2013;25:e67.

[13] Moffat KL, Neal RA, Freed LE, Guilak F. Chapter 13 - Engineering Functional Tissues: In Vitro Culture Parameters A2 - Lanza, Robert. In: Langer R, Vacanti J, editors. Principles of Tissue Engineering (Fourth Edition). Boston: Academic Press; 2014. p. 237-59.

[14] Hubka KM, Dahlin RL, Meretoja VV, Kasper FK, Mikos AG. Enhancing chondrogenic phenotype for cartilage tissue engineering: monoculture and coculture of articular chondrocytes and mesenchymal stem cells. Tissue Eng,Part B 2014;20:641-54.

[15] Leferink AM, Santos D, Karperien M, Truckenmüller R, Van Blitterswijk C, Moroni L. Differentiation capacity and maintenance of differentiated phenotypes of human mesenchymal stromal cells cultured on two distinct types of 3D polymeric scaffolds. Integrative biology 2015;7:1574-86.

[16] Vinardell T, Sheehy EJ, Buckley CT, Kelly DJ. A comparison of the functionality and in vivo phenotypic stability of cartilaginous tissues engineered from different stem cell sources. Tissue Eng,Part A 2012;18:1161-70.

[17] Darwiche S, Scaletta C, Raffoul W, Pioletti DP, Applegate LA. Epiphyseal chondroprogenitors provide a stable cell source for cartilage cell therapy. Cell Medicine 2012;4:23-32.

[18] Studer D, Cavalli E, Formica FA, Kuhn GA, Salzmann G, Mumme M, et al. Human chondroprogenitors in alginate–collagen hybrid scaffolds produce stable cartilage in vivo. Journal of tissue engineering and regenerative medicine 2017;11:3014-26.

[19] Solchaga LA, Tognana E, Penick K, Baskaran H, Goldberg VM, Caplan AI, et al. A rapid seeding technique for the assembly of large cell/scaffold composite constructs. Tissue Eng 2006;12:1851-63.

[20] Thevenot P, Nair A, Dey J, Yang J, Tang L. Method to analyze three-dimensional cell distribution and infiltration in degradable scaffolds. Tissue Eng,Part C 2008;14:319-31.

[21] Pei M, Solchaga LA, Seidel J, Zeng L, Vunjak-Novakovic G, Caplan AI, et al. Bioreactors mediate the effectiveness of tissue engineering scaffolds. The FASEB Journal 2002;16:1691-4.

[22] Wendt D, Marsano A, Jakob M, Heberer M, Martin I. Oscillating perfusion of cell suspensions through three-dimensional scaffolds enhances cell seeding efficiency and uniformity. Biotechnol Bioeng 2003;84:205-14.

[23] Xie J, Jung Y, Kim SH, Kim YH, Matsuda T. New technique of seeding chondrocytes into microporous poly (l-lactide-co-ε-caprolactone) sponge by cyclic compression force-induced suction. Tissue Eng 2006;12:1811-20.

[24] Vega SL, Kwon MY, Burdick JA. Recent advances in hydrogels for cartilage tissue engineering. European cells & materials 2017;33:59.

[25] Horák D, Kroupová J, Šlouf M, Dvořák P. Poly (2-hydroxyethyl methacrylate)-based slabs as a mouse embryonic stem cell support. Biomaterials 2004;25:5249-60.

[26] Loh QL, Choong C. Three-dimensional scaffolds for tissue engineering applications: role of porosity and pore size. Tissue Eng,Part B 2013;19:485-502.

[27] Antons J, Marascio M, Aeberhard P, Weissenberger G, Hirt-Burri N, Applegate L, et al. Decellularised tissues obtained by a CO2-philic detergent and supercritical CO2. European Cells and Materials 2018;36:81-95.

[28] Sun TL, Kurokawa T, Kuroda S, Ihsan AB, Akasaki T, Sato K, et al. Physical hydrogels composed of polyampholytes demonstrate high toughness and viscoelasticity. Nat Mater 2013;12:932.

[29] Moghadam MN, Pioletti DP. Improving hydrogels′ toughness by increasing the dissipative properties of their network. J Mech Behav Biomed Mater 2015;41:161-7.

[30] Chung HJ, Park TG. Surface engineered and drug releasing pre-fabricated scaffolds for tissue engineering. Adv Drug Del Rev 2007;59:249-62.

[31] Paterson SM, Shadforth AM, Shaw JA, Brown DH, Chirila TV, Baker MV. Improving the cellular invasion into PHEMA sponges by incorporation of the RGD peptide ligand: the use of copolymerization as a means to functionalize PHEMA sponges. Materials Science and Engineering: C 2013;33:4917-22.

[32] Liao IC, Moutos FT, Estes BT, Zhao X, Guilak F. Composite three-dimensional woven scaffolds with interpenetrating network hydrogels to create functional synthetic articular cartilage. Adv Funct Mater 2013;23:5833-9.

[33] Mow VC, Wang CC, Hung CT. The extracellular matrix, interstitial fluid and ions as a mechanical signal transducer in articular cartilage. Osteoarthr Cartil 1999;7:41-58.

[34] Chen J-L, Duan L, Zhu W, Xiong J, Wang D. Extracellular matrix production in vitro in cartilage tissue engineering. Stem Cells 2014;8:14-5.

[35] Zuscik MJ, Hilton MJ, Zhang X, Chen D, O'Keefe RJ. Regulation of chondrogenesis and chondrocyte differentiation by stress. The Journal of clinical investigation 2008;118:429-38.

[36] Mow VC, Guo XE. Mechano-electrochemical properties of articular cartilage: their inhomogeneities and anisotropies. Annual review of biomedical engineering 2002;4:175-209.

[37] Nassajian Moghadam M. Self-heating hydrogel for mechanically-controlled drug release. EPFL; 2015.

[38] Buscemi L, Ramonet D, Klingberg F, Formey A, Smith-Clerc J, Meister J-J, et al. The single-molecule mechanics of the latent TGF-β1 complex. Curr Biol 2011;21:2046-54.

[39] Li Z, Kupcsik L, Yao SJ, Alini M, Stoddart MJ. Mechanical load modulates chondrogenesis of human mesenchymal stem cells through the TGF-β pathway. J Cell Mol Med 2010;14:1338-46.

[40] Baker BM, Chen CS. Deconstructing the third dimension–how 3D culture microenvironments alter cellular cues. J Cell Sci 2012;125:3015-24.

[41] Humphrey JD, Dufresne ER, Schwartz MA. Mechanotransduction and extracellular matrix homeostasis. Nature reviews Molecular cell biology 2014;15:802-12.

[42] Jaalouk DE, Lammerding J. Mechanotransduction gone awry. Nature reviews Molecular cell biology 2009;10:63-73.

[43] Salinas EY, Hu JC, Athanasiou K. A Guide for Using Mechanical Stimulation to Enhance Tissue-Engineered Articular Cartilage Properties. Tissue Eng,Part B 2018.

[44] Behrens F, Kraft EL, Oegema Jr TR. Biochemical changes in articular cartilage after joint immobilization by casting or external fixation. J Orth Res 1989;7:335-43.

[45] Babalola OM, Bonassar LJ. Parametric finite element analysis of physical stimuli resulting from mechanical stimulation of tissue engineered cartilage. J Biomech Eng 2009;131:061014.

[46] O'Conor CJ, Case N, Guilak F. Mechanical regulation of chondrogenesis. Stem Cell Res Ther 2013;4:61.

[47] Guilak F, Butler DL, Goldstein SA, Baaijens FP. Biomechanics and mechanobiology in functional tissue engineering. J Biomech 2014;47:1933-40.

[48] Valonen PK, Moutos FT, Kusanagi A, Moretti MG, Diekman BO, Welter JF, et al. In vitro generation of mechanically functional cartilage grafts based on adult human stem cells and 3D-woven poly (ε-caprolactone) scaffolds. Biomaterials 2010;31:2193-200.

[49] Huang AH, Farrell MJ, Mauck RL. Mechanics and mechanobiology of mesenchymal stem cell-based engineered cartilage. J Biomech 2010;43:128-36.

[50] Martin I, Jakob M, Schäfer D, Dick W, Spagnoli G, Heberer M. Quantitative analysis of gene expression in human articular cartilage from normal and osteoarthritic joints. Osteoarthritis and Cartilage 2001;9:112-8.

[51] Kemppainen JM, Hollister SJ. Differential effects of designed scaffold permeability on chondrogenesis by chondrocytes and bone marrow stromal cells. Biomaterials 2010;31:279-87.

[52] Lefebvre V, Smits P. Transcriptional control of chondrocyte fate and differentiation. Birth Defects Res C Embryo Today Rev 2005;75:200-12.

[53] Leung VY, Gao B, Leung KK, Melhado IG, Wynn SL, Au TY, et al. SOX9 governs differentiation stage-specific gene expression in growth plate chondrocytes via direct concomitant transactivation and repression. PLoS Genet 2011;7:e1002356.

[54] Gu S, Boyer TG, Naski MC. Basic helix-loop-helix transcription factor Twist1 inhibits transactivator function of master chondrogenic regulator Sox9. J Biol Chem 2012;287:21082-92.

[55] Lee H-p, Gu L, Mooney DJ, Levenston ME, Chaudhuri O. Mechanical confinement regulates cartilage matrix formation by chondrocytes. Nat Mater 2017;16:1243.

[56] O'Conor CJ, Leddy HA, Benefield HC, Liedtke WB, Guilak F. TRPV4-mediated mechanotransduction regulates the metabolic response of chondrocytes to dynamic loading. Proceedings of the National Academy of Sciences 2014;111:1316-21.

[57] Abdel-Sayed P, Darwiche SE, Kettenberger U, Pioletti DP. The role of energy dissipation of polymeric scaffolds in the mechanobiological modulation of chondrogenic expression. Biomaterials 2014;35:1890-7.

[58] Mouw JK, Connelly JT, Wilson CG, Michael KE, Levenston ME. Dynamic Compression Regulates the Expression and Synthesis of Chondrocyte-Specific Matrix Molecules in Bone Marrow Stromal Cells. Stem Cells 2007;25:655-63.

[59] Schätti O, Grad S, Goldhahn J, Salzmann G, Li Z, Alini M, et al. A combination of shear and dynamic compression leads to mechanically induced chondrogenesis of human mesenchymal stem cells. Eur Cell Mater 2011;22:214-25.

[60] Lee JK, Huwe LW, Paschos N, Aryaei A, Gegg CA, Hu JC, et al. Tension stimulation drives tissue formation in scaffold-free systems. Nat Mater 2017;16:864.

[61] Heyland J, Wiegandt K, Goepfert C, Nagel-Heyer S, Ilinich E, Schumacher U, et al. Redifferentiation of chondrocytes and cartilage formation under intermittent hydrostatic pressure. Biotechnol Lett 2006;28:1641-8.

[62] Panadero J, Lanceros-Mendez S, Ribelles JG. Differentiation of mesenchymal stem cells for cartilage tissue engineering: Individual and synergetic effects of three-dimensional environment and mechanical loading. Acta Biomater 2016;33:1-12.

[63] Goetzke R, Sechi A, De Laporte L, Neuss S, Wagner W. Why the impact of mechanical stimuli on stem cells remains a challenge. Cell Mol Life Sci 2018:1-16.

[64] Erickson IE, Huang AH, Chung C, Li RT, Burdick JA, Mauck RL. Differential maturation and structure–function relationships in mesenchymal stem cell-and chondrocyte-seeded hydrogels. Tissue Eng,Part A 2008;15:1041-52.

[65] Li Z, Yao S-J, Alini M, Stoddart MJ. Chondrogenesis of human bone marrow mesenchymal stem cells in fibrin–polyurethane composites is modulated by frequency and amplitude of dynamic compression and shear stress. Tissue Eng,Part A 2009;16:575-84.

[66] Liu F, Kozanek M, Hosseini A, Van de Velde SK, Gill TJ, Rubash HE, et al. In vivo tibiofemoral cartilage deformation during the stance phase of gait. J Biomech 2010;43:658-65.

[67] Finlay S, Seedhom BB, Carey DO, Bulpitt AJ, Treanor DE, Kirkham J. In Vitro Engineering of High Modulus Cartilage-Like Constructs. Tissue Eng,Part C 2016;22:382-97.

[68] Li K, Zhang C, Qiu L, Gao L, Zhang X. Advances in application of mechanical stimuli in bioreactors for cartilage tissue engineering. Tissue Eng,Part B 2017;23:399-411.

[69] Buschmann MD, Gluzband YA, Grodzinsky AJ, Hunziker EB. Mechanical compression modulates matrix biosynthesis in chondrocyte/agarose culture. J Cell Sci 1995;108:1497-508.

[70] Davisson T, Kunig S, Chen A, Sah R, Ratcliffe A. Static and dynamic compression modulate matrix metabolism in tissue engineered cartilage. J Orth Res 2002;20:842-8.

[71] Thorpe S, Buckley C, Vinardell T, O'Brien FJ, Campbell V, Kelly DJ. Dynamic compression can inhibit chondrogenesis of mesenchymal stem cells. Biochem Biophys Res Commun 2008;377:458-62.

[72] Hunter CJ, Mouw JK, Levenston ME. Dynamic compression of chondrocyte-seeded fibrin gels: effects on matrix accumulation and mechanical stiffness. Osteoarthritis and Cartilage 2004;12:117-30.

[73] Hong S, Sycks D, Chan HF, Lin S, Lopez GP, Guilak F, et al. 3D printing of highly stretchable and tough hydrogels into complex, cellularized structures. Adv Mater 2015;27:4035-40.

[74] Annabi N, Nichol JW, Zhong X, Ji C, Koshy S, Khademhosseini A, et al. Controlling the porosity and microarchitecture of hydrogels for tissue engineering. Tissue Eng,Part B 2010;16:371-83.

[75] Zhao X. Multi-scale multi-mechanism design of tough hydrogels: building dissipation into stretchy networks. Soft Matter 2014;10:672-87.

[76] Long R, Hui C-Y. Fracture toughness of hydrogels: measurement and interpretation. Soft Matter 2016;12:8069-86.

[77] Regeneration gets physical. Nat Mater 2017;16:1163.

[78] Mak A. The apparent viscoelastic behavior of articular cartilage—the contributions from the intrinsic matrix viscoelasticity and interstitial fluid flows. J Biomech Eng 1986;108:123-30.

[79] Gong JP, Katsuyama Y, Kurokawa T, Osada Y. Double-network hydrogels with extremely high mechanical strength. Adv Mater 2003;15:1155-8.

[80] Abdurrahmanoglu S, Can V, Okay O. Design of high-toughness polyacrylamide hydrogels by hydrophobic modification. Polymer 2009;50:5449-55.

[81] Henderson KJ, Zhou TC, Otim KJ, Shull KR. Ionically cross-linked triblock copolymer hydrogels with high strength. Macromolecules 2010;43:6193-201.

[82] Li J, Suo Z, Vlassak JJ. Stiff, strong, and tough hydrogels with good chemical stability. Journal of Materials Chemistry B 2014;2:6708-13.

[83] Karami P, Wyss C, Khoushabi A, Schmocker A, Broome M, Moser C, et al. Composite double-network hydrogels to improve adhesion on biological surfaces. ACS Appl Mater Interfaces 2018.

[84] Chen Q, Zhu L, Chen H, Yan H, Huang L, Yang J, et al. A Novel Design Strategy for Fully Physically Linked Double Network Hydrogels with Tough, Fatigue Resistant, and Self-Healing Properties. Adv Funct Mater 2015;25:1598-607.

[85] Yuan N, Xu L, Wang H, Fu Y, Zhang Z, Liu L, et al. Dual physically cross-linked double network hydrogels with high mechanical strength, fatigue resistance, notch-insensitivity, and self-healing properties. ACS Appl Mater Interfaces 2016;8:34034-44.

[86] Bai R, Yang Q, Tang J, Morelle XP, Vlassak J, Suo Z. Fatigue fracture of tough hydrogels. Extreme Mechanics Letters 2017;15:91-6.

[87] Nakajima T, Furukawa H, Tanaka Y, Kurokawa T, Osada Y, Gong JP. True chemical structure of double network hydrogels. Macromolecules 2009;42:2184-9.

[88] Sun J-Y, Zhao X, Illeperuma WR, Chaudhuri O, Oh KH, Mooney DJ, et al. Highly stretchable and tough hydrogels. Nature 2012;489:133.

[89] Kamata H, Akagi Y, Kayasuga-Kariya Y, Chung U-i, Sakai T. “Nonswellable” hydrogel without mechanical hysteresis. Science 2014;343:873-5.

[90] Pennella F, Cerino G, Massai D, Gallo D, Labate GFDU, Schiavi A, et al. A survey of methods for the evaluation of tissue engineering scaffold permeability. Ann Biomed Eng 2013;41:2027-41.

[91] Roylance D. Mechanics of Materials. New York: John Wiley & Sons; 1996.

[92] Moghadam MN, Kolesov V, Vogel A, Klok H-A, Pioletti DP. Controlled release from a mechanically-stimulated thermosensitive self-heating composite hydrogel. Biomaterials 2014;35:450-5.

[93] Haimovici N. Three years experience in direct intraarticular temperature measurement. Progress in clinical and biological research 1982;107:453-61.

[94] Becher C, Springer J, Feil S, Cerulli G, Paessler HH. Intra-articular temperatures of the knee in sports–An in-vivo study of jogging and alpine skiing. BMC Musculoskel Disord 2008;9:46.

[95] Moghadam MN, Abdel-Sayed P, Camine VM, Pioletti DP. Impact of synovial fluid flow on temperature regulation in knee cartilage. J Biomech 2015;48:370-4.

[96] Abdel-Sayed P, Moghadam MN, Salomir R, Tchernin D, Pioletti DP. Intrinsic viscoelasticity increases temperature in knee cartilage under physiological loading. J Mech Behav Biomed Mater 2014;30:123-30.

[97] Abdel-Sayed P, Vogel A, Nassajian Moghadam M, Pioletti D. Cartilage self-heating contributes to chondrogenic expression. European Cells and Materials 2013;26:171-8.

[98] Ito A, Nagai M, Tajino J, Yamaguchi S, Iijima H, Zhang X, et al. Culture temperature affects human chondrocyte messenger RNA expression in monolayer and pellet culture systems. PloS one 2015;10:e0128082.

[99] Hojo T, Fujioka M, Otsuka G, Inoue S, Kim U, Kubo T. Effect of heat stimulation on viability and proteoglycan metabolism of cultured chondrocytes: preliminary report. Journal of orthopaedic science 2003;8:396-9.

[100] Tonomura H, Takahashi KA, Mazda O, Arai Y, Shin-Ya M, Inoue A, et al. Effects of heat stimulation via microwave applicator on cartilage matrix gene and HSP70 expression in the rabbit knee joint. J Orth Res 2008;26:34-41.

[101] Chen J, Li C, Wang S. Periodic heat shock accelerated the chondrogenic differentiation of human mesenchymal stem cells in pellet culture. PLoS One 2014;9:e91561.

[102] Mabvuure N, Hindocha S, S Khan W. The role of bioreactors in cartilage tissue engineering. Current stem cell research & therapy 2012;7:287-92.

[103] Wimmer MA, Grad S, Kaup T, Hänni M, Schneider E, Gogolewski S, et al. Tribology approach to the engineering and study of articular cartilage. Tissue Eng 2004;10:1436-45.

Chapter 2: Experimental Method to Characterize the Strain Dependent Permeability of Tissue Engineering Scaffolds*

2-1 Abstract

Permeability is an overarching mechanical parameter encompassing the effects of porosity, pore size, and interconnectivity of porous structures. This parameter directly influences transport of soluble particles and indirectly regulates fluid pressure and velocity in tissue engineering scaffolds. The permeability also contributes to the viscoelastic behavior of visco-porous material under loading through frictional drag mechanism. We propose a straightforward experimental method for permeability characterization of tissue engineering scaffolds. In the developed set-up a step-wise spacer was designed to facilitate measurement of the permeability under different compressive strains while maintaining similar experimental conditions during the successive measurements. As illustration of the method, we measured the permeability of scaffolds presenting different average pore sizes and subjected to different compression values. Results showed an exponential relationship between the permeability and the average pore size of the scaffolds. Furthermore, the trend of the permeability decrease with compressive strains was depending on pore sizes of the scaffolds. The permeability also appeared to play a role in relaxation behavior of the scaffolds.

Keywords: Scaffolds, Permeability, Pore size, Compressive strain, Frictional drag

* This chapter has been published in Journal of Biomechanics (Volume 49, 2016, 3749–3752).

2-2 Introduction

Permeability is considered as an integrative variable for tissue engineering (TE) scaffolds reflecting the role of contributing parameters in their architectures such as porosity, pore size, interconnectivity and orientation of pores to flow direction [1]. The permeability of the scaffold not only influences infiltration and diffusion of soluble particles in TE applications but also passively controls the velocity and pressure fields of fluid phase inside the scaffold under mechanical stimulation.

From another point of view, the permeability can be understood as a primary mechanical determinant defining frictional drag that is the resistance of a 3D biomaterial for flowing fluid through its tortuous structure [2, 3]. Accordingly, permeability can be controlled to tune viscoelastic behavior of biomaterials under loading. Specifically, energy dissipation and stress relaxation of TE scaffolds are key viscoelastic features in dynamic and static loading regimes, respectively. Interestingly, these mechanobiological variables have been shown to be significantly influential on cellular response of load bearing tissues [4, 5].

Obviously, permeability is varied under compressive strain due to the deformed scaffold's internal structure and geometry. Different theoretical models have been developed to establish relationships between the strain and permeability for biological tissues such as cartilage (interested reader is referred to [6-9]). While many experimental studies have been performed to measure the permeability of biological tissues and scaffolds (see [10] for a review), only very few techniques have been developed to quantify the corresponding strain dependent permeability of the scaffolds. In a pioneer work for tissue engineered scaffolds, O'Brien *et al* [11] developed an experimental set-up allowing to measure the permeability of highly porous natural polymeric scaffolds (porosity higher than 95%) under different strain conditions. However, their system necessitates disassembly and reassembly steps of the rig for measurements of the permeability under different compressive strains. This technical approach impacts the reliability of the permeability measurement as permeability quantification is highly dependent on the initial and boundary conditions.

Kenneth *et al* [12] tested synthetic PVA scaffolds under confined compression to indirectly quantify strain dependent permeability according to the biphasic theoretical model for cartilage [6]. The employed model for permeability determination in that study was based on linear infinitesimal strain theory, while the range of applied compressive strain caused large deformation and nonlinear behavior. Therefore, the predicted permeability values from

confined compression experimental data based on the assumed model were not reliable anymore. In particular, Ateshian *et al* [13] have already discussed the limitation of indirect estimation of the permeability from creep or stress-relaxation experiments when finite deformation biphasic theory is used [13]. They showed low sensitivity of the reaction force vs. time data in confined compression (e.g., stress relaxation or creep tests) to large variations of the permeability function parameters. The difficulty of the indirect methods resides in the parameters estimation of the mathematical function for samples with different porosities, pore sizes, interconnectivity and viscoelastic properties, which indeed requires several experiments.

In this work, we present a general experimental technique to accurately characterize strain dependent permeability of tissue engineering scaffolds. In the proposed test rig, we designed a step-wise spacer for straightforward characterization of the permeability under different compressions while preserving initial and boundary conditions. As example, we applied this method to recently developed viscoelastic scaffolds presenting different average pore sizes subjected to different compression values.

2-3 Materials and Methods

Macroporous scaffolds with different average pore sizes and crosslinking density (3 groups) of pHEMA-EGDMA were prepared by salt leaching method as reported elsewhere [3, 4]. Each swelled scaffold was cut with an 8 mm diameter punch and the thickness was sized to 3 mm using a custom-made cutting tool. The equilibrium Young modulus of hydrated scaffolds were determined through applying successive compressive strains (10, 15 and 20%) with the Instron uniaxial testing machine (Instron E3000, Norwood, Massachusetts, USA) as described elsewhere [14]. Unconfined stress relaxation tests of 20% strain were also performed for fine and coarse pore size scaffolds at 50 µm/s and 5 µm/s compression rates as schematically depicted in Figure 1-a (See supplemental data for detail).

Micro-computed tomography (µCT) scans (Skyscan 1076, Bruker-microCT, Kontich, Belgium) of freeze-dried scaffolds (n=3) were used to calculate with CTAn software (Bruker-microCT) the average and the distribution of pore sizes in dried state (See supplemental data for detail). By measuring the bulk geometry of the scaffolds in hydrated as well as in dried states, the pores volumetric expansion (PVE) was evaluated. We then estimated the corresponding average pore size change as cubic root of PVE ($\sqrt[3]{PVE}$) [15]. Finally, by multiplying this value to obtained results from µCT of dried scaffolds, the hydrated state characteristics were calculated (Table S1). The porosity ϕ was determined by measuring the

volume V and weighting the mass of the swelled m_{wet} and the dried scaffolds m_{dried} according to Eq. 1.

$$\phi = \frac{(m_{wet} - m_{dried})/\rho_{water}}{V} \times 100 \qquad (1)$$

We modified a previously proposed set-up by O'Brien *et al* [11] for measuring strain dependent permeability of scaffolds. In the developed set-up as illustrated in Figure 1-b, we used a step-wise spacer, which allows measurements of the permeability in different compressive strains (10%, 18%, 27%, and 35%) in one assembly.

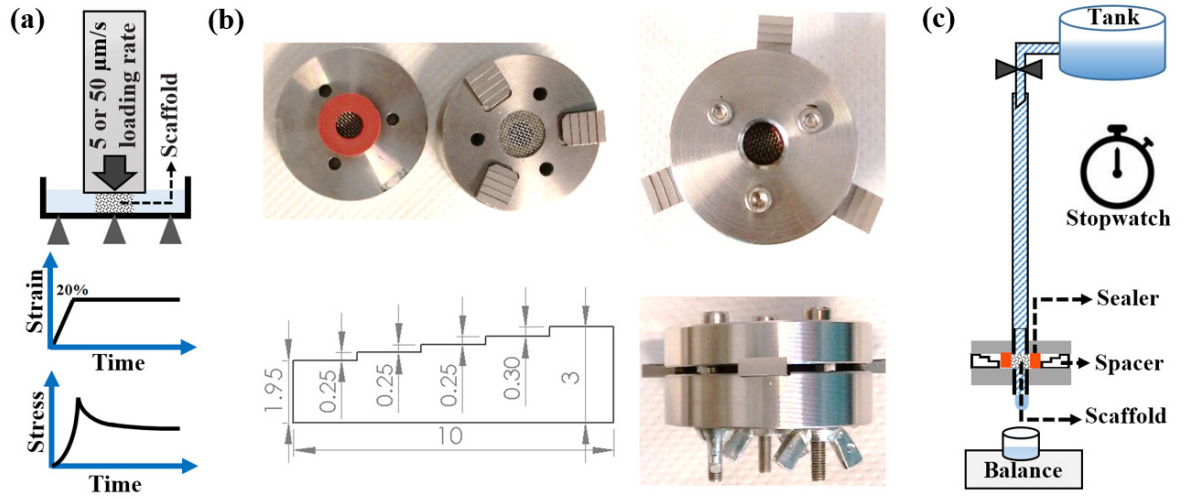

Figure 1. Employed test rigs for scaffolds evaluation. (a) Schematic illustration of the stress relaxation test. (b) Permeability chamber with stepwise spacer and the sealant. (c) Schematic of the experimental setup to measure permeability of a scaffold under different compressive strains.

Before measuring the permeability of scaffold, we needed to insure that our set-up is leakproof. For this purpose, a thick cylindrical sealant (3.5 mm thickness, 7 mm internal and 15 mm outer diameter) was designed to guarantee the sample's sealing while maintaining a uniform deformation. It was made of a silicon rubber (Elastosoil M4601, Wacker Chemie, Munich, Germany) and we obtained its equilibrium Young modulus by sequential compressive strains of 5, 10, 15 and 20% considering stress relaxation after each step [14]. The level of pre-strain resulting in required sealing force to prevent any leakage under the applied experimental conditions was then evaluated using Hooke's law and press fit's equations for thick walled cylinders.

To calculate the permeability, as schematically shown in Figure 1-c, after stress equilibrium, the flow rate was measured under constant water head condition using the weight of the flowing

water passing the scaffold (n=4-6) and a stopwatch. The permeability k of the scaffold was calculated using Eq. 2 based on Darcy's law [10, 16].

$$k = \frac{QL\mu}{A\rho gh} \quad (2)$$

where, μ represents the dynamic fluid viscosity (0.001 Pa.s for water), A is the actual scaffold cross section (πr^2 = 2.83E-05 m^2), L stands for the thickness of the sample (m), h is the constant fluid head (2.04 m), Q denotes the measured volumetric flow rate (m^3/s), ρ is the density of the fluid (1000 kg/m^3 for water) and g is the gravity constant (9.81 m/s^2). The thickness of sample decreases in Eq. 2 in case of different compressive strains corresponding to steps of the spacer (3.00, 2.70, 2.45, 2.20 and 1.95 mm, respectively).

2-4 Results

We developed different types of viscoelastic scaffolds having elastic modulus (0.76 to 1.2 MPa) within the range of articular cartilage by tuning the crosslinker (Cr) percentage of the base material and pore size as reported in Table 1. The average pore size and porosity for the three types of scaffolds ranged from 162 to 271 μm and 63% to 68% as reported in Table 1. The obtained results from the stress relaxation tests (Figure 2-d) revealed that the initial decay rate and relaxation time of transient stress were significantly different between fine and coarse pores size scaffolds (Table S2).

Table 1. Important characteristics of the developed viscoelastic scaffolds.

Scaffold type	4%Cr-Fine pore size	6%Cr-Medium pore size	8%Cr-Coarse pore size
Equilibrium Young modulus - (kPa)	760±63	1008±163	1201±154
Time to relax 90% of transient stress at 5 μm/s rate - (s)	581.5±76	378±30	341±45.5
Average pore size - d (μm)	162±5	196±4	271±5
Range of distribution of pore sizes within ± σ - (μm)	107-216	127-266	175-367
Porosity - $\boldsymbol{\phi}$ (%)	68±2	65±3	63±3

The compressive modulus of the rubber sealant was 1226 ± 154 kPa and, therefore, with any value higher than 5% pre-strain of the sealer, leakproof condition for permeability measurement could be insured. Typical measurement times varied between 2 to 60 minutes (after reaching steady state condition) depending on the scaffold pore size and the applied compression. Performed permeability measurements revealed significant decrease in the permeability as the pore size of the scaffolds was reduced (Figure 2-a), and the trend for this reduction was exponential (Figure 2-b). Moreover, dramatic permeability drop under compressive strain was

observed for scaffolds presenting smaller pore sizes. In fact, for scaffolds with coarse pore sizes (d=271 µm), we observed almost a linear trend for the permeability decrease under compressive strains up to 20%. On the contrary, for scaffolds with the fine pore size (d=162 µm), this trend was nonlinear and decreasing exponentially (Figure 2-c).

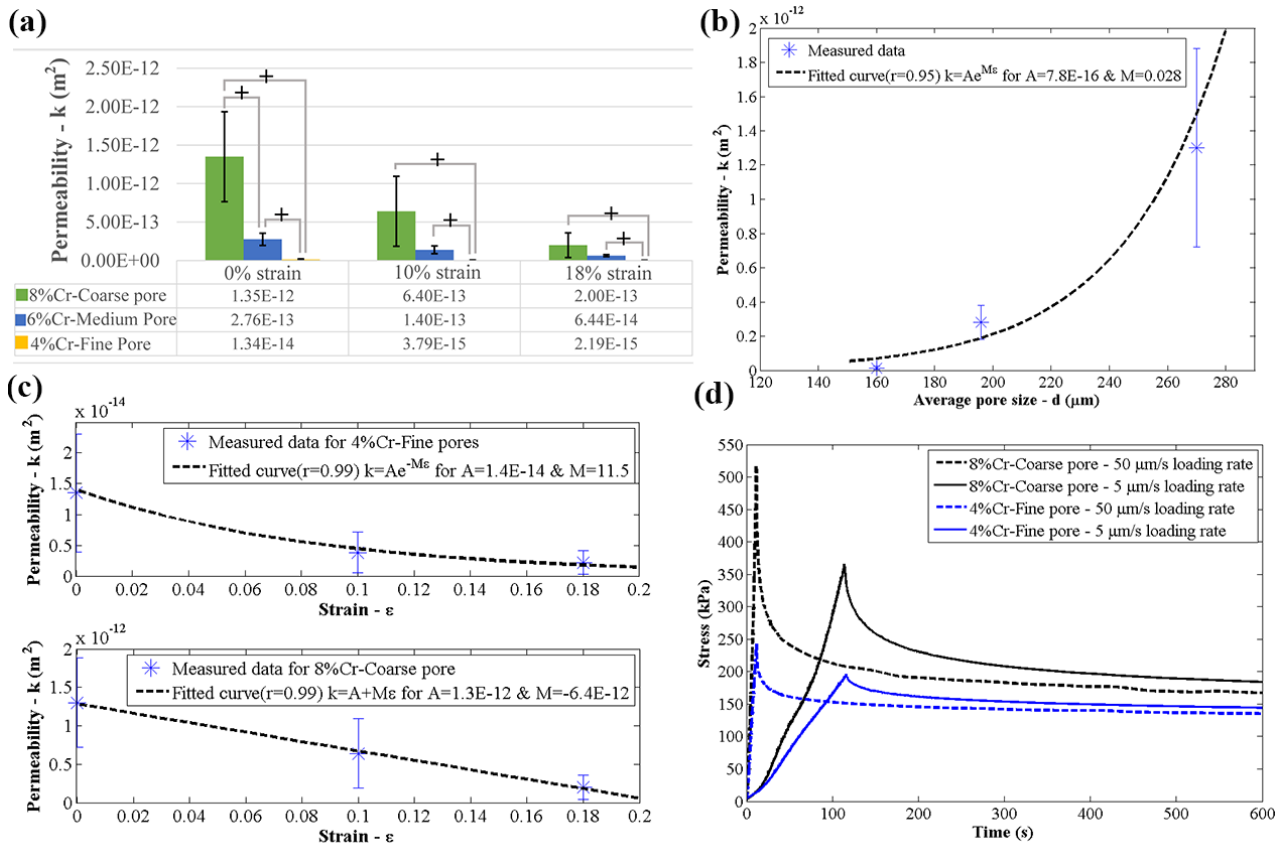

Figure 2. Results of permeability and rate dependent stress relaxation measurements for viscoelastic scaffolds under compressive strain. (a) Comparison of permeability for different groups of scaffolds; plus (+) symbol shows significant difference ($p<0.05$) using Student t-test (n=4-6). (b) Trend of permeability with average pore size of the scaffolds in 0% strain condition. (c) Strain dependent permeability trend for fine and coarse pore size scaffolds up to 20% strain. (d) Representative stress relaxation curves of 20% strain for fine and coarse pore size scaffolds at 5 and 50 µm/s loading rates.

2-5 Discussion

A fairly simple indeed reliable experimental method for permeability measurement of the scaffolds under compressive strain was presented. Our measurements revealed that the permeability is an exponential function of the average pore size of the scaffolds in strain free condition. Additionally, we observed that the decreasing trend of permeability under compressive strain is quite different depending on pore sizes of the scaffolds. The scaffolds having fine pore size (d=162 µm) showed an exponential drop in permeability under compression similar to established cartilage model [6, 9]; coarse pore size scaffolds (d=271

μm), however, indicated almost linear strain dependent permeability reduction. The permeability also appeared to play a role in relaxation behavior of the scaffolds. The release of compression-induced fluid pressure during decaying phase was easier in coarse pore size scaffolds with higher permeability resulting in faster initial decay rate and shorter relaxation time compared to fine pores scaffolds. It is worth mentioning that the complex interaction of entangled chains of polymer network is also reported to be an important mechanism for stress relaxation in covalently crosslinked structures [17, 18].

In the present work, we assumed isotropic material properties for our scaffolds since pores are randomly distributed and oriented within the entire volume (Figure S1). Our permeability measurement for coarse pore size scaffolds in strain free condition is comparable with reported values by Spain *et al* [19] ($1.81\pm3.6\times10^{-12}$ m^2) which used synthetic scaffolds with similar characteristics such as porosity range (ranged from 51 to 70%) as our scaffolds. On the other hand, the reported values of permeability in O'Brien *et al* [11] study, for scaffolds in the range of our fine pore size scaffolds, are higher than our measurements. This is not surprising since the porosity of the scaffolds in their study (ϕ>95%) is much higher than our scaffolds (ϕ <70%). It is worth mentioning, according to the semi-empirical Kozeny-Carmen equation [10, 20], the permeability is a function of the porosity of the porous media.

We proposed the stepwise spacer to eliminate disassembly and reassembly of the rig for measurements of the permeability under different compressive strains. In the proposed set-up of O'Brien *et al* [11], by reinstalling the rig for each measurement, the same experimental condition between different compression values may not be conserved and, therefore, the obtained results could reflect large variations. In the present set-up, the sealant geometry was designed to have large enough thickness for providing required sealing force after rig assembly. This strategy prevents pressure loss in the chamber during measurement. In addition, its smaller internal radius leads to integration of the sealant and scaffold due to the elastic behavior of the sealant which blocks fluid to pass around the sample (radial sealing by interface pressure due to press fitting). The previously proposed systems (compressing sample edges by sealant axially) for sealing by others such as Sell *et al* [21] and O'Brien *et al* [11] are appropriate for soft samples but would damage the structure of stiffer scaffolds under large compressive strain (e.g., 40%). Likewise, glue solution for sealing is not usually practical for hydrated samples. In addition, it is difficult to maintain the amount of glue to prevent water leakage across the edges of the sample while not blocking effective pores of the sample. It is worth mentioning that the measurement of permeability in other fields such as soil mechanics, composites and textiles has

an impressive literature (e.g., see [22]) which could be instructive for development of new systems for biomaterials characterization.

The main limitation of the present set-up is that with provided 20 kPa pressure head, it is difficult to measure the permeability of scaffolds with values less than order of 10^{-16}-m^2 due to very slow flow rate and long required time for passing a detectable amount of water without evaporation. Indeed increasing pressure head is possible, however, in high pressure measurements we should take into account the effect of fluid induced strain inside the scaffold [8, 9].

Characterization of strain dependent permeability of tissue engineering scaffolds is critical in load-bearing applications due to its considerable effect on solutes transport, oxygen tension, fluid pressure and velocity fields as well as scaffolds viscoelastic behavior. All of these biophysical factors may influence cellular differentiation and therefore neo-tissue formation. In our experiments, we identified remarkable differences in permeability trend between scaffolds presenting different averages in pore size. This observation suggests that relying on expressions for permeability as a function of compressive strain such as exponential function proposed for cartilage may not be good enough predictive for all types of tissue engineering scaffolds. Direct experimental characterization should be preferred.

Supporting Information

Corresponding supplementary data can be found at the end of this chapter.

2-6 Acknowledgments

This work was supported by the Swiss National Science Foundation (#310030_149969 / 1).

2-7 References

[1] Li S, de Wijn JR, Li J, Layrolle P, de Groot K. Macroporous biphasic calcium phosphate scaffold with high permeability/porosity ratio. Tissue Eng 2003;9:535-48.

[2] Mow VC, Kuei S, Lai WM, Armstrong CG. Biphasic creep and stress relaxation of articular cartilage in compression: theory and experiments. J Biomech Eng 1980;102:73-84.

[3] Nasrollahzadeh N, Pioletti DP. Development of dissipative scaffolds with different mechanisms of dissipation. In the procceeding of 10th International Conference on the Mechanics of Time Dependent Materials, . Paris-France2016.

[4] Abdel-Sayed P, Darwiche SE, Kettenberger U, Pioletti DP. The role of energy dissipation of polymeric scaffolds in the mechanobiological modulation of chondrogenic expression. Biomaterials 2014;35:1890-7.

[5] Chaudhuri O, Gu L, Klumpers D, Darnell M, Bencherif SA, Weaver JC, et al. Hydrogels with tunable stress relaxation regulate stem cell fate and activity. Nat Mater 2016;15:326-34.

[6] Lai W, Mow V. Drag-induced compression of articular cartilage during a permeation experiment. Biorheology 1979;17:111-23.

[7] Lai W, Mow VC, Roth V. Effects of nonlinear strain-dependent permeability and rate of compression on the stress behavior of articular cartilage. J Biomech Eng 1981;103:61-6.

[8] Holmes MH. A theoretical analysis for determining the nonlinear hydraulic permeability of a soft tissue from a permeation experiment. Bull Math Biol 1985;47:669-83.

[9] Holmes M, Mow V. The nonlinear characteristics of soft gels and hydrated connective tissues in ultrafiltration. J Biomech 1990;23:1145-56.

[10] Pennella F, Cerino G, Massai D, Gallo D, Labate GFDU, Schiavi A, et al. A survey of methods for the evaluation of tissue engineering scaffold permeability. Ann Biomed Eng 2013;41:2027-41.

[11] O'Brien FJ, Harley BA, Waller MA, Yannas IV, Gibson LJ, Prendergast PJ. The effect of pore size on permeability and cell attachment in collagen scaffolds for tissue engineering. Technol Health Care 2007;15:3-17.

[12] Ng KW, Torzilli PA, Warren RF, Maher SA. Characterization of a macroporous polyvinyl alcohol scaffold for the repair of focal articular cartilage defects. Journal of tissue engineering and regenerative medicine 2014;8:164-8.

[13] Ateshian G, Warden W, Kim J, Grelsamer R, Mow V. Finite deformation biphasic material properties of bovine articular cartilage from confined compression experiments. J Biomech 1997;30:1157-64.

[14] Scholten PM, Ng KW, Joh K, Serino LP, Warren RF, Torzilli PA, et al. A semi-degradable composite scaffold for articular cartilage defects. Journal of Biomedical Materials Research Part A 2011;97:8-15.

[15] Offeddu G, Ashworth J, Cameron R, Oyen M. Structural determinants of hydration, mechanics and fluid flow in freeze-dried collagen scaffolds. Acta Biomater 2016.

[16] Darcy H, Darcy H, Darcy H. Les fontaines publiques de la ville de Dijon1856.

[17] Mitchell J. The rheology of gels. Journal of Texture Studies 1980;11:315-37.

[18] Kapnistos M, Lang M, Vlassopoulos D, Pyckhout-Hintzen W, Richter D, Cho D, et al. Unexpected power-law stress relaxation of entangled ring polymers. Nat Mater 2008;7:997-1002.

[19] Spain T, Agrawal C, Athanasiou K. New technique to extend the useful life of a biodegradable cartilage implant. Tissue Eng 1998;4:343-52.

[20] Carman PC. Flow of gases through porous media: Academic press; 1956.

[21] Sell S, Barnes C, Simpson D, Bowlin G. Scaffold permeability as a means to determine fiber diameter and pore size of electrospun fibrinogen. Journal of Biomedical Materials Research Part A 2008;85:115-26.

[22] Arbter R, Beraud J, Binetruy C, Bizet L, Bréard J, Comas-Cardona S, et al. Experimental determination of the permeability of textiles: A benchmark exercise. Composites Part A: Applied Science and Manufacturing 2011;42:1157-68.

Supplemental data for Chapter 2

Morphological characterization of scaffolds in hydrated state

Dried state μCT scan of tissue engineering scaffolds is a more straightforward method for morphological characterization provided that we could verify the minimal structural differences between hydrated and dried scaffolds. Normal drying of the hydrated scaffolds either at room temperature or inside an oven may cause significant shrinkage of the scaffolds. By optimal freeze-drying procedure, however, we can keep this change as minimal as possible. For this purpose, the hydrated scaffold was put inside a 2 ml Eppendorf tube and carefully frozen in liquid nitrogen while avoiding direct contact of scaffold and nitrogen. Then the frozen samples were vacuumed dried for 72 hours and scanned afterwards (Figure S1) for morphological characterization in dried state. The measurement parameters were set as 40 kV for voltage, 100 mA for current, 18 mm for spatial resolution, 400 mS for exposure time and 0.42° for rotation steps without using any filter.

By measuring the bulk geometry of the scaffolds in hydrated as well as in dried states, we could estimate the pores volumetric expansion (PVE). We then estimated the corresponding average pore size change as cubic root of PVE ($\sqrt[3]{PVE}$). The calculation showed that PVE is always less than 1.2 for our freeze dried scaffolds, leading to pore size change of 1.06 as reported in Table 1. This estimation method has recently been reported for collagen based scaffolds elsewhere in which they also confirmed it by direct μCT measurements in hydrated state [1].

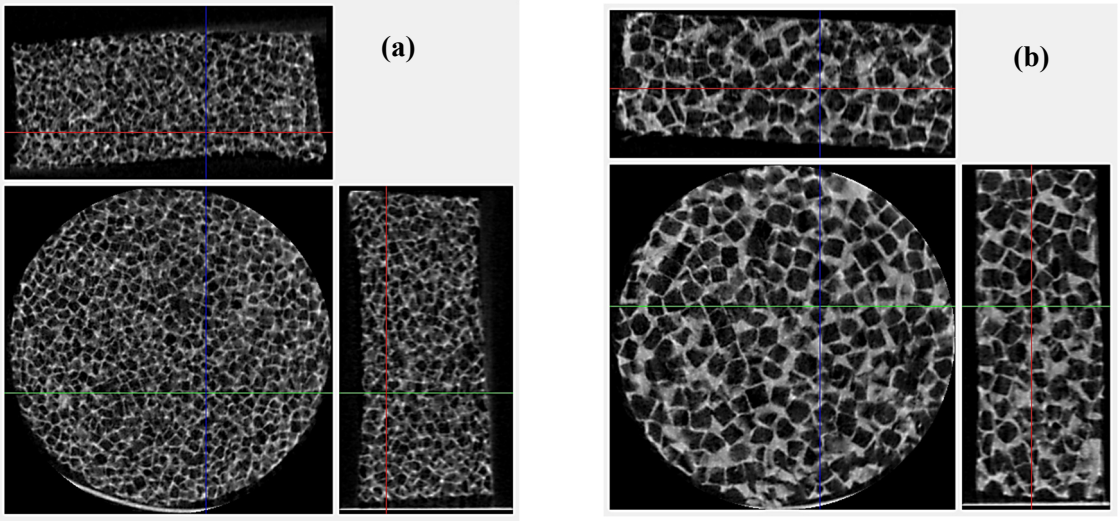

Figure S1. Micro-CT scans of freeze-dried scaffolds from different views (Disks diameter ~ 7 mm). (a) 4%Cr-Fine pores. (b) 8%Cr-Coarse pores.

Table S1. Pore size change estimation using bulk geometry of the scaffold in hydrated and freeze-dried states.

Scaffold type	4%Cr-Fine	6%Cr-Medium	8%Cr-Coarse
Pores volumetric expansion [PVE] - (m^3)	1.16±0.03	1.15±0.02	1.18±0.02
Expansion ratio [$\sqrt[3]{PVE}$] - (m)	R=1.05	R=1.045	R=1.06
Average pore size of the dried scaffold - (μm)	155	188	255
Estimated Avg. pore size of hydrated scaffolds - (μm)	162	196	271

To further evaluate this problematic issue, we also performed an Environmental Scanning Electron Microscopy (ESEM) assessment for hydrated samples as illustrated in Figure S2 using Philips XL30 ESEM-FEG. The pressure and temperature in environmental chamber of the ESEM were adjusted to reduce humidity of the sample. The geometry of representative pores was measured by imageJ software and compared in different humidity conditions. There was no significant difference when we reduced the humidity from 100% to 20%. It was not possible to conduct the test in less humid condition anymore, since the sample was moved (due to reducing pressure inside the chamber to dry the sample) and we could not track the target pores for comparison of the geometry. These results confirm the minimal morphological differences of hydrated and freeze-dried scaffolds.

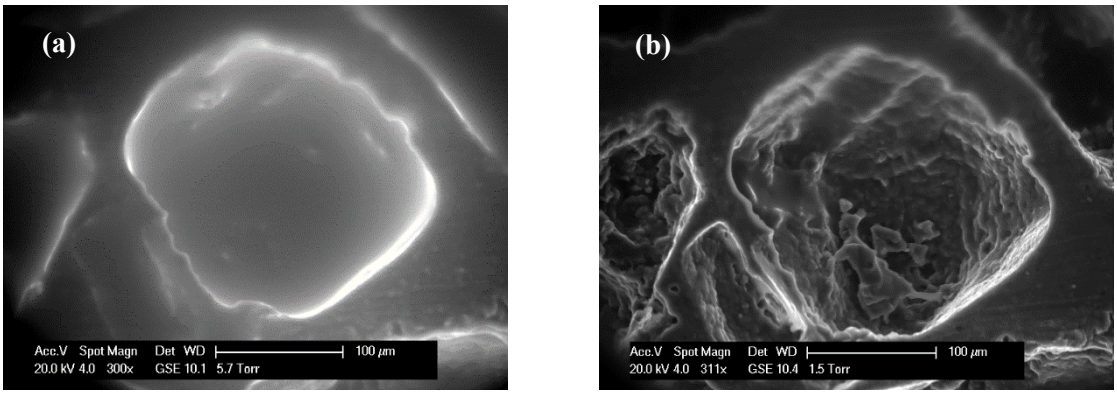

Figure S2. ESEM of a macroporous scaffold at different humidity conditions. (a) 100% humidity. (b) 20% humidity.

Rate dependent stress relaxation

Unconfined stress relaxation tests were performed on hydrated scaffolds at either 5 μm/s or 50 μm/s speed of plunger for 20% compressive strain with E3000 Instron testing machine. Modified Maxwellian model as Eq. S1 was used [2] to analyze the relaxation behavior of fine and coarse pore size scaffolds.

$$\sigma(t) = \sigma_e + \sum_{i=1}^{3} \sigma_i e^{-t/\tau_i} \qquad \text{(S1)}$$

where, σ_e is the equilibrium stress after infinite time and $\sigma_i e^{-t/\tau_i}$ represents transient decaying stress with time. We utilized Matlab curve fitting tool to estimate parameters of the model that best predicted measured data. The initial decay rate of stress ratio [2] can be calculated as:

$$\frac{1}{\sigma_{peak}}\frac{d\sigma(t)}{dt}|_{t=0} = \sum_{i=1}^{3} -\frac{\sigma_i}{\sigma_{peak}\tau_i} \quad \text{(S2)}$$

In addition we determined the time ($t_{r90\%}$) required for the sample to relax 90% of transient stress ($\sigma_{r90\%}$) as defined by eq. (S3):

$$\sigma_{r90\%} = \sigma_{peak} - 0.9(\frac{\sigma_{peak} - \sigma_e}{\sigma_{peak}}) \quad \text{(S3)}$$

The obtained results from the stress relaxation tests, demonstrated completely different viscoelastic behavior between 4%Cr with fine pore sizes and 8%Cr scaffolds having coarse pore sizes at two rates of compression. The σ_{peak} was significantly higher for 50 µm/s loading rate than 5 µm/s in corresponding groups. Scaffolds with 4%Cr and fine pore size indicated smaller σ_{peak} than 8%Cr scaffolds with coarse pore size. The initial decay rate of stress ratio and relaxation times ($t_{r90\%}$) were significantly different between fine and coarse pore size scaffolds at two rates of compression. Results of stress relaxation experiments revealed a longer $t_{r90\%}$ for scaffolds with 4%Cr and fine pore sizes than 8%Cr scaffolds having coarse pore size either at 50 µm/s or 5 µm/s compression rates. Accordingly, the higher initial decay rate was not surprising for 8%Cr scaffolds with coarse pore size compared to lower initial decay rate of scaffolds with 4%Cr having fine pores. Specifically, faster loading rate resulted in higher initial decay rate as well as shorter time for transient stress relaxation.

Generally, a variety of factors such as base material composition, crosslinking type, porosity and pore size of the polymeric scaffolds are contributing to the viscoelastic behavior. The concentration of crosslinker was the dominant contributing factor to σ_{peak} or generally stiffness of the developed scaffolds while the role of average pore size and permeability were less significant. In fact, increasing crosslinking density leads to a stronger polymer network with higher stiffness. It is worth mentioning that, in the same material composition, σ_{peak} would be higher in scaffolds having lower permeability due to greater fluid pressurization inside pores. On the other hand, both average pore size and crosslinking density appear to play a role in relaxation behavior of the scaffolds. The release of compression-induced fluid pressure during decaying phase is easier in coarse pore size scaffolds with higher permeability resulting

in faster decay rate and shorter relaxation time. In addition, the complex interaction of entangled chains of polymer network is reported to be an important mechanism for stress relaxation in covalently crosslinked structures [3, 4].

Table S2. Results of rate dependent stress relaxation experiments.

Test Config.	Peak stress (σ_{peak}) - kPa	relaxation time ($t_{r90\%}$) - s	Initial relaxation decay rate ($\dot{r}_0$) - kPa/s
8%Cr-Coarse pore at 5 µm/s	382±42	341±45.5	-0.038±0.004
8%Cr-Coarse pore at 50 µm/s	521±54	140±5	-0.250±0.014
4%Cr-Fine pore at 5 µm/s	200±5	581.5±76	-0.016±0.003
4%Cr-Fine pore at 50 µm/s	249.5±12	232±58	-0.169±0.040
Statistical analysis	* + ^ #	* + ^ #	* + ^ #

*: t-test comparison between 8%Cr-Coarse pores and 4%Cr-Fine pores at 5 µm/s.
+: t-test comparison between 8%Cr-Coarse pores and 4%Cr-Fine pores at 50 µm/s.
^: Paired t-test comparison between 5 µm/s and 50 µm/s loading rate for 8%Cr-Coarse pores scaffolds.
#: Paired t-test comparison between 5 µm/s and 50 µm/s loading rate for 4%Cr-Fine pores scaffolds.

Supplemental Reference:

[1] Offeddu G, Ashworth J, Cameron R, Oyen M. Structural determinants of hydration, mechanics and fluid flow in freeze-dried collagen scaffolds. Acta Biomater 2016.

[2] Tang J, Tung MA, Zeng Y. Characterization of gellan gels using stress relaxation. J Food Eng 1998;38:279-95.

[3] Mitchell J. The rheology of gels. Journal of Texture Studies 1980;11:315-37.

[4] Kapnistos M, Lang M, Vlassopoulos D, Pyckhout-Hintzen W, Richter D, Cho D, et al. Unexpected power-law stress relaxation of entangled ring polymers. Nat Mater 2008;7:997-1002.

Chapter 3: Development of an Effective Cell Seeding Technique: Simulation, Implementation and Analysis of Contributing Factors[†]

3-1 Abstract

Cell seeding in a biomaterial is an important process for tissue engineering applications. It helps to modulate tissue formation or to control initial conditions for mechanobiological studies. The compression release-induced suction (CRIS) seeding technique leads to active infiltration of the cell suspension toward the central region of the scaffold. Its effectiveness, however, may significantly vary depending on several controlling factors such as the rate of loading and unloading or scaffold architecture. We utilized a 2D axisymmetric finite element model to numerically evaluate the influence of a seeding loading regime on suction pressure and infiltration velocity of the cell suspension. The *in vitro* application of optimized CRIS seeding obtained from simulation showed significant effectiveness over a static seeding method. As simulation results predicted, the permeability of the scaffold directly influenced CRIS seeding effectiveness *in vitro*. By supplementing an optimized CRIS loading regime with slow rotation after seeding treatment, cell distribution through thickness was improved especially for scaffolds showing low permeability. Finally, we systematically analyzed the relative importance of permeability, thickness or coating on cell seeding efficiency and uniformity using a full factorial design of experiments. We observed that permeability has a higher impact on the CRIS seeding than scaffold coating and thickness.

Keywords: Cell seeding, active infiltration, scaffold, permeability, coating, after seeding treatment.

[†] This Chapter has been published in Tissue Engineering Part C: Methods (Volume 23, Number 8, 2017)

3-2 Introduction

Cell seeding in a biomaterial is an important process for tissue engineering (TE) applications that can help to control and modulate tissue formation [1]. Intuitively, seeding of cells within a 3D biomaterial may seem to be straightforward due to the available void volume inside a highly porous and permeable scaffold. However, this is not the case for a thick scaffold presenting low permeability, being tortuous and having hydrophobic properties [2-4]. An efficient and uniform distribution of cells is essential to obtain a normalized initial condition either for *in vitro* experiments such as mechanobiological studies or for clinical applications. A homogeneous artificial tissue should be formed initially since there is no chance to modify cell distribution and density following an ineffective cell seeding [3].

Several static or dynamic methods have been developed for cell seeding. For the static method, the most used technique is based on surface pipetting and depends mainly on gravity for infiltration of cells inside tortuous pores of the scaffold [5]. For the dynamic seeding method, an external force is applied to facilitate the cell penetration toward the center of the scaffold [6]. Flow perfusion [2, 7], centrifugation [8, 9], orbital shaking [6, 10] and the spinner flask [2, 10] are the most utilized techniques in dynamic cell seeding methods. These studies have shown that active motions of solution containing cells can improve cells distribution inside the scaffold in comparison to static methods.

Among different dynamic seeding methods, the compression release-induced suction (CRIS) has been reported as a promising approach for cartilage TE [11]. Since most of the bioreactors in cartilage biotechnology are based on compression loading regime [12], the CRIS could be easily adapted from existing setups. By applying a compression followed by an unloading to a porous scaffold, the solution around the scaffold containing cells is infiltrated toward the central region of the scaffold. However, even for this mechanism of induced driving force, the seeding outcome may significantly vary depending on parameters such as the rate of loading and unloading, the scaffold's permeability, or the cell-scaffold interface. In a systematic approach, the cell seeding efficiency and uniformity should be evaluated for the contributing factors in their pertinent range. This can be accomplished by determining the role of scaffold related characteristics on seeding process while controlling cell infiltration force dynamics.

In this study, we first simulated CRIS by a 2D axisymmetric poroelastic finite element model. A what-if analysis was performed to find best parameters of the CRIS seeding loading regime

to induce optimum medium infiltration. Cell seeding was then experimentally implemented according to the best loading regimes obtained from numerical calculations. To enhance cell distribution in the scaffold, we further evaluated the effect of an after seeding treatment during re-swelling time. Finally, to obtain a more profound insight on the proposed seeding process, the relative contribution of the scaffold's permeability, thickness and coating were evaluated using a full factorial design of experiments.

3-3 Materials and Methods

3-3-1 Scaffold fabrication and preparation

Macroporous scaffolds of poly 2-hydroxyethyl methacrylate (pHEMA) crosslinked with ethylene glycol dimethacrylate (EGDMA) were prepared by a salt leaching method as described elsewhere [13, 14]. Briefly, we utilized fixed 35/65% polymer to salt volumetric ratio with 4% and 8% crosslinking density (Cr) for fine (200-250 μm) and coarse (355-500 μm) salt particles, respectively. The hydrated scaffolds were sized with an 8 mm diameter punch and a custom made cutting tool covering 1.7 to 3.1 mm thickness ranges. The scaffolds were imaged by scanning electron microscopy (SEM) before and after CRIS loading regime. For this purpose, the hydrated scaffolds before and after optimized CRIS loading (3 per group) were frozen in liquid nitrogen and the frozen samples were vacuum-dried for 72 hrs. The samples were then coated with a layer of 30 nm gold and imaged using a XLF30-FEG instrument (FEI, Hillsboro, Oregon, USA).

The characterization process of the scaffolds are reported in detail elsewhere [14], and we used the corresponding values for our model development. Briefly, we measured the equilibrium Elastic modulus (Eeq) of hydrated scaffolds while applying sequential compressive strain, followed by stress relaxation after each step, using the Instron uniaxial testing machine (Instron E3000, Norwood, Massachusetts, USA) [15]. For the Poisson ratio (υ), an evaluation with a digital camera was performed to capture the radial deformation and the pictures were processed by ImageJ (NIH, Bethesda, Maryland, USA). A novel custom made set-up was designed with step-wise spacer for strain dependent permeability characterization of the scaffold based on Darcy's law. The porosity was directly calculated by measuring the volume and mass of the hydrated scaffold as well as its dried state mass.

Before the seeding process, sterilization was carried out by autoclaving 200 ml bottles of phosphate-buffered saline (PBS) containing the scaffolds. Human plasma fibronectin (HPFN)

(Sigma Aldrich, St. Louis, Missouri, USA) was used for coating the scaffolds to evaluate the cell-scaffold interface effect on seeding efficiency and uniformity. Scaffolds were coated in a 48 well plate containing 2.2 µl/mm^3 of coating solution (25 µg/ml) while mildly agitating (10 Hz) for 1 hour after 3 manual compressions. Thereafter, they were incubated at 4^{o}C overnight and washed 3 times with PBS before using in seeding experiments. Successful adsorption of HPFN to the pHEMA scaffolds was previously confirmed by immunohistochemistry as shown elsewhere [13].

3-3-2 Simulation of compression release-induced suction seeding

In order to numerically calculate time dependent induced pressure gradient and medium infiltration due to compression/decompression of the scaffold, we developed a poroelastic finite element (FE) model based on Biot's theory [16] using COMSOL Multiphysics software (Burlington, MA, USA). After the mesh convergence study, a what-if analysis was performed on parameters of seeding loading regime in different case studies to understand the influence of loading/unloading rates, delay time and compressive strain on the induced suction pressure and velocity fields inside the scaffold.

In the model, the 2D axisymmetric cross section of cylindrical scaffold having 3 mm thickness and 4 mm radius was divided to finite elements as illustrated in Figure 1-a. We assumed isotropic mechanical behavior for the two types of scaffold. Corresponding measured values given in Table 1 were utilized for each scaffold model, while considering Biot–Willis Coefficient of 1 for both scaffolds. The strain dependent permeability (k_ε) of the scaffold was implemented in the model using a curve-fitted expression to the measured data up to 35% strain. Additionally, the porosity (ϕ) was also assumed to be strain dependent as $\phi_\varepsilon = 1 - \frac{1-\phi_0}{\lambda}$, in which ϕ_0 is the initial porosity and $\lambda = 1 - \varepsilon$ represents the stretch ratio [17].

To simulate the seeding working mechanism, a prescribed displacement according to the loading regime scheme (Figure 1-b) was applied on the top boundary of the model. The loading regime expressed by a combination of two smoothed falling and rising ramp functions having parametric starting points and ramp rates. A zero pressure ($p_f = 0$) boundary condition was assigned on the outer edge (r = 4 mm) of the axisymmetric model during the time of the simulation to allow exchange of the fluid phase. A time dependent boundary condition for the pressure of the top part (z = 3 mm) was assigned by using a smoothed step function to reflect the effect of plunger separation at the end of the unloading step allowing fluid infiltration from

the top boundary. The frictionless impermeable roller boundary condition was applied for the bottom boundary (z = 0) of the model.

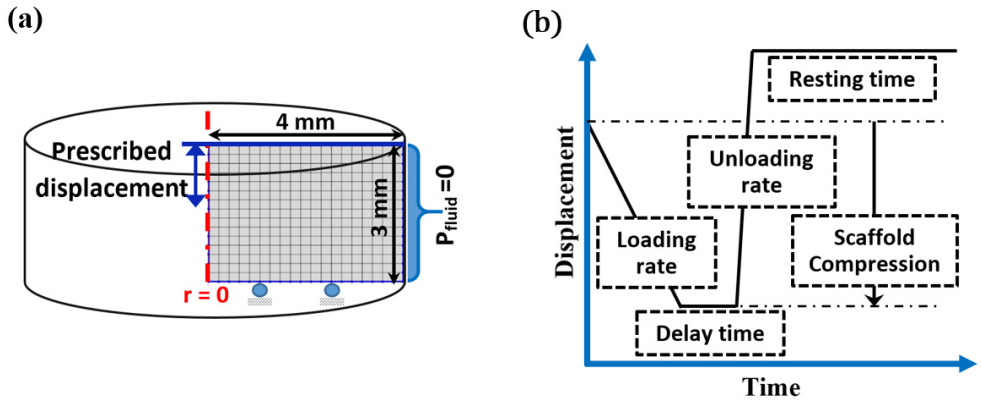

Figure 1. Modeling of CRIS loading regime. (a) 2D axisymmetric geometry of the cylindrical scaffold. (b) Scheme of prescribed displacement for CRIS loading regime.

Table 1. Measured material properties of the scaffolds used in the FE model (mean ± standard deviation).

Scaffold type	Eeq (Mpa)	ν	ϕ (%)	k_0 (m^2)	k_ε
4% Cr - Fine P.	0.76 ±0.06	0.25±0.2	68 ±2	1.34E-14 ±9.59E-15	$k_0 e^{-11.5\varepsilon}$
8% Cr - Coarse P.	1.2 ±0.15	0.23±0.4	63 ±3	1.35E-12 ±5.84E-13	$k_0 + 8.0E^{-12}\varepsilon + 1.2E^{-11}\varepsilon^2$

Cr: crosslinking density. P.: Pores

3-3-3 Cell culture

Human epiphyseal chondro-progenitors cells were prepared as described elsewhere [18] and distributed in standard polystyrene tissue culture flasks (75 cm^2) for monolayer expansion. Cell Culture Medium (CCM) was made from Dulbecco's Modified Eagle Medium with L-Glutamine, 4,5 g/l D-Glucose and Sodium pyruvate, (Life Technologies, Paisley, UK) supplemented with 10% fetal bovine serum (Sigma, St. Louis, MO, USA) and 1% L-Glutamine (Life Technologies, Paisley, UK). Culture flasks containing cells were incubated in standard conditions (at 37 °C with 5% CO_2) and the CCM was changed twice a week in monolayer culture period. Following 90% confluence, cells were trypsinized for passage (up to passage 7) or usage in seeding experiments.

3-3-4 Cell seeding implementation and after seeding treatment

In vitro CRIS cell seeding was performed using a custom-made set-up compatible with a uniaxial testing machine (Instron E3000) as shown in Figure 2-a. The scaffolds were placed in cylinders of 11 mm diameter and 10 mm height. Then 2.6 µl/mm^3 of cell suspension (5×10^6 cells/ml) were pipetted onto the scaffolds inside the cylinders. Each cylinder was covered with

a cap equipped with a piston to ensure sterile conditions under the loading machine (Figure 2-b). The scaffolds were subjected to predefined seeding loading regime obtained from the simulation and lasting for 5 cycles. Control static seeding was also conducted by means of surface pipetting on preconditioned scaffolds (after 24 hours recovery).

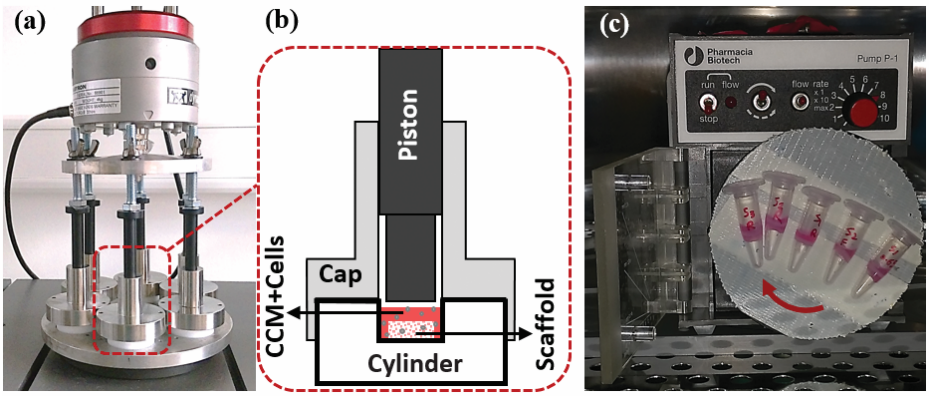

Figure 2. Cell seeding method. (a) Compression release-induced suction cell seeding implementation using a custom-made setup. (b) Schematic of a seeding chamber in detail. (c) Slow rotation after seeding treatment.

We supplemented CRIS technique by a dynamic after seeding treatment (AST) and compared it with a static condition. Following CRIS seeding, we used a dynamic slow rotation AST [19] by employing the rotating plate of a peristaltic pump (Pump P-1, Pharmacia Biotech Inc., NJ, USA). For this purpose, seeded scaffolds were located in the middle of the 1.5 ml Eppendorf tubes and remaining cells suspension in the seeding cylinder was pipetted on the top surface of the scaffold inside the Eppendorf tube. Next, the Eppendorf tubes were rotated (10 rpm) inside a standard incubator (Figure 2-c) for 2 periods, each lasting one hour. Between two periods of rotation, suspended scaffolds inside Eppendorf tubes were inverted. After this step, cell inoculated scaffolds were transferred to 48 well plates without CCM and incubated for 45 minutes to ensure cell attachment. Then, 1 ml fresh CCM was added to each well and seeded scaffolds were evaluated after overnight incubation.

3-3-5 Experimental design to identify contributing factors to cell seeding

In order to evaluate the relative importance of scaffold permeability, coating and thickness in cell seeding efficiency and distribution, a systematic experimental design was carried out. The range of studied factors was selected in such a way to cover an anticipated application for functional tissue engineering. We performed a full factorial design (FFD) with 8 experiments (each triplicate) for this analysis as described in detail elsewhere [20]. Briefly, the linear model with interaction according to Eq. 1 was chosen to fit the experimental observations.

$$\vec{y} = a_0 + \sum_{i=1}^{n} a_i x_i + \sum_{i \neq j}^{n} a_{ij} x_{ij} + \sum_{i \neq j \neq k}^{n} a_{ijk} x_{ijk} + \vec{e} \qquad (1)$$

where $\vec{y}$ is the vector of experimental response in different configurations, $\vec{e}$ is the error between observations and model predictions, x_i is an examined factor, a_0 is a constant effect (grand mean), a_i are the main half effects corresponding to factors x_i, a_{ij} are the first order interaction half effects corresponding to factors x_i and x_j and so on. Using the least square technique, the main effects and interactions are estimated in such a way that the error between the model prediction and the experimental value is minimized. The percentage of the a_i/a_0 and a_{ij}/a_0 are calculated afterwards presenting the relative role of the main half effects and interactions.

3-3-6 Cell seeding assessment

We measured cell seeding efficiency (CSE) and distribution metric (DM) to evaluate the seeding technique. The CSE is defined as the percentage of cells attached to the scaffold versus the initial number of cells used for the seeding[2, 11]. The attached number of cells was determined by counting the number of remaining cells from the medium outside the scaffold and subtracting that value to the initial cell number used for seeding. To determine the DM, seeded scaffolds were cut in half; one half was used for the quantitative and one for the qualitative distribution measurements (Figure 3). For the quantitative cell distribution evaluation, 3D CellTiter Glo assay (Promega Corporation, Madison, USA) was used according to manufacturer's instructions. Briefly, a 5 mm punch was used to separate the core from the periphery and assay results in each section were recorded using a Wallac 1420 VICTOR 2 multi-label plate reader (Wallac Oy, Turku, Finland). The relative distribution of cells in the central to the periphery sections was defined as the ratio of normalized values by weight of sections for each scaffold (Maximum value 1).

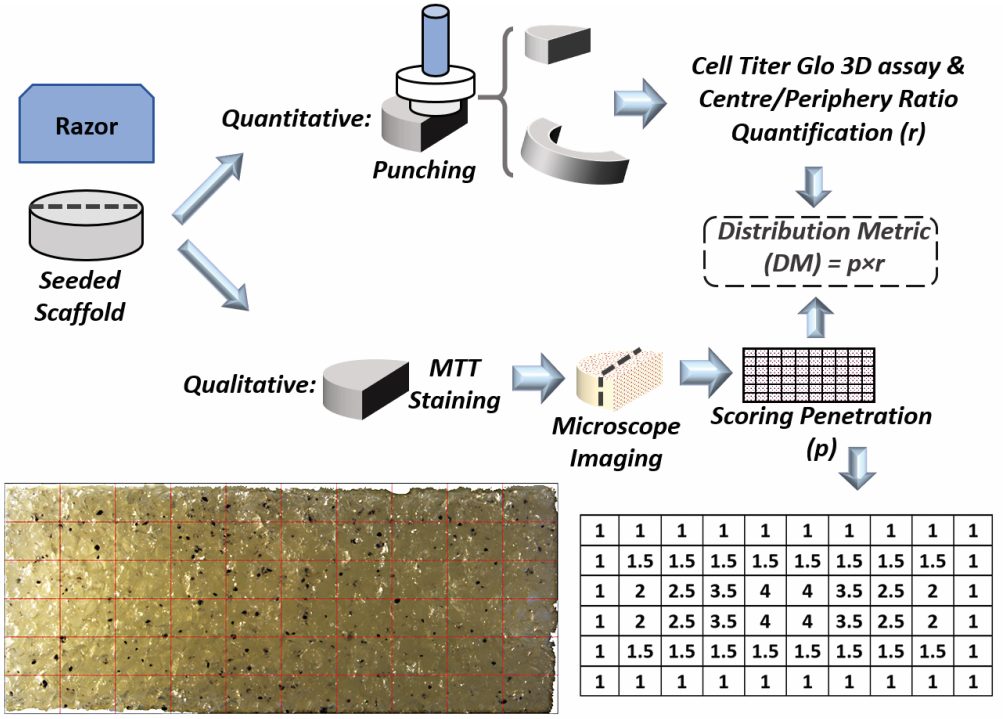

Figure 3. Schematic procedure of distribution metric (DM) evaluation.

For the qualitative cell distribution evaluation, the second half of the seeded scaffold was labelled with MTT cell proliferation reagent (Roche Corporation, Indianapolis, USA) to observe the cell distribution visually. After staining according to the manufacturer's instructions, three images were captured from each scaffold from top surface, bottom surface and perpendicular cross section of the scaffold using a Stereomicroscope (LEICA MZ 16 1FA). The cross section image was manually image processed using ImageJ (NIH, Bethesda, Maryland, USA) software for cells penetration. For this purpose, the cross section of the scaffold was gridded to 10 x 6 partitions with predefined scores as depicted in Fig. 3. The penetration score was calculated over the whole grid for each seeded scaffold and divided by 100, which provides the score of an ideal case. The qualitative penetration score was then multiplied by the obtained value for the 3D CellTiter Glo assay as the weighting coefficient to result in the distribution metric (DM).

We also performed live/dead staining of cell-seeded scaffolds with R37601 sensitive two-color fluorescence cell imaging kit (Molecular Probes, USA) to assess cell viability. For this purpose, after staining the samples with mixed live and dead dyes (as provided in the kit diluted 2x with PBS) for 20 min at 25°C, the samples were washed three times with PBS. Thereafter, green (live) and red (dead) florescence images were taken at wavelengths adjusted

for fluorophores of interest by confocal microscopy (LEICA TCS SP8) with a 20x objective and analyzed with ImageJ.

3-3-7 Statistical analysis

Student t-test was used to compare DM values between static seeding and optimized CRIS seeding followed either by static or dynamic after seeding treatments (n=3). Significant factors for DM and CSE values in FFD were identified by a half normal probability plot to distinguish standing out effects which cannot be due to experimental variation [21]. Moreover, analysis of variance (ANOVA, F-test) was performed with P-value of 0.05 to determine significant half-effects and interactions.

3-4 Results

3-4-1 Scaffold morphology before and after CRIS loading

SEM was employed to compare the scaffold morphology before and after CRIS loading regime. As illustrated in Figure 4, there is no significant difference in pore size and pores orientation for the two types of scaffolds before (left column images) and after CRIS loading (right column images). The pore size distributions were between 120-240 μm for 4%Cr density and fine pore scaffolds and 220-400 μm for 8%Cr density and coarse pore scaffolds. Yet, in higher magnification images, we could observe a few more micro-fissures inside the pores after loading that can slightly increase pores fenestration of scaffolds. Since the applied strain is below plastic deformation limit, the scaffolds exhibit shape recovery after unloading. However, even if we could not see significant morphological changes, the macromolecular network of the polymeric scaffold can potentially experience deformation-induced bonds rupture [22], rearrangement and disentanglement [23] according to “Mulins effect” [24] following CRIS loading.

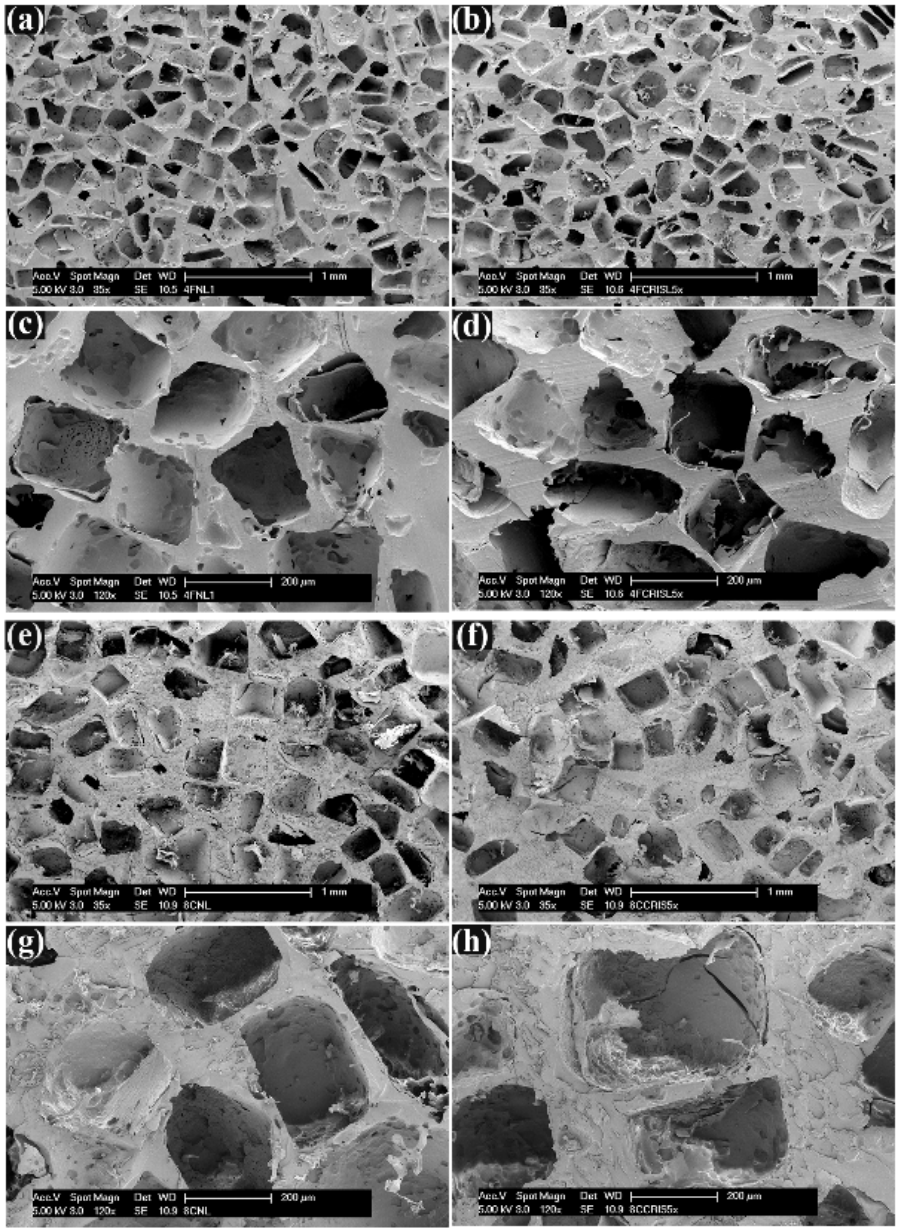

Figure 4. Scanning electron microscopy images before (left column) and after (right column) optimized CRIS loading. (a-d) 4%Cr-Fine pore sizes scaffold. (e-f) 8%Cr-Coarse pore sizes scaffolds.

3-4-2 Simulated CRIS seeding loading regime

We derived the average suction pressure and the infiltration velocity of the 2D axisymmetric surface over the simulation time and compared their maximum values in a number of case studies. Derived values for some cases are reported in Table 2 to elaborate the conducted what-if analysis. For better illustration of the induced suction pressure and velocity fields, the rainbow and arrow surface plots are combined and shown in Fig. 5 at the middle and end of unloading step for the third case study. As can be seen, the medium infiltration is dominant at

the outer edges of the cylindrical scaffold for both types of scaffold. Obviously, the medium infiltration is considerably shallower for fine pore size scaffold with low permeability.

Table 2. Seeding loading parameters used in simulations for reported case studies and corresponding derived values for maximum suction pressure (Pf) and Darcy's velocity (Ud) inside two types of scaffold.

Case	Loading rate (mm/s)	UnL. rate (mm/s)	Delay time (s)	Strain (%)	4Cr-Fine pores model		8Cr-Coarse pores model	
					P_f (pa)	U_d (mm/s)	P_f (pa)	U_d (mm/s)
1	5	10	3	35	-10975	2.01E-01	-23023	2.14
2	5	10	0.3	35	-6834.2	1.48E-01	-23738	2.07
3*	**0.05**	**10**	**3**	**35**	**-54228**	**5.56E-01**	**-24647**	**2.53**
4	0.05	10	0.3	35	-51431	5.28E-01	-24784	2.14
5	0.05	10	3	30	-51551	5.34E-01	-16288	1.91
6	0.05	10	3	20	-41162	4.22E-01	-7180.2	1.67
7	5	1	3	35	-13585	1.23E-01	-7884.8	1.48E-01
8	5	1	0.3	35	-8316.8	8.57E-02	-7681	1.51E-01
9	0.05	1	3	35	-41722	2.93E-01	-7708.2	1.33E-01
10	0.05	1	0.3	35	-39892	2.81E-01	-7536.3	1.29E-01

* Case 3 (bold) resulted in the best suction pressure and infiltration velocity, irrespective of scaffold type.

As anticipated, our simulation showed that faster unloading and larger strain enhanced medium suction into the scaffold. This can be verified for the role of unloading rate by comparing induced suction pressure and medium infiltration velocity in cases 1-6 and 7-10 for two types of scaffold with different mechanical and morphological characteristics. Likewise, the improving effect of higher compressive strain can be seen from cases 3, 5, and 6. Interestingly, while the rate of loading was not as important parameter for the permeable scaffold, they were important for scaffold showing lower permeability. Derived results from cases 1, 2 and 3, 4 revealed the significance of slow loading rate on improved infiltration velocity and suction pressure. Likewise, longer delay time leads to more effective medium suction for fine pore size scaffolds depending on loading/unloading rates. This can be clearly highlighted when comparing cases 1 and 2 or 7 and 8. The shorter the times for loading and unloading, the more pronounced is the role of time delay.

According to the CRIS simulation results, case 3 (bold) has the best seeding loading parameters, irrespective of scaffold type. This CRIS seeding would follow a slow compression loading of 0.05 mm/s until 35% strain. Then, after a 3 sec delay time, an abrupt unloading of

10 mm/s causes infiltration of the CCM containing cells into the instantaneously developed empty pores.

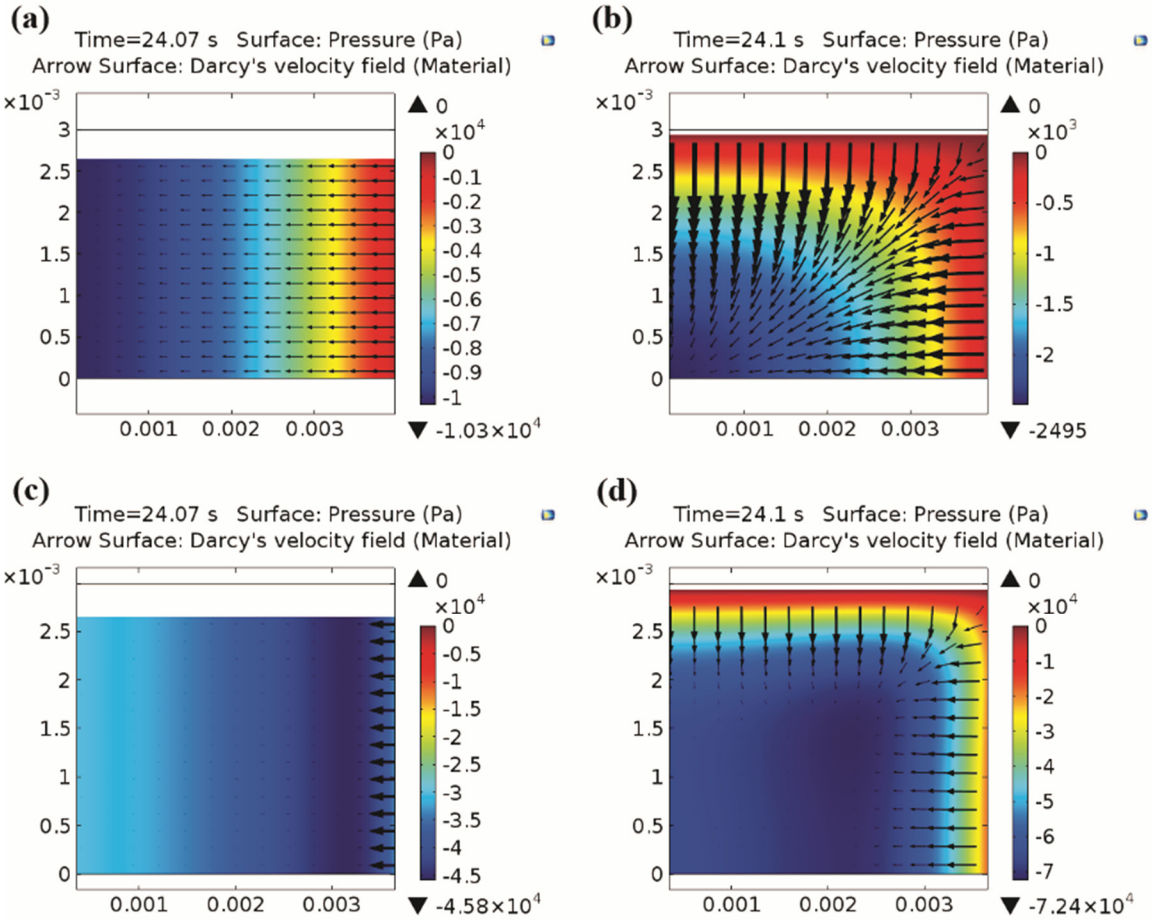

Figure 5. Graphical illustration of suction pressure (color map) and velocity fields (arrows) during unloading step for the third case study. (a-b) Permeable scaffolds. (c-d) Scaffolds having low permeability.

3-4-3 Cell seeding and post-seeding treatments

We implemented experimental cell seeding by choosing the optimized seeding regime given by the third (numerical) case, and lasting for 5 cycles followed by a 20 second resting period after each repetition. The considered resting time gives enough pause for passing a transient condition before starting a new cycle. Control static surface pipetting for cell seeding was also carried out on preconditioned scaffolds having the same loading history. We utilized HPFN coated scaffolds having 2.5 mm thickness and 8 mm diameter for comparison of different seeding strategies. Distribution of MTT stained cells are representatively shown in Figure 6 for two types of scaffold and extracted results are displayed in Figure 7.

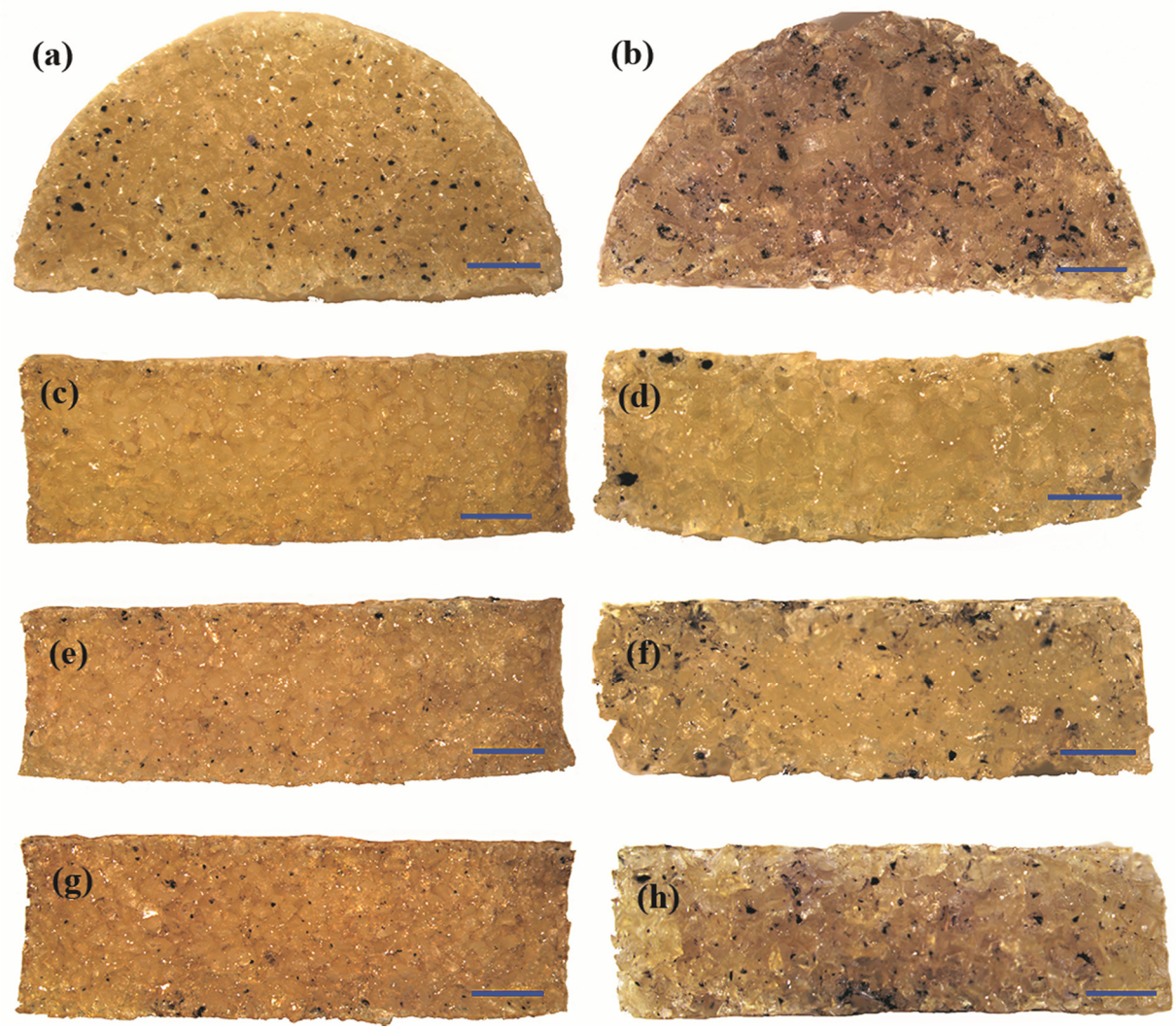

Figure 6. MTT-stained cells showing distribution of cells for different seeding strategies (first row: top surface, second row: cross section for static seeding, third row: CRIS + static incubation, last row: CRIS with slow rotation AST. Scale bar: 1 mm). (a, c, e & g) The labeled cells inside 4%Cr-Fine pore size scaffolds. (b, d, f & h) The labeled cells inside 8%Cr-Coarse pore size scaffolds.

Despite a fairly uniform distribution on the top surface for all cases, we observed quite different patterns through cross sections of the scaffolds. It is clear that without CRIS loading regime, very poor cell penetration can be achieved irrespective of scaffold type. There is a significant difference for distribution metric between static surface pipetting and CRIS seeding methods. As simulation results predicted, the permeability of the scaffold directly influenced CRIS seeding effectiveness. A more permeable scaffold provides a higher cell distribution metric. Additionally, while slow rotation AST slightly improved cells distribution for permeable scaffolds, its overall influence on cells penetration was significant for scaffolds showing low permeability. Moreover, live/dead staining of cell-scaffold constructs revealed very good cell survival after the proposed seeding process. Figure 8, illustrates strong signal

from abundant live cells (Green stain) inside two types of scaffold after seeding, while showing only a few dead cells (Red stain).

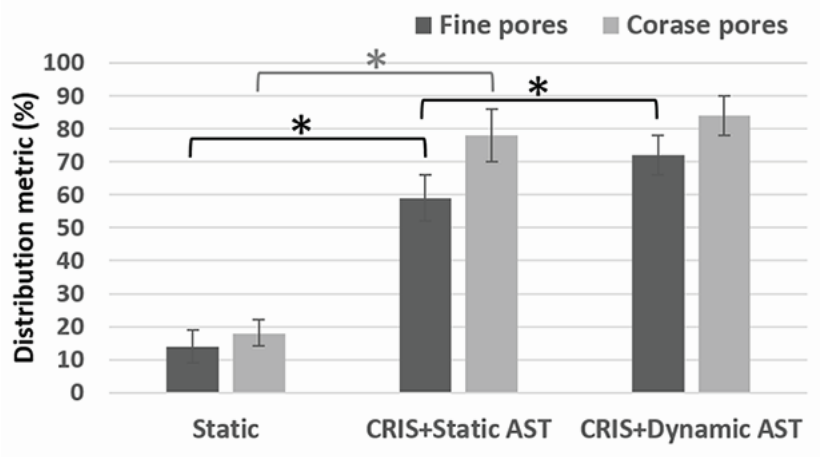

Figure 7. Comparison of distribution metric for different seeding strategies. Asterisk symbol (*) shows significant difference (Student t-test, $p<0.05$).

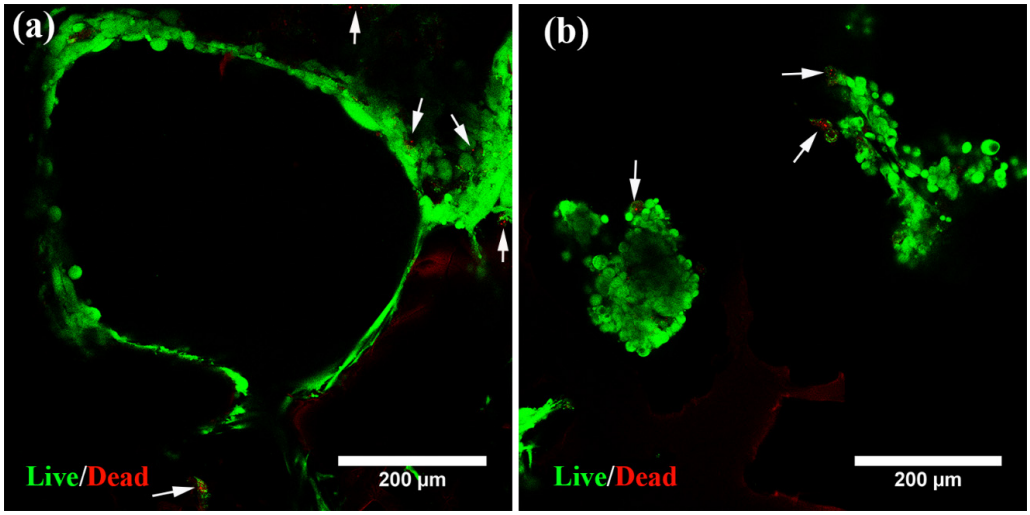

Figure 8. Live/dead staining of human epiphyseal chondro-progenitor cells after cell seeding. (a) 8%Cr-Coarse pore size scaffold. (b) 4%Cr-Fine pore size scaffold. Green color shows distribution of live cells inside pores and red color is the stain for dead cells indicated by arrows.

3-4-4 Systematic analysis of main effects on seeding results

To identify the relative importance of contributing factors to seeding results, we used 8 mm diameter scaffolds having 1.7 or 3.1 mm thickness, high ($k_0=O(10^{-12})$) or low ($k_0=O(10^{-14})$) permeability and with fibronectin coating (25 µg/ml) or no coating conditions. In order to standardize each factor state for the sake of computation [20], -1 code was used for low permeability, no coating condition and 1.7 mm thickness states, while high permeability,

HPFN coating and 3.1 mm thickness states were coded as +1. The coded experimental configurations and obtained responses for CSE and DM (mean and standard deviation) are reported in Table 3. Due to the augmentation effect of dynamic after-seeding treatment, all experiments of this phase were accomplished by applying the slow rotation AST.

The results of analysis of the main effects and interactions for cell seeding efficiency and distribution metric are highlighted in Figure 9. It is clear that relative importance of permeability (a_1) is higher than coating (a_2) and thickness (a_3) for both responses. By looking at the extracted results, we can observe that CSE and DM responses are higher for permeable scaffolds. Our results have shown that HPFN coating improved CSE, which is a result of better cell attachment, while thickness had a negative effect on cell seeding efficiency. Given the half normal probability plot, it can be observed that scaffold permeability, coating, and thickness were influential on CSE response, while just scaffold permeability affects the DM. All interactions were neither important for cell seeding efficiency nor for the DM response. Analysis of variance also confirmed the half normal plot since all graphically determined contributing factors were significant ($p<0.05$).

Table 3. Matrix of experiment for the full factorial design and corresponding responses (mean ± standard deviation).

	Matrix of Exp.			**Response - y (%)**	
Run	k	c	t	DM	CSE
1	-1	-1	-1	65±5	61±5
2	-1	-1	1	79±6	58±4
3	-1	1	-1	76±7	71±6
4	-1	1	1	70±6	66±4
5	1	-1	-1	80±1	76±7
6	1	-1	1	81±4	68±5
7	1	1	-1	87±6	84±4
8	1	1	1	89±4	76±6

Eight experimental configurations are shown by coded values for permeability (k), coating (c), and thickness (t) columns.
CSE: cell seeding efficiency.
DM: distribution metric.

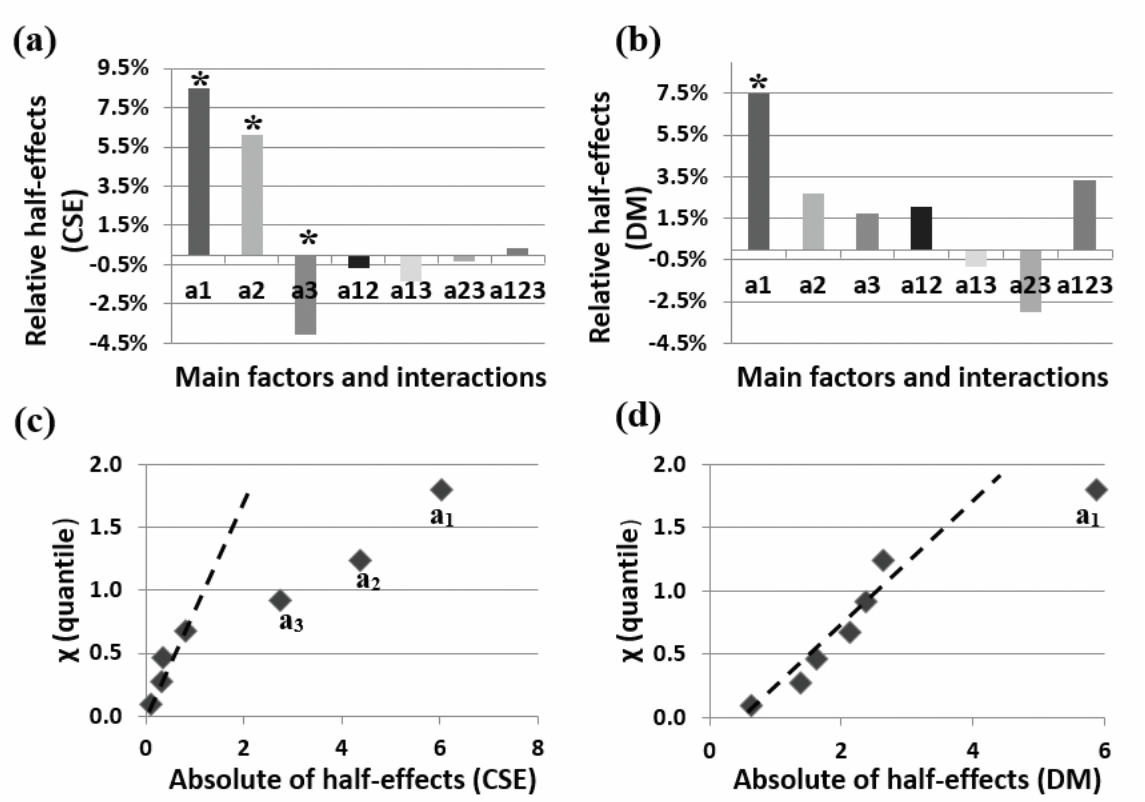

Figure 9. Relative half effects (up) and corresponding half normal probability (bottom) plots for permeability (a_1), coating (a_2) and thickness (a_3) factors. (a, c) Extracted results for cell seeding efficiency. (b, d) Extracted results for distribution metric. Asterisk symbol (*) stands for the significant factors. Significant half-effects are away from straight line covering normally distributed half-effect which could be due to normal experimental variation.

3-5 Discussion

Preparation of a cells-3D support construct is one of the most challenging issues in functional tissue engineering taking into consideration the demanding physiological constraints which govern scaffold design. Indeed, strictly controlled structural and mass transport properties are required for load bearing after transplantation, maintaining cells retention, viability and differentiation [4, 25, 26]. Accordingly, two types of scaffolds having different mechanical and morphological characteristics were employed [14] as models for evaluating the influential parameters for cell seeding. A compression release induced suction technique was used for cell seeding inside these pre-formed scaffolds.

A what-if analysis was performed on parameters of seeding regime by numerical simulation of compression-induced suction in different case studies. We observed that fast unloading and large strain considerably enhanced medium suction toward the center of the scaffold for both types of scaffolds. On the other hand, the influence of slow loading and delay time between

loading and unloading steps were just significant for scaffolds showing low permeability. These numerical results could be explained by the fact that permeability of a scaffold determines the ease of fluid flow inside the pores. During loading steps, fluid pressurization phenomenon occurs due to the resistance of the scaffold porous structure to the fluid seepage. For scaffolds with low permeability, release of this internal hydrostatic pressure can take longer time compared to permeable scaffolds [14]. Therefore, by decreasing the loading rate or increasing the delay time, fluid pressure would have more time to be relaxed before the unloading step. Otherwise, when the unloading step is begun, in the core region, the fluid flow is still capable of reaching outside in contrast to inward velocity field at the edge of the scaffold. This is clearly observable for rapid loading and short delay time in Figure 10 for scaffolds with low permeability (Figure 10-c, d). In permeable scaffolds, on the contrary, induced velocity field is unidirectional toward the central region during the unloading step regardless of rapid loading rate and short delay time (Figure 10-a, b).

Additionally, from the numerical results obtained, it can be observed that permeability directly affects the suction pressure and infiltration velocity for the two types of scaffolds. For example, under slow loading and rapid unloading rate conditions, the maximum induced suction pressure is twice as high in scaffolds with lower permeability. On the other hand, as permeable scaffolds would show less resistance to fluid flow through the pores, even with lower suction pressure in this condition, infiltration velocity is more than four times faster than scaffolds having low permeability.

Xie *et al.* [11], applied compression up to 50% with the same loading and unloading rate of 5 mm/s. According to our simulation, this loading regime could be optimum for highly permeable and soft scaffolds. We showed that for scaffolds with low permeability, rapid loading rates in CRIS seeding technique should be avoided to have optimized medium suction. Moreover, a rapid loading rate leads to higher peak stress compared to a slow loading rate and this might result in damage to the scaffolds [14, 27]. We should also notice that the microstructure of the stiff scaffolds could be destroyed by increasing a compressive strain up to 50%. In our case, the plastic deformation of the highly crosslinked scaffolds (8% crosslinking density and coarse pores) were measured to be around 35%. Yet, our soft scaffolds with low permeability (4% crosslinker and fine pores) showed elastic deformation up to 40%.

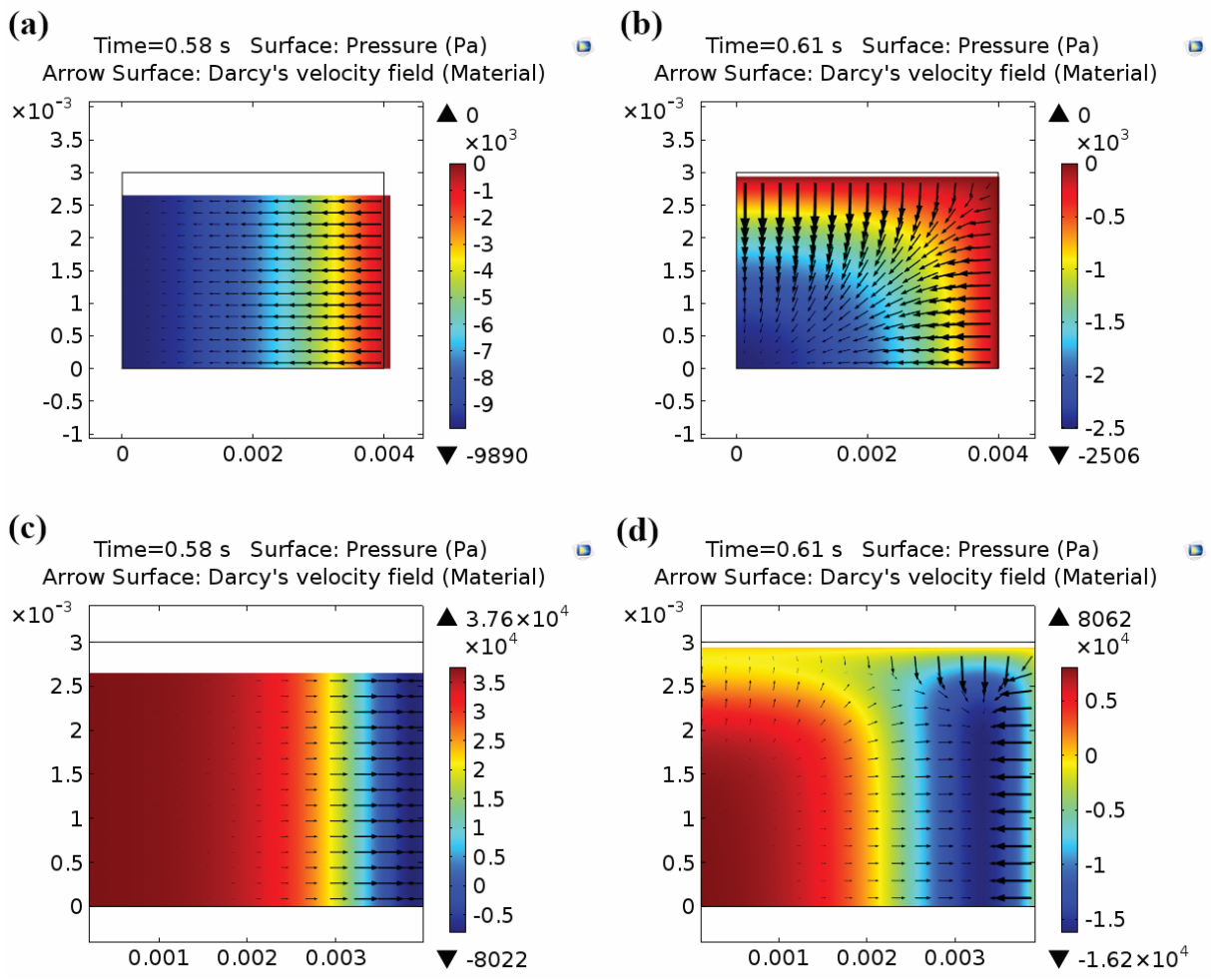

Figure 10. Graphical illustration of suction pressure (color map) and velocity fields (arrows) during unloading step for the fast loading/unloading with short delay time. (a-b) Permeable scaffolds. (c-d) Scaffolds having low permeability.

Performed experimental cell seeding according to the optimal loading regime obtained from the simulation showed significant improvement on cell penetration compared to static surface pipetting. We also observed an enhancing role of slow rotation AST (dynamic incubation) after optimized CRIS loading regime, especially for scaffolds showing low permeability. We could explain the AST working mechanism by the hypothesis that the cell penetration in the scaffold is due to the active fluid movement inside the tortuous pores of the scaffold during the re-swelling period. Apparently, after several loading-unloading steps, the hydrated scaffolds had some loss of fluid inside the pores. Therefore, by providing dynamic movement of cell suspension around the scaffold after initial shallow suction, there can be an active movement of cells deep inside the scaffold compared to static incubation.

We have shown high cell viability for the optimized CRIS seeding followed by slow rotation AST. Obviously, the rate of loading and the amount of strain are important factors on

transmitted stress on cells and therefore overall cells viability. The unloading rate should not be important on cells viability since we are releasing the maximal applied stress on cells during unloading. The peak stress in optimum loading regime was always less than 1.5 MPa which is the physiological stress in native cartilage during walking [28]. Likewise, 35% strain is not exceeding the reported physiologic magnitude of dynamic strains following activity (ranging between 15–35%) [29]. Thus, the proposed optimum loading regime is not in a non-physiologic level and would not transfer damaging forces to cells. Generally, applying an external force in dynamic seeding techniques will improve cell distribution, however the nature of this dynamic force (e.g., harsh centrifugation [9]) might reduce cells viability. Evidently, the proposed CRIS with slow rotation AST, as applied dynamic force does not affect cell viability but it did enhance cell distribution within the scaffolds.

Our systematic experimental design indicated that the scaffold permeability (a_1) is the most significant factor for both cell seeding efficiency and distribution compared to coating (a_2) and thickness (a_3). Conventionally, porosity, average pore size and distribution of pore size are used as primary characteristic parameters of tissue engineering scaffolds, while interconnectivity, fenestration size, fenestration distribution, and orientation of pores are used as secondary indicative parameters of a porous structure. The difficulty of characterizing some of these parameters is the reason why it is difficult to find all of them in publications [30]. In practice, permeability is an overarching mechanical parameter encompassing the effects of all mentioned morphological features. Therefore, permeability as a robust quantitative determinant has been suggested for evaluating porous structures [30, 31]. Accordingly, we selected permeability to study influence of morphological characteristics of the scaffold (e.g., pore size, interconnectivity and porosity) on cell infiltration.

The considered range for permeability ($O(10^{-14}) < k_0 < O(10^{-12})$) was wide enough to reflect its role considering the reported values in the literature [31] for functional TE applications. In correlation with the study of Melchels *et al*, [4] our results indicated direct influence of permeability on cell seeding efficiency and uniformity. Obviously, the more permeable the scaffold is, the easier solute transport is within the structure and accordingly cell infiltration. On one hand, the literature has clearly reported the effective role of higher permeability and larger pore size on vascularization of scaffolds and bone in-growth in the field of bone tissue engineering[32, 33]. On the other hand, it has been shown that cartilaginous matrix synthesis by chondrocytes is enhanced inside scaffolds having smaller pore size and lower permeability

(mimicking more similarly *in vivo* cartilage environment) [26, 34]. Taken together, a trade-off between seeding outcome and chondrogenesis should be considered for cartilage TE when designing scaffold permeability, while this not the case for osteogenesis in bone TE.

While scaffold coating was also contributing to cell seeding efficiency, it has had a minor effect on distribution of cells within scaffolds. Different concentrations of fibronectin have been used in the literature for coating scaffolds mostly between 10 to 20 µg/ml [13, 35, 36]. We used 25 µg/ml to clearly differentiate the coating and no coating conditions. Since fibronectin has the RGD (arginine–glycine–aspartic acid) cell recognition sequence, it enhances functionality of the scaffolds and cell-scaffold interface interaction [37]. In fact, scaffold coating with fibronectin modulates binding sites for cell attachment, therefore, it is expected to influence the cell seeding efficiency. Interestingly, previous studies also demonstrated that fibronectin coated scaffolds facilitate cell proliferation as well as neo-tissue formation supporting use of bioactive scaffolds for TE application [35, 38].

Increasing scaffold thickness reduced the CSE response, while it had negligible effect on the distribution metric. The scaffold thickness range (1.7 and 3.1 mm) used in the present study reflected the anticipated application which is for human knee cartilage where the thickness is roughly between 2 to 3 mm [39]. Controlling the cell distribution in the scaffold is an important aspect for clinical application, where different scaffold thickness might be required based on lesion location. Undoubtedly, we can maintain the concentration of cells by initially using higher amounts of cells for thicker scaffolds to compensate its negative influence on CSE.

One limitation of the performed numerical study was considering isotropic and homogenous mechanical properties for the scaffold. Although this was appropriate to particularly study the role of different parameters, one can imagine a numerical analysis of the scaffold mimicking the anisotropic poroviscoelastic cartilage having depth-dependent structural heterogeneity. Experimentally, we just investigated the influence of slow rotation after-seeding treatments during re-swelling time over static incubation. Due to expected enhancing role of dynamic conditions such as orbital shaking, one could have compared different dynamic after seeding treatments and rank them accordingly. The effect of coating concentration on seeding results should also be studied. It could be interesting to find the minimum and maximum coating concentration to detect the threshold and saturation point.

Improved spatial distribution in dynamic seeding methods compared to poor uniformity of static seeding highlights the role of external force to actively control medium infiltration during the seeding process. This external driving force was provided in our seeding method by optimized CRIS seeding loading regime supplemented with slow rotation AST during re-swelling time of the scaffold. Permeability, coating and thickness of scaffolds are contributing to the seeding outcome regardless of the seeding strategy. However, we have shown that the role of permeability is more pronounced than coating and thickness of the scaffolds in the CRIS seeding method. In conclusion, this study presents a systematic analysis of scaffold mechanical and morphological characteristics, geometry, and surface functionality with regards to effectiveness of a seeding strategy. This approach helps to identify the key parameters affecting seeding process in cell-scaffold based tissue engineering. In particular, controlling cell seeding in scaffolds is important in developing TE products which have to be compliant with regulatory aspects necessitating reproducible and consistent procedures.

3-6 Acknowledgments

We thank Sandra Jaccoud for her precious technical support. We also appreciate the advice of Dr. Jean Marie Furbringer for design and analysis of systematic experiments. This work was supported by the Swiss National Science Foundation (#310030_149969 / 1).

3-7 References

[1] Hasegawa T, Miwa M, Sakai Y, Niikura T, Lee S, Oe K, et al. Efficient cell-seeding into scaffolds improves bone formation. J Dent Res 2010;89:854-9.

[2] Wendt D, Marsano A, Jakob M, Heberer M, Martin I. Oscillating perfusion of cell suspensions through three-dimensional scaffolds enhances cell seeding efficiency and uniformity. Biotechnol Bioeng 2003;84:205-14.

[3] Solchaga LA, Tognana E, Penick K, Baskaran H, Goldberg VM, Caplan AI, et al. A rapid seeding technique for the assembly of large cell/scaffold composite constructs. Tissue Eng 2006;12:1851-63.

[4] Melchels FP, Barradas AM, Van Blitterswijk CA, De Boer J, Feijen J, Grijpma DW. Effects of the architecture of tissue engineering scaffolds on cell seeding and culturing. Acta Biomater 2010;6:4208-17.

[5] Burg K, Holder W, Culberson C, Beiler R, Greene K, Loebsack A, et al. Comparative study of seeding methods for three-dimensional polymeric scaffolds. Journal of biomedical materials research 2000;52:576-.

[6] Vitacolonna M, Belharazem D, Hohenberger P, Roessner ED. Effect of dynamic seeding methods on the distribution of fibroblasts within human acellular dermis. Cell Tissue Banking 2015:1-10.

[7] Alvarez-Barreto JF, Linehan SM, Shambaugh RL, Sikavitsas VI. Flow perfusion improves seeding of tissue engineering scaffolds with different architectures. Ann Biomed Eng 2007;35:429-42.

[8] Roh JD, Nelson GN, Udelsman BV, Brennan MP, Lockhart B, Fong PM, et al. Centrifugal seeding increases seeding efficiency and cellular distribution of bone marrow stromal cells in porous biodegradable scaffolds. Tissue Eng 2007;13:2743-9.

[9] Thevenot P, Nair A, Dey J, Yang J, Tang L. Method to analyze three-dimensional cell distribution and infiltration in degradable scaffolds. Tissue Eng,Part C 2008;14:319-31.

[10] Almarza AJ, Athanasiou KA. Seeding techniques and scaffolding choice for tissue engineering of the temporomandibular joint disk. Tissue Eng 2004;10:1787-95.

[11] Xie J, Jung Y, Kim SH, Kim YH, Matsuda T. New technique of seeding chondrocytes into microporous poly (l-lactide-co-ε-caprolactone) sponge by cyclic compression force-induced suction. Tissue Eng 2006;12:1811-20.

[12] O'Conor CJ, Case N, Guilak F. Mechanical regulation of chondrogenesis. Stem Cell Res Ther 2013;4:61.

[13] Abdel-Sayed P, Darwiche SE, Kettenberger U, Pioletti DP. The role of energy dissipation of polymeric scaffolds in the mechanobiological modulation of chondrogenic expression. Biomaterials 2014;35:1890-7.

[14] Nasrollahzadeh N, Pioletti DP. Experimental method to characterize the strain dependent permeability of tissue engineering scaffolds. J Biomech 2016;49:3749-52.

[15] Scholten PM, Ng KW, Joh K, Serino LP, Warren RF, Torzilli PA, et al. A semi-degradable composite scaffold for articular cartilage defects. Journal of Biomedical Materials Research Part A 2011;97:8-15.

[16] Biot MA. Mechanics of deformation and acoustic propagation in porous media. J Appl Phys 1962;33:1482-98.

[17] Heneghan P, Riches PE. Determination of the strain-dependent hydraulic permeability of the compressed bovine nucleus pulposus. J Biomech 2008;41:903-6.

[18] Darwiche S, Scaletta C, Raffoul W, Pioletti DP, Applegate LA. Epiphyseal chondroprogenitors provide a stable cell source for cartilage cell therapy. Cell Medicine 2012;4:23-32.

[19] Hausherr TC, Nuss K, Thein E, Applegate L, Pioletti D. Human Bone Progenitor Cells for Clinical Application: What Kind of Immune Reaction Does Fetal Xenograft Tissue Trigger in Immuno-Competent Rats? Cell Transplantation 2016;DOI: 10.3727/096368916X693789.

[20] Box GE, Hunter JS, Hunter WG. Statistics for Experimenters: Design, Innovation, and Discovery. 2nd edition ed. New York: Wiley-Interscience; 2005.

[21] Taylor G. Analysis of experiments by using half-normal plots. The Statistician 1994:529-36.

[22] Bueche F. Molecular basis for the Mullins effect. J Appl Polym Sci 1960;4:107-14.

[23] Hanson DE, Hawley M, Houlton R, Chitanvis K, Rae P, Orler EB, et al. Stress softening experiments in silica-filled polydimethylsiloxane provide insight into a mechanism for the Mullins effect. Polymer 2005;46:10989-95.

[24] Mullins L. Softening of rubber by deformation. Rubber chemistry and technology 1969;42:339-62.

[25] Hollister SJ. Porous scaffold design for tissue engineering. Nat Mater 2005;4:518-24.

[26] Kemppainen JM, Hollister SJ. Differential effects of designed scaffold permeability on chondrogenesis by chondrocytes and bone marrow stromal cells. Biomaterials 2010;31:279-87.

[27] Tang J, Tung MA, Zeng Y. Characterization of gellan gels using stress relaxation. J Food Eng 1998;38:279-95.

[28] Barker M, Seedhom B. The relationship of the compressive modulus of articular cartilage with its deformation response to cyclic loading: does cartilage optimize its modulus so as to minimize the strains arising in it due to the prevalent loading regime? Rheumatology 2001;40:274-84.

[29] Sanchez-Adams J, Leddy HA, McNulty AL, O'Conor CJ, Guilak F. The mechanobiology of articular cartilage: bearing the burden of osteoarthritis. Current rheumatology reports 2014;16:1-9.

[30] Li S, de Wijn JR, Li J, Layrolle P, de Groot K. Macroporous biphasic calcium phosphate scaffold with high permeability/porosity ratio. Tissue Eng 2003;9:535-48.

[31] Pennella F, Cerino G, Massai D, Gallo D, Labate GFDU, Schiavi A, et al. A survey of methods for the evaluation of tissue engineering scaffold permeability. Ann Biomed Eng 2013;41:2027-41.

[32] Hutmacher DW, Schantz JT, Lam CXF, Tan KC, Lim TC. State of the art and future directions of scaffold-based bone engineering from a biomaterials perspective. Journal of tissue engineering and regenerative medicine 2007;1:245-60.

[33] Murphy CM, Haugh MG, O'Brien FJ. The effect of mean pore size on cell attachment, proliferation and migration in collagen–glycosaminoglycan scaffolds for bone tissue engineering. Biomaterials 2010;31:461-6.

[34] Nehrer S, Breinan HA, Ramappa A, Young G, Shortkroff S, Louie LK, et al. Matrix collagen type and pore size influence behaviour of seeded canine chondrocytes. Biomaterials 1997;18:769-76.

[35] Bhati R, Mukherjee D, McCarthy K, Rogers S, Smith D, Shalaby S. The growth of chondrocytes into a fibronectin-coated biodegradable scaffold. Journal of biomedical materials research 2001;56:74-82.

[36] Attia M, Santerre JP, Kandel RA. The response of annulus fibrosus cell to fibronectin-coated nanofibrous polyurethane-anionic dihydroxyoligomer scaffolds. Biomaterials 2011;32:450-60.

[37] Chung HJ, Park TG. Surface engineered and drug releasing pre-fabricated scaffolds for tissue engineering. Adv Drug Del Rev 2007;59:249-62.

[38] Roy DC, Hocking DC. Recombinant fibronectin matrix mimetics specify integrin adhesion and extracellular matrix assembly. Tissue Eng,Part A 2012;19:558-70.

[39] Shepherd D, Seedhom B. Thickness of human articular cartilage in joints of the lower limb. Ann Rheum Dis 1999;58:27-34.

Chapter 4: Hydrogels Preserving Hysteresis for Enhanced Mechanical and Mechanobiological Performances

4-1 Abstract

Dissipation is a key attribute for defect growth resistance and durability of biomaterials under mechanical loading. A new paradigm is also emerging on the role of dissipative phenomena in mechanobiology of load-bearing tissues. Therefore, an interesting potential exists to employ dissipation for these two different but complementary goals in the development of biomaterials. Herein, a novel combination of flow-dependent and flow-independent dissipation sources is proposed to enhance both fatigue resistance and mechanobiological performance of hydrogels. Given hydrogel as a biphasic material, we supplemented the solid network intrinsic dissipation with a fluidic frictional drag dissipation. Accordingly, a dually porous yet low permeable pHEMA based hydrogel is developed via hybrid crosslinking strategy presenting weak physical and strong covalent bonds. In contrast to widely reported tough hydrogels without sufficient load support capability, our proposed design allowed development of fatigue-resistant hydrogels presenting a range of compressive stiffness, dissipation and water content similar to articular cartilage. Moreover, the preserved mechanical hysteresis during cyclic compression positively impacted the mechanobiological feature of the hydrogel, as chondrogenesis was favored in these cell-laden hydrogels. The competent design of dissipation sources in the development of hydrogels opens therefore new possibilities for fine tuning their mechanical behavior and increasing their biological function.

Keywords: Hydrogel, energy dissipation, fatigue resistance, cartilage, mechanobiology.

4-2 Introduction

The structural similitude of hydrogels with soft tissues as a water-swollen solid network makes them promising materials to regenerate damaged tissues. Apart from biological key features, a challenging set of mechanical properties including stiffness, resilience, strength, damping, toughness, and fatigue resistance would be necessary for hydrogels to withstand demanding mechanical loadings [1-4]. In particular, dissipation is a key feature for resisting defect growth and durability of biomaterials under mechanical loading. It is well established that damping of input energy via mechanical hysteresis in dissipation zone protects the loaded hydrogel by shielding the crack tip and thus improves its toughness [5, 6]. A new paradigm is also emerging on the role of dissipative phenomena in mechanobiology of load-bearing tissues. Indeed, cartilage can dissipate a considerable part of the input energy due to its rich viscoelastic nature and this phenomenon corresponds to its physiological function in diarthrodial joints [7-9]. Interestingly, chondro-progenitor cells were shown to be sensitive to the dissipation level of cell-scaffold constructs following cyclic compression [9]. Likewise, viscoelasticity of hydrogels was recently presented as a key feature to regulate cartilage formation [10] and osteogenic differentiation [11]. Design of dissipative attributes in the development of hydrogels can therefore be a strategic approach to improve mechanical and mechanobiological performances.

The basic mechanical characteristics of a load-bearing biomaterial depend on the required physiological stress/strain range of the target tissue. In case of articular cartilage, a tough biomaterial with a relatively high stiffness (~1 MPa) and moderate deformability (< 50%) [1, 12, 13] is required to withstand harsh biomechanical loading in joints [1, 2]. Therefore, a combination of high stiffness and dissipative capacity is necessary for corresponding load-bearing hydrogels. However, a merely stiff and dissipative hydrogel does not necessarily present a fatigue resistance performance. There is a supplemental complexity in the development of a load-bearing biomaterial as the different sources of dissipation must be carefully designed for a robust behavior under fatigue loading.

The mechanical dissipation is generally considered as a global variable and quantified by the area of hysteresis loop when the material is under cyclic loading. Various dissipative hydrogels have been developed with different strategies including double network (DN) [14, 15], hybrid systems [16, 17], block copolymers [18, 19], polyion complexes [3, 20] and hydrophobically modified [21-23] hydrogels. They all follow the same idea of dissipating

imposed input energy by incorporating different sacrificial elements into the network. However, covalent DN hydrogels, for instance, pose a practical shortcoming as one of the networks is permanently sacrificed to dissipate energy upon initial loading and the source of dissipation is vanished for subsequent cycles of loading. Since hydrogels having a dissipation source from destructive processes are not fatigue resistance, reversible dissipation mechanisms have been proposed for a robust mechanical performance. In particular, sacrificial bonds in physical hydrogels disengage temporarily, and bonds reforming capability (partially or fully) is possible over a recovery time [3, 20, 24]. These hydrogels, therefore, represent a kind of fatigue resistance behavior following discontinuous loading scheme, but not cyclic loading. A major limitation for reversible processes (e.g., ionic bonds) is the reassociation time needed to give back the hydrogel its initial properties. Moreover, most of physical hydrogels usually have poor stiffness in physiological strain range such as the one found in cartilage, and therefore, their load support capability is very limited [4, 19, 24-26]. Despite development of a few physical hydrogels with high stiffness, the lack of chemical stability [16, 18] (weakness against mobile ion), low water content [3, 20], long recovery time after loading [3, 16, 17, 20], time consuming and complex fabrication process [23] limit their application.

Given hydrogel as a biphasic material, its mechanical dissipation can be due to flow-dependent or flow-independent processes. Despite a surge of interest in the development of different molecular structures for hydrogels to modulate intrinsic dissipation sources [5, 15, 27, 28] (which by definition are flow-independent), there are only a few studies considering flow-dependent dissipation [29]. However, this kind of dissipation is a salient aspect in soft biological tissues such as cartilage [7-9]. Fluidic phase contribution to support load is also a well-recognized phenomenon in this tissue [1, 7, 8, 12]. Accordingly, to obtain a material that could successfully sustain the demanding physiological loading conditions pertaining for example in knee cartilage, we hypothesize that load-bearing hydrogels should be developed by considering flow-independent as well as flow-dependent mechanisms.

A timely efficient hybrid crosslinking system from a single precursor would be highly appreciated for potential biomedical applications. By following the sacrificial bonds principle [3, 15, 18], a fatigue-resistant single network (SN) hydrogel can be developed via a hybrid crosslinking strategy [5]. Crosslinked poly [2-hydroxyethyl methacrylate] (pHEMA) based hydrogel presents a SN system with tunable contribution of hybrid bonds. In one hand,

different weak physical bonds including hydrophobic associations [30], hydrogen bonding [31], and chains entanglement [32] can be formed in pHEMA hydrogel *per se*. On the other hand, the stiffness and the dissipation level of pHEMA hydrogels can be significantly enhanced if the network is copolymerized by a short length crosslinker such as ethylene glycol dimethacrylate (EGDMA) [33] to build strong covalent bonds. Furthermore, the proper balance of hydrophilic and hydrophobic elements inside the pHEMA network intrinsically controls the swelling of the hydrogel in physiological condition and prevents degraded mechanical properties [23, 28, 34]. A careful combination of physical and covalent bonds can lead to a hybrid crosslinking system with enhanced intrinsic dissipation capacity and fatigue resistance capability. In parallel, we aim to incorporate different extent of flow-dependent dissipation and load support into the system by controlling the morphological architecture of the hydrogel.

Herein, we report that by an optimized combination of dissipation sources, either dependent or not on the flow, fatigue-resistant hydrogels can be developed presenting similar range of compressive stiffness, dissipation and water content to cartilage. Permeability of the hydrogel is introduced as a source for flow-dependent dissipation and hydrogel material composition for intrinsic network dissipation. Surprisingly, we discovered that with a water content close to the one of the cartilage (~70%), stiffness and dissipative capacity of porous p(HEMA-co-EGDMA) hydrogels (presenting combination of dissipation sources) are higher than corresponding conventional hydrogels (deprived of flow-dependent dissipative mechanism) having the same material composition. We showed that hydrogels with the same level of stiffness and energy dissipation may differently sustain fatigue loading depending on their preserved or shrank hysteresis curve during cyclic loadings. Additionally, we found that chondrogenesis is favored in the cell-laden constructs preserving mechanical hysteresis with effective contribution of frictional drag dissipation during cyclic compression rather than in constructs having destructive sources of dissipation.

4-3 Results and Discussion

4-3-1 Conventional hydrogels with intrinsic dissipation sources

Considering a timely efficient one-pot polymerization process, we chose the biocompatible p(HEMA) based hydrogels reinforced with EGDMA crosslinker to design a hybrid crosslinked SN system. The conventional p(HEMA-co-EGDMA) based hydrogels are

referred to xCr-yW, where x and y stand respectively for EGDMA molar and initial water content (IWC) volumetric ratios to HEMA (Cr and W are abbreviations for crosslinking and water). We developed 5 groups of dissipative and stiff hydrogels (in MPa range) and probed the role of material composition in physical (weak) and covalent (strong) bonds formation. We then highlighted contribution of different bonds to the mechanisms of dissipation and fatigue resistance performance. The energy dissipation (ED) during cyclic loading (15% cyclic strain over 10% pre-strain at 1 Hz) was defined as the area of the corresponding hysteresis loop. As fatigue resistance metrics, we employed i) the differential value of the energy dissipation ($\Delta ED = ED_i - ED_{100}$, i stands for the cycle number) normalized by the energy dissipation of a reference cycle taken at the 100th cycle (ED_{100}) and ii) the load support capability of hydrogel before and after fatigue loading. Representative hysteresis loop evolution and time dependent load support of hydrogels in sequential stress relaxation test before and after one hour fatigue loading (3600 cycles) are shown in Figure 1-a and b.

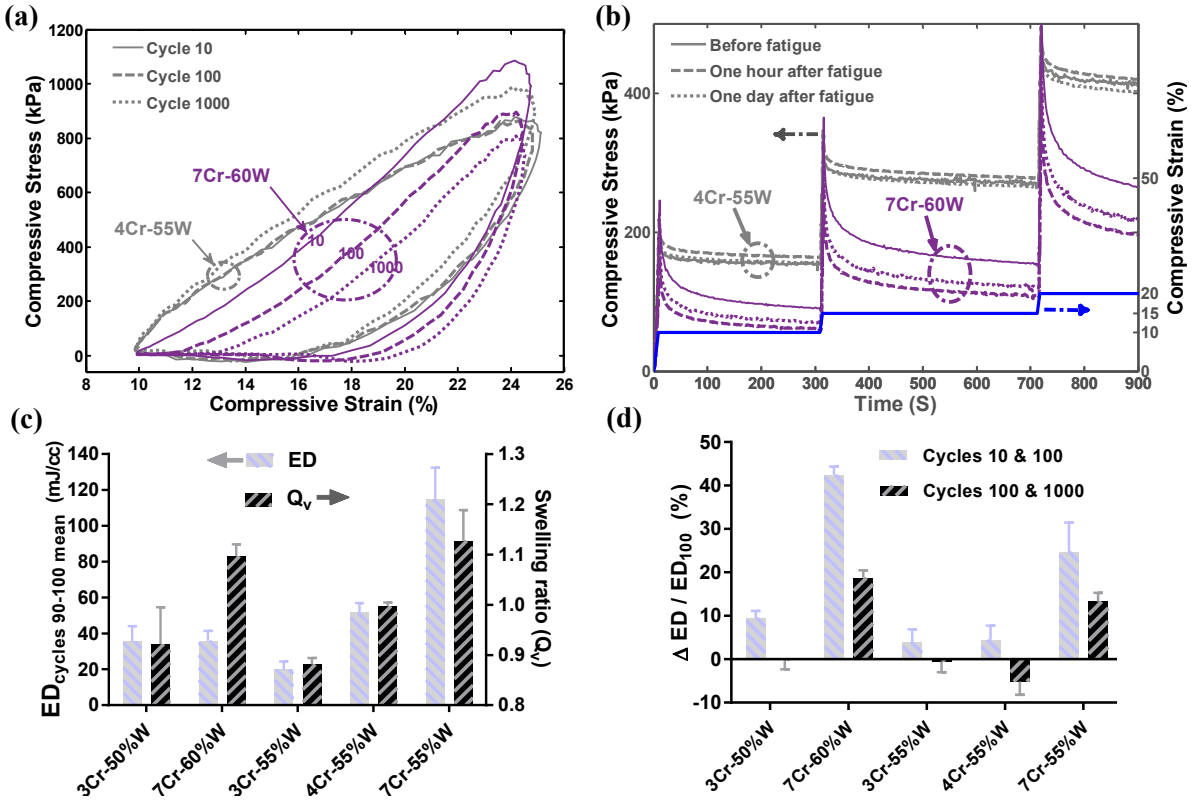

Figure 1. Single network p(HEMA-co-EGDMA) dissipative hydrogels characteristics. (a) Hysteresis loop evolution of 4Cr-55W (gray) and 7Cr-60W (purple) hydrogels during cyclic loading demonstrating the preserved and reduced energy dissipation (ED) level, respectively. (b) Time dependent load support (left axis) of 4Cr-55W (gray) and 7Cr-60W (purple) hydrogels in sequential stress relaxation (ramp and hold strain in blue, right axis) tests before and after fatigue load demonstrating the recoverability of the 4Cr-55W hydrogels and permanent damage for the 7Cr-60W hydrogels. (c) Energy dissipation per unit volume (ED averaged over the 90th to 100th loading cycles, left axis) and swelling ratio (Qv, right axis). (d) The differential value of the energy dissipation

during repeated loadings at 1 Hz for cycle i = 10 and i = 1000 normalized with value of cycle i = 100, $\left(ED_i - ED_{100} / ED_{100}\right)$.

The preserved hysteresis during cyclic loadings arises from a stable dissipation source which is necessary for a robust fatigue behavior. Regardless of the level of stiffness and dissipation in hydrogels, the dissipation origin should be reversible and non-destructive. As shown in Figure 1-c and d, even for hydrogels with similar ED level, e.g. 3Cr-50W and 7Cr-60W, significantly different fatigue performance can be observed. The 7Cr-60W hydrogel shows the weakest fatigue resistance metrics (Figure 1-d and Figure S1-a) despite its lower stiffness (Figure S1-b) than 3Cr-50W, 4Cr-55W and 7Cr-55W hydrogels. Indeed, the higher covalent crosslinking density of 7Cr-55W hydrogel provides a stiffer network and a higher dissipative capacity compared to its 3Cr and 4Cr counterparts prepared with the same water content. However, this strategy of higher covalent crosslinking density comes at the expense of reducing fatigue performance, as 7Cr-55W hydrogel displays a shrunk hysteresis curve during cyclic loading (Figure S1-c). On the other hand, the optimal balance between weak and strong bonds in case of 4Cr-55W hydrogel presents a fairly stiff and dissipative hydrogel with robust fatigue resistance thanks to non-destructive dissipation mechanisms.

A high density of strong covalent bonds can over constrain the hydrogels network, reduce its resilience and hinder the role of reversible bonds for energy dissipation. As a consequence, the network may either experience chains fracture between two crosslinks or bonds rupture at the crosslinking location upon large deformation (Figure 2-a). Both of these processes are highly dissipative, nevertheless causing permanent and not recoverable damage (even after a long recovery time) as it is observed in the reduced load support capability of the 7Cr-60W hydrogel after fatigue loading (Figure 1-b). Alternatively, incorporating a combination of non-destructive sacrificial bonds to a stable yet flexible network could lead to a proper dissipative biomaterial [5]. Therefore, we propose to design hybrid crosslinked SN hydrogels (3Cr-50W and 4Cr-55W) in which the network is sparsely populated by the covalent bonds and efficient contribution of the physical bonds as schematically illustrated in Figure 2-b. Preserving high dissipative capacity with non-destructive processes, however, can only be obtained with an increased polymer fraction (reduced water content) in the hydrogel structure.

The capability of pHEMA hydrogels to form different types of reversible bonds depends on the functionality and mobility of the chains in the network with nano-mesh sizes (Table S1). In particular, polar hydroxyl (OH) and carbonyl (C=O) side chains in pHEMA not only bring

hydrophilicity to the network but also allow hydrogen bonding or pendant group sliding/interaction within the chains. In parallel, hydrophobicity of methyl (CH_3) groups in pHEMA chain acts as a driving force to form a secondary structure via hydrophobic associations. These inherent attributes can lead to formation of physical bonds in pHEMA network, provided that the network flexibility allows it (Figure 2-b). This was confirmed by studying the swelling ratio (Q_v) of the developed hydrogels as shown in Figure 1-c. The 7Cr-55W hydrogel presented a mild swelling in water ($Q_v>1$) meaning that the hydrophilic tendency of the pHEMA chains in a constrained network overcame the chains attraction force that favors deswelling. In contrary, for the 3Cr-55W hydrogel, the shrinking forces prevailed ($Q_v<1$) thanks to the flexibility of its loosely crosslinked network. In case of 4Cr-55W hydrogels, the swelling and shrinking forces almost equilibrated ($Q_v\sim1$), further supporting the inverse correlation between network rigidity and physical bonds formation. It is worth mentioning that we observed a swelling behavior again in 3Cr and 4Cr hydrogels with more than 60% water content (Figure S2). This indicates that the imposed distance within chains mitigates the attraction force functionality despite the network mobility (Figure 2-c).

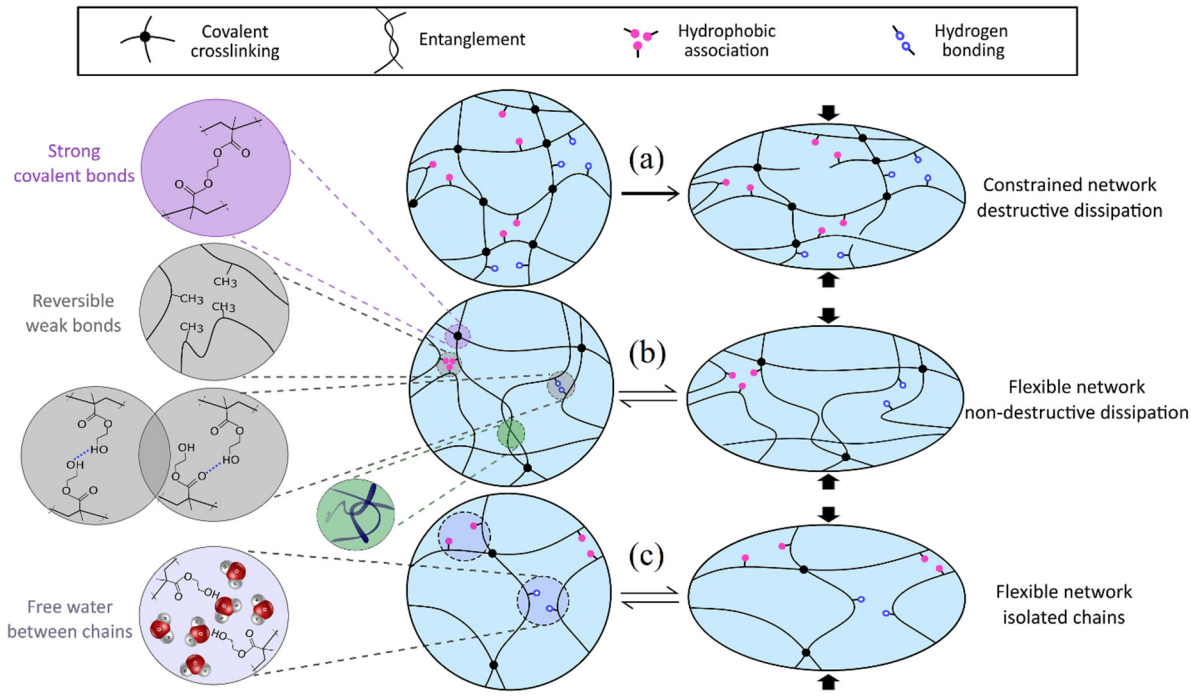

Figure 2. Schematic of the constrained and flexible SN p(HEMA-co-EGDMA) hydrogels. (a) High concentration of covalent bonds lead to destructive dissipation upon an applied deformation. (b) Optimal hybrid crosslinking dissipate input energy non-destructively. (c) Abundant free water within flexible network may however inhibit reversible physical bonds formation leading to isolated chains with inferior mechanical properties.

4-3-2 Porous hydrogels with flow-dependent and flow-independent dissipations

4-3-2-1 Heteroporous structure to enhance mechanical properties

Despite encouraging mechanical properties with IWC less than 60%, the stiffness and dissipative capacity of conventional p(HEMA-co-EGDMA) hydrogels significantly drop (Table 1) with a water content range close to the cartilage (65-80%) [7, 8]. Imposing a large amount of water in conventional pHEMA hydrogels not only loosens their networks and prevents adequate physical bonds formation [31, 35] but also may lead to phase separation with elastically inactive chains within the network [36]. In general, the higher portion of free water between chains decreases the corresponding potential for energy dissipation within the pHEMA network with isolated chains (Figure 2-c). In analogy, the amount of free water between the collagen and mineral phase of cortical bone and the physical bonds participation between tropocollagen molecules have a significant influence on the tissue mechanical characteristics [37]. Indeed, the presence of heterogeneous water compartments of different length scales (pore and bound water) within constituents of load bearing tissues maintains their optimal mechanical performance [7, 37]. Based on these observations, we propose to develop heteroporous hydrogels with a dual porosity design encompassing nano meshes and meso pores (Figure 3).

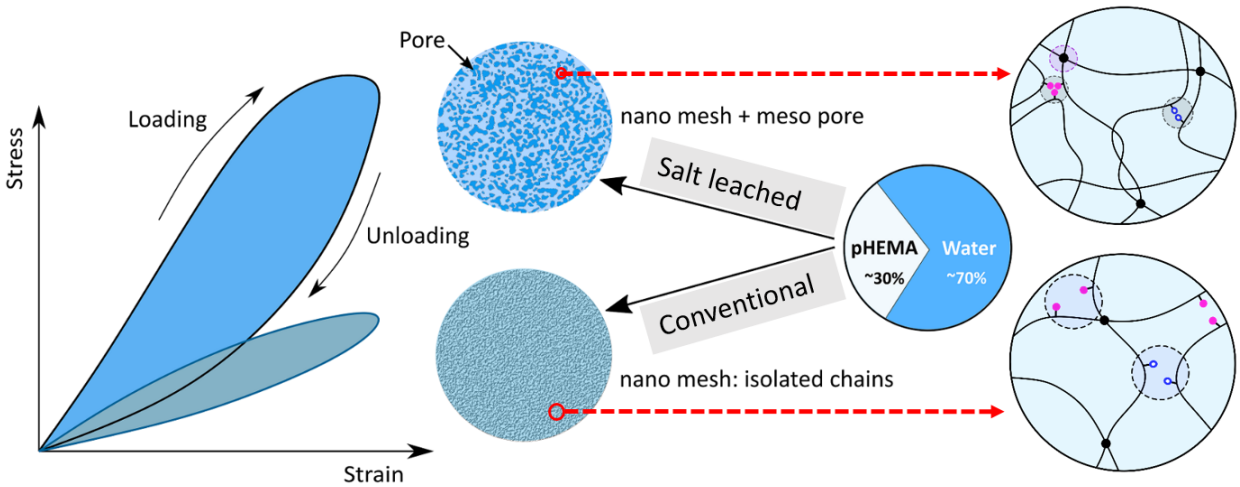

Figure 3. Heteroporous (obtained by salt leaching) versus conventional hydrogel design strategies in 70% water content condition (mimicking cartilage tissue). The patterned water distribution in different length scales lead to superior mechanical properties for salt-leached pHEMA hydrogels compared to conventional hydrogels in 70% water content.

Through the dual porosity design, not only water content close to that of cartilage is obtained for the hydrogel without isolated chains, but also different dissipative mechanisms of cartilage

can be mimicked. Hereafter, the heteroporous p(HEMA-co-EGDMA) hydrogels are simply defined as porous hydrogels with xCr-size configuration, where x stands for EGDMA molar ratio to HEMA, and size represents the size of the meso pores (extra fine, fine, medium, and coarse). By following the dual porosity strategy, we discovered that the stiffness and dissipative capacity of the porous p(HEMA-co-EGDMA) hydrogels, containing around 70% water, are significantly higher than their corresponding conventional hydrogels (Table 1). It was also observed that the mechanical properties of porous hydrogels could be further enhanced by changing the initiator of the polymerization process (Figure S3).

Table 1. Mechanical properties of conventional and heteroporous p(HEMA-co-EGDMA) hydrogels containing around 70% water in equilibrium state corresponding to the cartilage physiological water content.

Hydrogel	EWC (%)	ED (mJ/cc)	Eeq. (kPa)
3Cr-67W: conventional	68±1	5.5±0.51	148.05±9.17
3Cr Ext. Fine: heteroporous	69±1	12.55±0.72*	361.33±30.66*
4Cr-65W: conventional	67±1	7.51±1.03	293.75±54.58
4Cr-Ext. Fine: heteroporous	69±1	14.52±1.11*	506.41±67.76*

EWC: Equilibrium water content.
ED: Energy dissipation (10% static+15% at 1 Hz).
Eeq.: Equilibrium Young's modulus (10-20% strain).
* Significant difference between porous and corresponding conventional groups ($p < 0.01$, n=4).

4-3-2-2 Evaluation of dissipation mechanisms and characteristics of porous hydrogels

In porous p(HEMA-co-EGDMA) hydrogels, the intrinsic dissipation of solid network can be supplemented with a fluidic frictional drag dissipation. Flow field pressure and velocity in a porous medium are governed by its permeability which takes into account the contribution of important morphological features within the structure [38]. To impose different levels of solid-fluid interactions upon loading, we therefore modulate the permeability of the porous hydrogels by controlling the pore size. A multi-mechanism design for dissipative hydrogels can therefore combine different sources of flow-independent dissipation (either reversible or irreversible) as well as frictional drag forces. To this end, we developed 5 groups of porous hydrogels presenting different Cr densities and pore sizes while keeping the water content at 70% (Table S2). The morphological characteristics of the developed porous hydrogels are illustrated in Figure 4. We found that different degrees of stiffness, dissipation (Figure 5-a), and load support (Figure S5) are achievable only by changing the architecture of the hydrogels. Our results also showed that energy dissipation and stiffness are directly related to the Cr density and indirectly to the permeability (Figure 5-a) of the hydrogel. In a permeable hydrogel (coarse pore size, $k \sim 10^{-12}$), the flow dependent dissipation contribution is minor,

while it is a dominant dissipation source in poorly permeable hydrogel (finer pores, $k \leq 10^{-14}$). In parallel, Cr density modulates the intrinsic dissipation source of the polymeric network as discussed before.

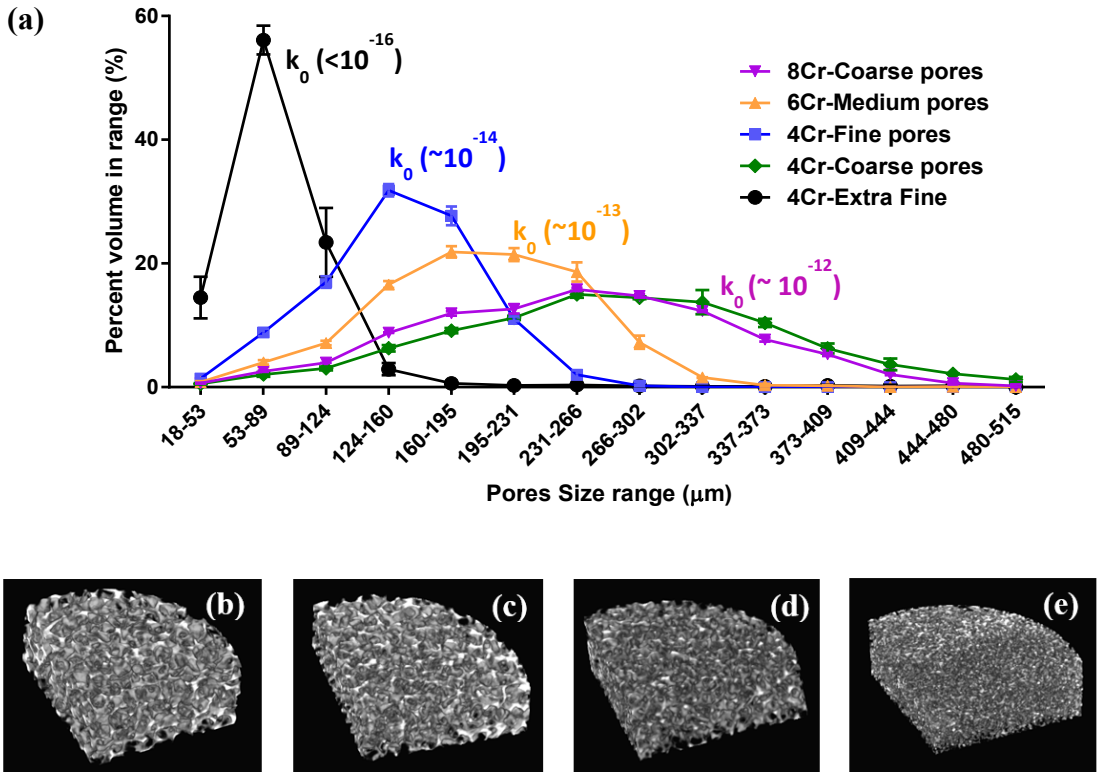

Figure 4. Porous hydrogels morphological characteristics. (a) Pores size distribution of the developed porous hydrogels determined by analysis of µCT scans and corresponding strain-free permeability (k_0). (b-e) Created three dimensional (3D) images using reconstructed µCT scans for porous hydrogel having coarse, medium, fine, and extra fine pores, respectively. Since the 3D images were almost the same for 4Cr and 8Cr-Coarse pores, 4Cr-Coarse image was not illustrated.

Via control of the hydrogel's permeability and material composition, we combined the fluidic and solid network dissipation sources. As shown in Figure 5-a, three porous hydrogels (4Cr-Fine, 6Cr-Medium and 8Cr-Coarse) present similar dissipation levels to human articular cartilage when subjected to a walking-like cyclic compression [9, 39] (defined as "standard regime": 10% static strain + 10% dynamic strain at 1 Hz). The contribution of the dissipation sources in these hydrogels was evaluated by computing the ratio of the ED obtained with lower frequency and larger dynamic strain (defined as "validation regime": 5% static strain + 15% dynamic strain at 0.1 Hz) to the ED of standard regime. Being a function of the loading rate, velocity of the fluid phase is decreased in the "validation regime" resulting in lower frictional drag dissipation. Accordingly, in the 4Cr-Fine hydrogel with poor permeability and effective contribution of flow-dependent dissipation, we observed a lower ED in the

"validation regime" compared to the "standard regime" (Figure 5-c, ED ratio ~ 0.7). Additionally, by applying a larger cyclic strain, an increased dynamic deformation is generated within the polymeric network, which in turn leads to a higher flow-independent dissipation. Therefore, the 8Cr-Coarse hydrogel with a dominant solid intrinsic dissipation showed higher ED level in the "validation regime" compared to the "standard regime" (Figure 5-c, ED ratio ~ 1.2). Finally, in the intermediate condition of the 6Cr-Medium hydrogel, no significant difference in the level of energy dissipation was observed between the two applied loading regimes. This indicates that the influence of the decreased frequency and the increased dynamic strain compensate each other in the 6Cr-Medium hydrogel confirming the contribution of the flow-dependent and the flow-independent dissipation sources. Additionally, to validate the inverse correlation of the flow-dependent dissipation source to the permeability, we increased the viscosity of the fluidic phase of the hydrogel by using glycerol instead of water for the ED evaluation. Indeed, the ED level was further amplified with glycerol compared to water (Figure S6) for the 4Cr-Fine hydrogel having a lower permeability compared to the 8Cr-Coarse hydrogel.

To further gain insight on the respective contribution of the solid and fluid phases on 8Cr-Coarse and 4Cr-Fine hydrogels viscoelastic behavior, a semi-inverse poro-viscoelastic model was developed following an iterative optimization process (Figure S7). It was shown that the release of the pressurized fluid is mainly contributing to the transient stress in the porous 4Cr-Fine hydrogels which are poorly permeable, while flow-dependent viscoelasticity has no influence for porous 8Cr-Coarse hydrogels with high permeability (Figure S8). In contrary, flow-independent viscoelasticity has minor effect on transient stress for 4Cr-Fine hydrogels, despite its dominant role for 8Cr-Coarse hydrogels.

While showing encouraging fatigue resistance metrics (Figure 5-b), the mechanical properties of 4Cr-Coarse hydrogel (ED and E_{eq}) are inferior compared to the cartilage ones (Figure 5-a). Our results showed that the dissipation and stiffness values corresponding to the cartilage ones could be either obtained by an increased Cr density of the network or by a reduced permeability of the porous structure. However, the obtained fatigue performance could be significantly different depending on the dominant mechanism of dissipation. Indeed, the contribution of destructive flow-independent processes (bonds rupture or chain fracture) is intensified for the 8Cr-Coarse hydrogels. In this case, the differential normalized value of the energy dissipation during cyclic deformation is about 65% for cycles 10 to 100 indicating

weak fatigue resistance (Figure 5-b). To better examine the effect of the irreversible process on the hydrogels mechanical behavior, the ED recoverability (EDr) was compared for two identical cyclic loading experiments in two consecutive days (Figure S9). We observed partial ED recovery of the 8Cr-Coarse hydrogels (Figure 5-d, EDr ~0.8) meaning that shrunk hysteresis in this case is partly influenced by the reversible processes. Moreover, to scrutinize hydrogels long-term durability, the ratio of load support (R_{ls}) in equilibrium state was evaluated before and after fatigue test with 3600 loading cycles. Despite presenting a slight recovery by a longer resting time, a significant drop on equilibrium load support (R_{ls}~2.5) was detected at 10% strain level for the 8Cr-Coarse samples (Figure 5-e). The R_{ls} value has almost linearly reached to 1.5 at 20% strain in these hydrogels.

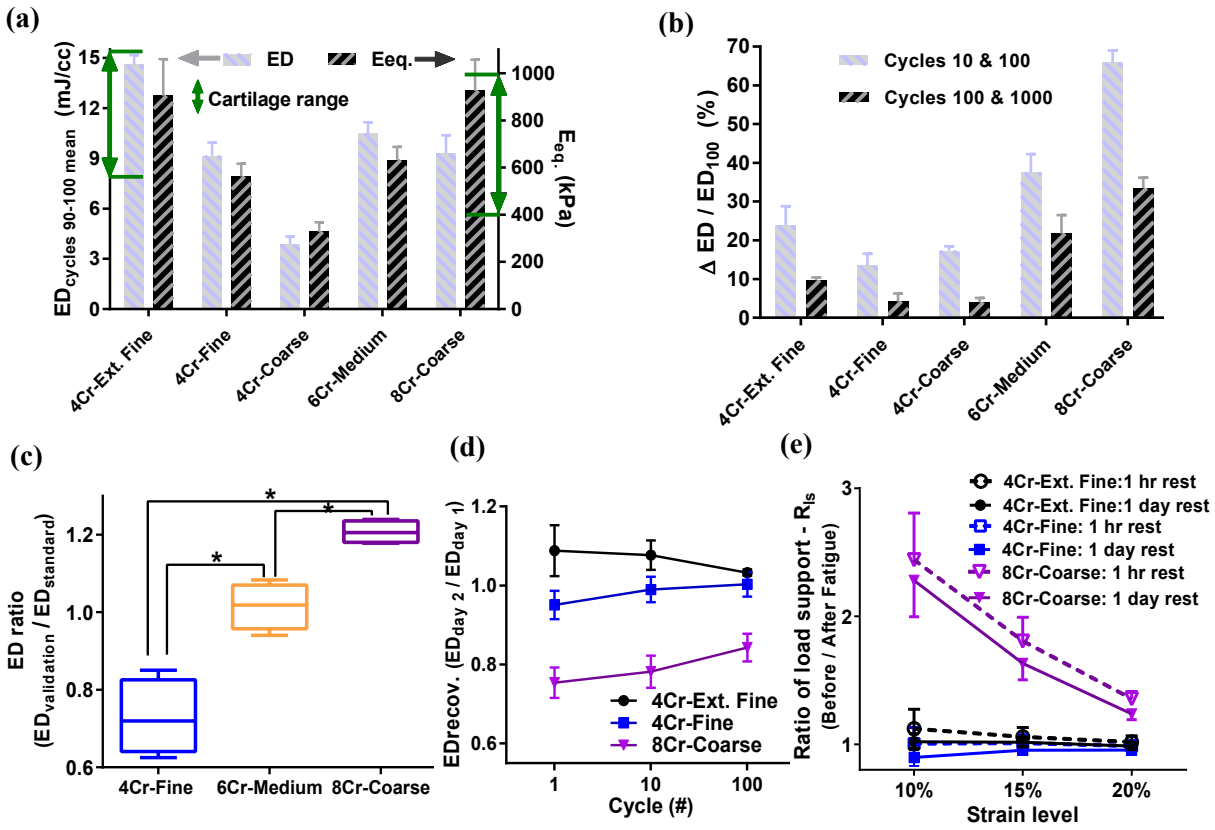

Figure 5. Mechanical characteristics of porous p(HEMA-co-EGDMA) hydrogels containing 70% water corresponding to the physiological cartilage value. (a) Energy dissipation level (ED, left axis) and equilibrium Young's modulus (Eeq, right axis) of the developed porous hydrogel along with the corresponding values for the cartilage in range of 10 to 20% strain [1, 9, 12, 40, 41]. (b) The differential normalized value of the energy dissipation upon standard loading regime for cycle 10 and 1000 with respect to cycle 100 as the reference cycle $(ED_i - ED_{100}/ED_{100})$. (c) Energy dissipation ratio of validation to standard loading regimes for porous hydrogels with similar dissipative capacity but different dissipation mechanisms (* significant difference with $p < 0.01$; n =4). (d) Recoverability of energy dissipation upon standard loading regime in two consecutive days while resting overnight in water after the first test. (e) Equilibrium load support ratio in sequential stress relaxation tests before and after fatigue loads.

In contrast, the non-destructive flow-dependent mechanism in the 4Cr-Fine and 4Cr-Ext.Fine porous hydrogels not only recapitulated cartilage mechanical properties, but also maintained hydrogels fatigue resistance and durability (Figure 5-b, d & e). Regardless of a slight hysteresis evolution (Figure 5-b) in all 4Cr compositions, the ED level (Figure 5-d, EDr ~1) and load support capability (Figure 5-e, R_{ls}~1) could be fully recovered. This means that non-destructive processes, such as reversible rearrangement of the network or fluid exchange, govern the hysteresis evolution in 4Cr porous hydrogels during cyclic loading. These self-healable dissipation sources can therefore protect these hydrogels over cycles of dynamic loading due to their recoverable nature (Figure S9). The developed 4Cr porous hydrogels with coarse, fine and extra fine pores have respectively similar morphology (Figure 4), dissipation level and stiffness (Figure 5-a) to 8Cr-Coarse porous hydrogel. Accordingly, it could be concluded that the fatigue resistance performance is not a function of morphology, dissipation level, and stiffness of the viscoelastic hydrogels but rather depends on the nature of dissipation source.

4-3-3 Mechanobiological performance of hydrogels with different dissipation mechanisms

Dynamic compression is the most widely employed loading regime in cartilage tissue engineering and mechanobiology, where stimulations up to 20% compressive strain have promoted chondrogenesis [39, 42, 43]. A direct correlation was also reported between the ED level of cell-seeded hydrogels and chondrogenic expression following cyclic compression [9]. They showed chondrogenic markers are at highest level for scaffold with dissipation level of healthy cartilage. In a recent study, hydrogels presenting a faster stress relaxation under compression, promoted cartilage formation [10], confirming the role of viscoelastic attributes on mechanobiology of cartilage [8, 9, 44]. We propose that the enhanced mechanical performance obtained by preserved hysteresis might be further applied to mechanobiological function of hydrogels. For this purpose, we examined the intracellular transcriptions of human chondro-progenitor cells [45] embedded in the 4Cr-Fine and 8Cr-Coarse dissipative hydrogels following mechanical stimulation. These two groups of hydrogels have a similar ED value (Figure 5-a), which is in the range of healthy cartilage, even though their respective ED originates from different sources. Having confirmed cells penetration and viability up to 10 days in the developed porous hydrogels (Figure S10 and S11), we performed an *in vitro*

mechanobiological experiment consisting of intermittent cyclic compressions (Figure S12-a) to evaluate cells differentiation.

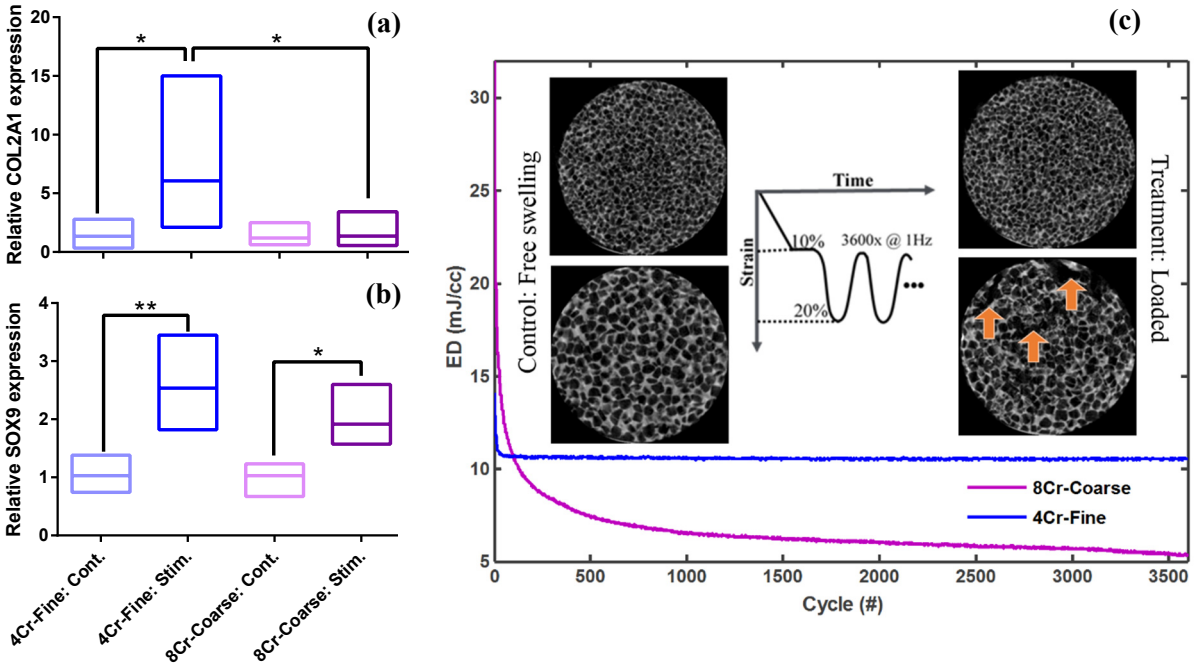

Figure 6. Chondrogenic markers expression for human chondro-progenitor cells when sedded into two types of porous hydrogel presenting similar dissipative capacity and water content to articular cartilage. (a-b) COL2A1 and SOX9 relative fold increase (depicted as mean value with minimum and maximum ranges) following cyclic compression in treatment (Stim.) group with respect to free swelling control (Cont.) group (* and ** mean significant difference with $p < 0.05$ and $p<0.01$, respectively; n =4). (c) Evolution of the energy dissipation level following cyclic compression for the two types of dissipative hydrogel undergoing mechanical stimulation. Internal fissures (shown by arrows) appeared inside the 8Cr-Coarse hydrogel structure after repeated loading.

Upregulation of chondrogenic markers (Collagen-2a1 (COL2A1), SRY-box 9 (SOX9), and Aggrecan (ACAN)) were observed in the two groups of dissipative hydrogels by mechanical stimulation (Stim.) relative to corresponding free swelling control groups (Cont.). However, following the mechanical stimulation, a higher relative fold increase was always observed for chondrogenic markers (Figure 6-a and b, Figure S12-b) in the 4Cr-Fine constructs compared to the 8Cr-Coarse hydrogels. Given different mechanisms of energy dissipation, the seeded cells in the two hydrogel groups did not receive the same physical signals despite applying a similar external loading on them.

In the hydrogel group deprived of reversible dissipation sources (8Cr-Coarse), the required physical cues cannot be kept at an appropriate chondro-inductive level via a constant loading regime over the entire period of the stimulation in particular due to internal damages in the hydrogel (Figure 6-c). *A contrario*, for the hydrogel presenting a preserved hysteresis loop (4Cr-Fine), the stimulation could be stabilized after a few preconditioning cycles. This latter

hydrogel could even sustain a 70% compressive strain without presenting a plastic deformation or defects unlike the 8Cr-Coarse hydrogel (Figure S13). Mechanical hysteresis has been recently proposed to be an overarching mechanobiological variable to encompass the solid and fluid related physical cues [9, 44]. Therefore, if the level of ED close to the one of cartilage is the target mechanobiological variable when applying a dynamic loading, hydrogels possessing non-destructive mechanisms of dissipation should be designed.

4-4 Conclusion

By developing hydrogels in which the flow-dependent and flow-independent dissipation processes can be independently controlled under cyclic loading, we showed that fatigue resistant hydrogels can be developed presenting similar extent of compressive stiffness, dissipation, and water content to cartilage. In these hydrogels, the reversible solid intrinsic dissipation sources act synergistically with the flow-induced dissipation source to damp the transferred mechanical energy to the hydrogels and to allow them sustaining cyclic loadings. While hydrogels having a dissipation mainly originating from non-destructive processes present a preserved hysteresis with a robust load support performance, the hysteresis loop in hydrogels with destructive dissipation is shrinking over of fatigue loading cycles causing a reduced load support capability. In the present study, it is further demonstrated that the mechanism of dissipation could play an important role in the chondrogenesis pathway. Indeed, chondrocytes differentiation is favored by the conditions, which mimic more similarly the cartilage extracellular characteristics (low permeability and mobile network). In such a local mechanical environment, different mechanosensitive elements including nucleus, ion channels, primary cilium, and cytoskeleton can be activated by an adequate frictional drag force, developed hydrostatic fluid pressure, and matrix deformation [8, 42]. The understanding and consequently the control of the different dissipation sources in the development of hydrogels open the possibility to obtain hydrogels with increased mechanical properties to be used in demanding mechanical loading environments and even to bring unforeseen new functionalities such as for example the control of cells fate for tissue engineering applications.

4-5 Experimental Section

Precursors of pHEMA hydrogels were prepared with different concentrations of EGDMA and bi-distillated water with respect to HEMA content. By adding the DPAP photo-initiator (0.1% of mol HEMA) to the mixture, the solution was transferred to cylindrical transparent molds

(6 mm diameter and 2.5 mm thickness) and covered with narrow microscope glass. After ultra violet (UV) polymerization for 15 min (365 nm, 2 mW/cm^2), as-prepared conventional hydrogels were used for swelling study and then for mechanical characterization once hydrogel disks equilibrated in water. Salt leaching method was employed for porous hydrogels fabrication following UV radiation or heating polymerization (details in Supplemental data) of target HEMA-EGDMA precursor inside Teflon molds containing sieved salt particles (Table S2). To remove entrapped salt particles, samples were kept in stirred water for one week during which the water was changed several time before saturation. The diameter and thickness of the hydrated porous hydrogels were sized using a punch and home-made cutting tool (8 mm, 2.5 mm).

The volumetric swelling ratio of the conventional hydrogels was calculated by measuring the volume of as prepared and swollen samples according to $Q_v = \frac{V_{swollen}}{V_{as\ prepared}}$. For this purpose, as prepared and swollen samples were weighted in air (W_{air}) and ethanol ($W_{eth.}$) and their corresponding volume was calculated as $V = \frac{(W_{air} - W_{eth.})}{\rho_{ethanol}}$ based on Archimedes' buoyancy principle. Similarly, the equilibrium water content (EWC) of the developed hydrogels (either homopororus or heteroporous) was determined via the volume of the hydrated ($W_{air}^{swollen}$) and weight of the dried (W_{dried}) samples as $EWC = \frac{(W_{air}^{swollen} - W_{dried})/\rho_{H2O}}{V_{swollen}}$. Micro-computed tomography (μCT Skyscan 1176, Bruker, Kontich, Belgium) scans of freeze-dried samples were employed for the morphological analysis. Pores distribution was evaluated by CTAn software (Bruker) and 3D images were created by AMIRA software (FEI Visualization Sciences Group, Burlington, MA, USA) using reconstructed μCT scans.

By measuring force and displacement during cyclic compression and calculating the hysteresis area upon loading and unloading, we experimentally quantified the amount of energy dissipation. Three sequential unconfined compressions and hold steps were applied on samples to evaluate time dependent load support over stress relaxation test (Figure S1 and Figure S4). Additionally, we utilized corresponding relaxed stress and strain values to evaluate the slope of the best linear fit as equilibrium Young modulus (Eeq.). Complete description of methods for mechanical and structural characterization of hydrogels can be found in supporting information.

The finite element model was developed using COMSOL Multiphysics (COMSOL Inc., Burlington, MA, USA) by employing Darcy's Law and Solid Mechanics modules to study the time dependent mechanical behavior of the porous hydrogels. Different parameters for a poro-viscoelastic model are required including equilibrium Young modulus (Eeq), strain dependent permeability (k(ε)), porosity (φ), Poisson ration (ν), and relaxation function (G(t)) which is usually approximated by a Prony Series (e.g., $G(t)= G + \sum G_i e^{-t/\tau i}$). Having measured Eeq, k(ε), ν and φ by relevant experiments, relaxation moduli (G_i) and times (τ_i) were estimated as reported in Table S3 by an iterative process using particle swarm optimization (detail in supplemental data-Figure S7) to obtain the same trend of stress relaxation for the model and the experimental data.

For mechanobiological study, cells infusion was carried out by an optimized compression released induced suction (CRIS) method as described in our previous work [46]. Hydrogels were then pre-cultured for 3 days in proliferation medium inside a standard incubator (37°C, 5% CO_2). After this step, differentiation medium was used and starting from day 5, the mechanical stimulation in standard loading regime was applied on 2 groups of porous hydrogels in a home-made compression bioreactor [9]. The stimulation time was 2 hours per day for a period of 4 days, while the corresponding control groups were preserved in equivalent condition but without applied loading. Detail process of mechanobiological experiment and analysis can be found in supporting information (Figure S12 and Table S4). The statistical significance between different study groups was determined by Student t-test when required (n=4).

Supporting Information

Corresponding supplementary data can be found at the end of this chapter.

4-6 Acknowledgments

We thank the Regenerative Therapy Unit of University Hospital of Lausanne (CHUV) and in particular Prof. Lee Ann Applegate for providing us human chondro-progenitor cells. This work was supported by the Swiss National Science Foundation (#310030_149969/1 and #CR23I3_159301).

4-7 References

[1] Moutos FT, Freed LE, Guilak F. A biomimetic three-dimensional woven composite scaffold for functional tissue engineering of cartilage. Nat Mater 2007;6:162.

[2] Liao IC, Moutos FT, Estes BT, Zhao X, Guilak F. Composite three-dimensional woven scaffolds with interpenetrating network hydrogels to create functional synthetic articular cartilage. Adv Funct Mater 2013;23:5833-9.

[3] Sun TL, Kurokawa T, Kuroda S, Ihsan AB, Akasaki T, Sato K, et al. Physical hydrogels composed of polyampholytes demonstrate high toughness and viscoelasticity. Nat Mater 2013;12:932.

[4] Chen Q, Zhu L, Chen H, Yan H, Huang L, Yang J, et al. A Novel Design Strategy for Fully Physically Linked Double Network Hydrogels with Tough, Fatigue Resistant, and Self-Healing Properties. Adv Funct Mater 2015;25:1598-607.

[5] Zhao X. Multi-scale multi-mechanism design of tough hydrogels: building dissipation into stretchy networks. Soft Matter 2014;10:672-87.

[6] Long R, Hui C-Y. Fracture toughness of hydrogels: measurement and interpretation. Soft Matter 2016;12:8069-86.

[7] Mow VC, Ratcliffe A, Poole AR. Cartilage and diarthrodial joints as paradigms for hierarchical materials and structures. Biomaterials 1992;13:67-97.

[8] Mow VC, Wang CC, Hung CT. The extracellular matrix, interstitial fluid and ions as a mechanical signal transducer in articular cartilage. Osteoarthr Cartil 1999;7:41-58.

[9] Abdel-Sayed P, Darwiche SE, Kettenberger U, Pioletti DP. The role of energy dissipation of polymeric scaffolds in the mechanobiological modulation of chondrogenic expression. Biomaterials 2014;35:1890-7.

[10] Lee H-p, Gu L, Mooney DJ, Levenston ME, Chaudhuri O. Mechanical confinement regulates cartilage matrix formation by chondrocytes. Nat Mater 2017;16:1243.

[11] Chaudhuri O, Gu L, Klumpers D, Darnell M, Bencherif SA, Weaver JC, et al. Hydrogels with tunable stress relaxation regulate stem cell fate and activity. Nat Mater 2016;15:326-34.

[12] Ateshian G, Warden W, Kim J, Grelsamer R, Mow V. Finite deformation biphasic material properties of bovine articular cartilage from confined compression experiments. J Biomech 1997;30:1157-64.

[13] Stok K, Oloyede A. Conceptual fracture parameters for articular cartilage. Clin Biomech 2007;22:725-35.

[14] Gong JP, Katsuyama Y, Kurokawa T, Osada Y. Double-network hydrogels with extremely high mechanical strength. Adv Mater 2003;15:1155-8.

[15] Gong JP. Materials both tough and soft. Science 2014;344:161-2.

[16] Li J, Illeperuma WR, Suo Z, Vlassak JJ. Hybrid hydrogels with extremely high stiffness and toughness. ACS Macro Letters 2014;3:520-3.

[17] Li J, Suo Z, Vlassak JJ. Stiff, strong, and tough hydrogels with good chemical stability. Journal of Materials Chemistry B 2014;2:6708-13.

[18] Henderson KJ, Zhou TC, Otim KJ, Shull KR. Ionically cross-linked triblock copolymer hydrogels with high strength. Macromolecules 2010;43:6193-201.

[19] Sun Y-n, Gao G-r, Du G-l, Cheng Y-j, Fu J. Super tough, ultrastretchable, and thermoresponsive hydrogels with functionalized triblock copolymer micelles as macro-cross-linkers. ACS Macro Letters 2014;3:496-500.

[20] Luo F, Sun TL, Nakajima T, Kurokawa T, Zhao Y, Sato K, et al. Oppositely Charged Polyelectrolytes Form Tough, Self-Healing, and Rebuildable Hydrogels. Adv Mater 2015;27:2722-7.

[21] Abdurrahmanoglu S, Can V, Okay O. Design of high-toughness polyacrylamide hydrogels by hydrophobic modification. Polymer 2009;50:5449-55.

[22] Hao J, Weiss R. Viscoelastic and mechanical behavior of hydrophobically modified hydrogels. Macromolecules 2011;44:9390-8.

[23] Zhang Y, Gao H, Wang H, Xu Z, Chen X, Liu B, et al. Radiopaque Highly Stiff and Tough Shape Memory Hydrogel Microcoils for Permanent Embolization of Arteries. Adv Funct Mater 2018;28:1705962.

[24] Sun J-Y, Zhao X, Illeperuma WR, Chaudhuri O, Oh KH, Mooney DJ, et al. Highly stretchable and tough hydrogels. Nature 2012;489:133.

[25] Hong S, Sycks D, Chan HF, Lin S, Lopez GP, Guilak F, et al. 3D printing of highly stretchable and tough hydrogels into complex, cellularized structures. Adv Mater 2015;27:4035-40.

[26] Hou J, Ren X, Guan S, Duan L, Gao GH, Kuai Y, et al. Rapidly recoverable, anti-fatigue, super-tough double-network hydrogels reinforced by macromolecular microspheres. Soft matter 2017;13:1357-63.

[27] Yuan N, Xu L, Wang H, Fu Y, Zhang Z, Liu L, et al. Dual physically cross-linked double network hydrogels with high mechanical strength, fatigue resistance, notch-insensitivity, and self-healing properties. ACS Appl Mater Interfaces 2016;8:34034-44.

[28] Zhang YS, Khademhosseini A. Advances in engineering hydrogels. Science 2017;356:eaaf3627.

[29] Baumberger T, Caroli C, Martina D. Solvent control of crack dynamics in a reversible hydrogel. Nat Mater 2006;5:552.

[30] Refojo MF. Hydrophobic interaction in poly (2-hydroxyethyl methacrylate) homogeneous hydrogel. J Polym Sci, Part A: Polym Chem 1967;5:3103-13.

[31] Morita S. Hydrogen-bonds structure in poly (2-hydroxyethyl methacrylate) studied by temperature-dependent infrared spectroscopy. Front Chem 2014;2:10.

[32] Peppas NA, Moynihan HJ, Lucht LM. The structure of highly crosslinked poly (2-hydroxyethyl methacrylate) hydrogels. J Biomed Mater Res A 1985;19:397-411.

[33] Moghadam MN, Pioletti DP. Improving hydrogels′ toughness by increasing the dissipative properties of their network. J Mech Behav Biomed Mater 2015;41:161-7.

[34] Kamata H, Akagi Y, Kayasuga-Kariya Y, Chung U-i, Sakai T. "Nonswellable" hydrogel without mechanical hysteresis. Science 2014;343:873-5.

[35] Choi S, Jhon MS, Andrade JD. Nature of water in synthetic hydrogels: III. Dilatometry, specific conductivity, and dielectric relaxation of poly (2, 3-dihydroxypropyl methacrylate). Journal of Colloid and Interface Science 1977;61:1-8.

[36] Karpushkin E, Dušková-Smrčková M, Šlouf M, Dušek K. Rheology and porosity control of poly (2-hydroxyethyl methacrylate) hydrogels. Polymer 2013;54:661-72.

[37] Granke M, Does MD, Nyman JS. The role of water compartments in the material properties of cortical bone. Calcif Tissue Int 2015;97:292-307.

[38] Nasrollahzadeh N, Pioletti DP. Experimental method to characterize the strain dependent permeability of tissue engineering scaffolds. J Biomech 2016;49:3749-52.

[39] Salinas EY, Hu JC, Athanasiou K. A Guide for Using Mechanical Stimulation to Enhance Tissue-Engineered Articular Cartilage Properties. Tissue Eng,Part B 2018.

[40] Boschetti F, Pennati G, Gervaso F, Peretti GM, Dubini G. Biomechanical properties of human articular cartilage under compressive loads. Biorheology 2004;41:159-66.

[41] Abdel-Sayed P, Moghadam MN, Salomir R, Tchernin D, Pioletti DP. Intrinsic viscoelasticity increases temperature in knee cartilage under physiological loading. J Mech Behav Biomed Mater 2014;30:123-30.

[42] O'Conor CJ, Case N, Guilak F. Mechanical regulation of chondrogenesis. Stem Cell Res Ther 2013;4:61.

[43] Finlay S, Seedhom BB, Carey DO, Bulpitt AJ, Treanor DE, Kirkham J. In Vitro Engineering of High Modulus Cartilage-Like Constructs. Tissue Eng,Part C 2016;22:382-97.

[44] Abdel-Sayed P, Pioletti DP. Strategies for improving the repair of focal cartilage defects. Nanomedicine 2015;10:2893-905.

[45] Darwiche S, Scaletta C, Raffoul W, Pioletti DP, Applegate LA. Epiphyseal chondroprogenitors provide a stable cell source for cartilage cell therapy. Cell Medicine 2012;4:23-32.

[46] Nasrollahzadeh N, Applegate LA, Pioletti DP. Development of an Effective Cell Seeding Technique: Simulation, Implementation, and Analysis of Contributing Factors. Tissue Eng,Part C 2017;23:485-96.

Supplemental Data for Chapter 4

Conventional hydrogels mechanical characterization

The equilibrium Young modulus (Eeq.) was measured by Instron uniaxial testing machine (Instron E3000, Norwood, Massachusetts, USA) through 3 sequential unconfined compressions-hold steps at 10, 15 and 20% compressive strains. Initial cross section area and thickness of samples were used to calculate stress-strain values from raw load-displacement data. The level of energy dissipation (ED) was obtained by applying 15% cyclic compression at 1 Hz over 10% static strain on hydrated samples in a water bath. A custom-written MATLAB script (The MathWorks, Natick, MA, USA) was used to extract the enclosed hysteresis area from the load-displacement (stress-strain) graphs.

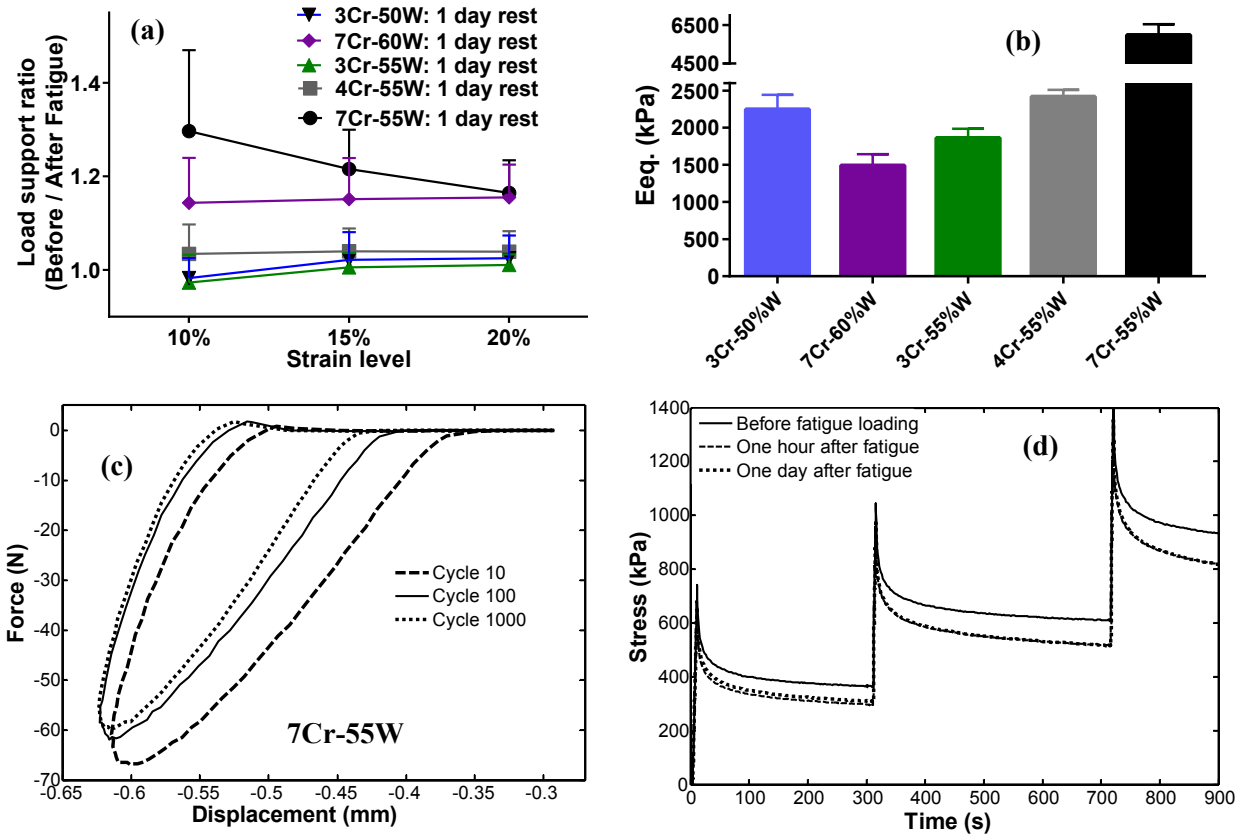

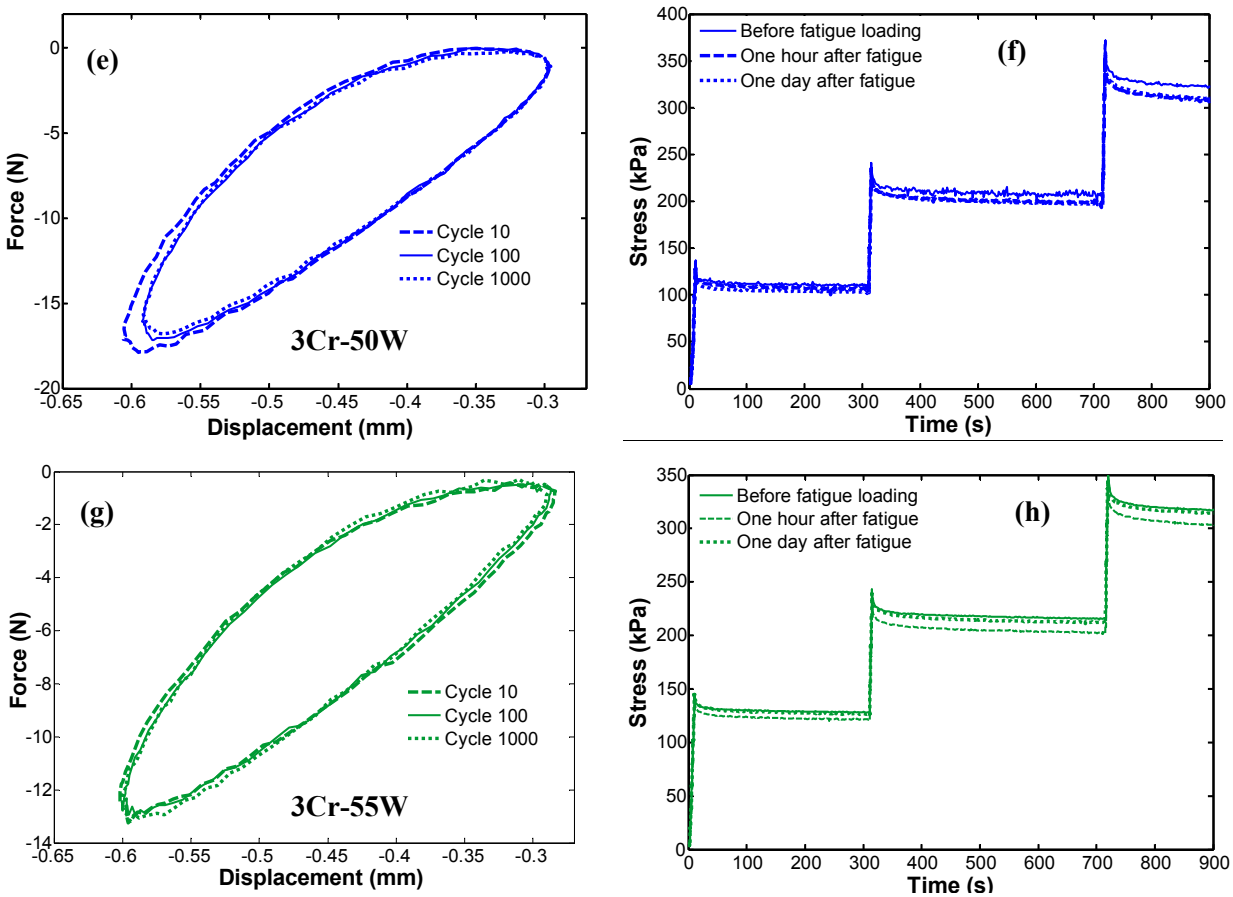

Figure S1. Homogeneous SN p(HEMA-co-EGDMA) hydrogels mechanical characteristics. (a) Equilibrium load support ratio before to after fatigue load in sequential stress relaxation tests (n=3 per group). (b) Equilibrium Young modulus (Eeq.) of the developed hydrogels (n=4 per group). (c,e & g) Representative hysteresis loop evolution for 7Cr-55W (black) 3Cr-50W (blue) and 3Cr-55W (green) during cyclic loading (Note: the representative curves for 7Cr-60W and 4Cr-55W were reported in the main part). (d, f and h) Representative time dependent load support of 7Cr-55W (black) 3Cr-50W (blue) and 3Cr-55W (green) in sequential stress relaxation (ramp and hold strain) tests before and after fatigue load of 3600 cycles (10% static strain + 15% dynamic strain at 1 Hz).

Evaluation of conventional hydrogels structural characteristics

By evaluating the polymer volume fraction immediately after polymerization (as prepared) in relaxed state (v_{ap}) and after swelling in water (v_{sw}), the average molecular weight between crosslinks (M_C) for hydrogel prepared in the presence of water can be determined using modified Flory–Rehner theory [1] by (S1):

$$\frac{1}{M_c} = \frac{2}{M_n} - \frac{\left(\frac{\bar{v}}{V_1}\right)[\ln(1 - v_{sw}) + v_{sw} + \chi {v_{sw}}^2]}{v_{ap}\left[\left(\frac{v_{sw}}{v_{ap}}\right)^{1/3} - \left(\frac{v_{sw}}{2v_{ap}}\right)\right]} \qquad \text{(S1)}$$

where M_n is the average chains length (considered here equal to 400 unit monomer of HEMA, M_n≈54000 g/mol) , $\bar{v}$ is the specific volume of polymer, V_1 is the molar volume of water (18.03 mL), and χ is the thermodynamics interaction parameter determined as:

$$\chi = 0.320 + 0.904\upsilon_{sw} \quad \text{(S2)}$$

The mesh size can then be calculated using equation (S3):

$$\xi = \upsilon_{sw}{}^{-1/3} \times \frac{2M_c C_n}{M_r} \times l \quad \text{(S3)}$$

Where ξ is the mesh size, M_r is the molecular weight of HEMA unit monomer (134.12 g/mol), C_n is the Flory characteristic ratio (6.9 for HEMA) and l the length of the bond along the polymer backbone (1.54 Å).

Table S1. Homogeneous SN p(HEMA-co-EGDMA) hydrogels characteristics[a]

Hydrogel	Q_v	υ_{sw}	v_{ap}	χ	M_c *(g/mol)*	ξ *(nm)*	Appearance[b]
3%Cr-50%W	0.92 ±0.07	0.55 ±0.01	0.50 ±0.05	0.82	3842 ±861	3.72 ±0.45	
7%Cr-60%W	1.10 ±0.02	0.37 ±0.02	0.41 ±0.02	0.65	1931 ±354	3.00 ±0.23	
3%Cr-55%W	0.88 ±0.01	0.52 ±0.01	0.46 ±0.01	0.79	9210 ±948	5.90 ±0.32	
4%Cr-55%W	1.00 ±0.01	0.50 ±0.01	0.50 ±0.01	0.77	13120 ±176	7.13 ±0.07	
7%Cr-55%W	1.13 ±0.06	0.39 ±0.01	0.44 ±0.01	0.67	2492 ±151	3.36 ±0.08	

a: All average molecular weights (M_c) were calculated by assuming M_n=54000 g/mol.
b: The horizontal black line has 10 mm length.

Increased initial water content (IWC) and swelling behavior of 3Cr and 4Cr conventional hydrogels

Despite deswelling of 3Cr-55W and neutral state of 4Cr-55W hydrogels, the swelling forces prevail polymeric chains attraction forces for higher IWCs (e.g., 60, 65 and 70%). In these compositions, free water portion between chains was large enough to avoid formation of a new secondary structure that favors shrinkage of the network. We also observed slightly larger swelling in case of 4Cr-65W compared to 3Cr-65W hydrogels (IWC~65% was detected as

maximum swelling condition) indicating more efficient attraction forces between chains in more resilient network (lower crosslinking density) thanks to a higher degree of freedom within the network.

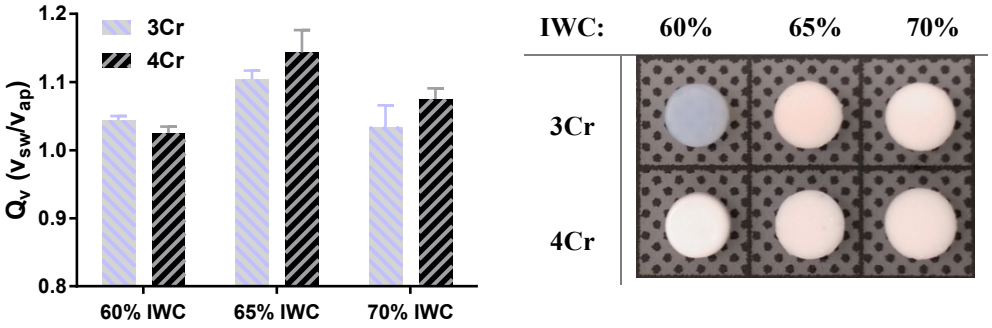

Figure S2. Swelling behavior of 3 and 4Cr p(HEMA-co-EGDMA) hydrogels when IWC is higher than 60%.

Effect of initiator type on porous hydrogels mechanical properties

By testing different initiator for the polymerization process, we realized that the mechanical properties of porous hydrogels could be improved with different initiator agents. Since porous hydrogels do not initially contain high water amount, contrary to conventional hydrogels, we could employ heat polymerization without significant loss of water during the fabrication process instead of UV polymerization by 2,2-dimethoxy-2-phenylacetophenone (DPAP[57 mg/mL ethano]). We therefore utilized 40 µl ammonium persulfate (AP[100 mg/mL water]) and 40 µl sodium metabisulfite (SM[100 mg/mL water]) redox initiator solution (AP-SM, polymerization time: 2 hours) instead of 40 µl photo initiator solution (DPAP, polymerization time: 15 minutes) for 1 ml HEMA and compared the corresponding mechanical properties of porous 4Cr-Fine hydrogel.

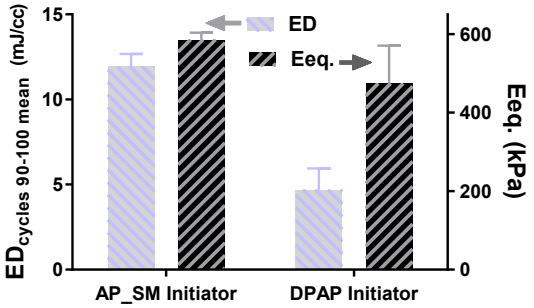

Figure S3. Equilibrium Young modulus (Eeq.) in range of 10 to 20% compressive strain and the level of ED by applying 10% dynamic strain over 10% static strain at 1 Hz on 4Cr-Fine porous hydrogels prepared with different initiator agents.

Porous hydrogels structural characteristics

The salt particles were manually separated with the stainless steel sieves in 7 different sizes from 100 to 500 μm. Then, different salt groups were combined with predefined ratio according to the Table S2 to control the permeability of the porous hydrogels while keeping the same equilibrium water content (EWC). Permeability (k) of the hydrogels were measured based on Darcy's law in 0% and around 20% compressive strains by a recently developed customized experimental set-up [2]. Briefly, the flow rate was measured under constant water head condition by measuring the weight of traversing water through the porous hydrogels in a period of time (See chapter 2).

Table S2. Porous p(HEMA-co-EGDMA) hydrogels characteristics

Hydrogel Type	Salt Size (μm)	EWC (%)	k at 0% strain (m^2)	k at 20% strain (m^2)
8%Cr-Coarse Pores	300-350: 60% 400-500: 40%	67±3	1.76E-12 ±5.04E-13	1.22E-12 ±3.72E-13
6%Cr-Medium Pores	250-300: 55% 300-350: 45%	68±2	5.10E-13 ±2.65E-13	2.08E-13 ±4.22E-14
4%Cr-Fine Pores	200-250: 80% 150-200: 20%	68±2	1.09E-14 ±1.55E-14	2.35E-15 ±3.07E-15
4%Cr-Coarse Pores	300-350: 60% 400-500: 40%	69±2	O(E-12)[a]	O(E-12)[a]
4%Cr-Extra Fine	100-150: 100%	69±1	< O(E-16)[b]	< O(E-16)[b]

a: we estimate permeability of 4Cr-Coarse samples to be in the same order of 8Cr-Coarse hydrogels considering their similar pores distribution (Figure 4-Chapter 4), EWC and morphology (the samples stiffness was not adequate for a reliable measurement based on radial sealing method [2]).
b: it was difficult to precisely measure the permeability of porous 4Cr-Ext. Fine hydrogels due to very slow flow rate and long required time for passing a detectable amount of water without evaporation. However, we can safely estimate based on our previous work that the permeability of this group is lower than 10^{-16} m^2.

Porous hydrogels mechanical characterization

All the samples preconditioned firstly to consider the effect of loading history of cell seeding step on mechanical properties of porous hydrogels. For this purpose, samples were submitted to a predefined loading regime (30-35% compressive strain for 5 times) according to the compression-induced suction (CRIS) seeding method [3] and then rested overnight before all characterization tests. Sequential stress relaxation tests were carried out as described for the conventional hydrogels. However, to measure energy dissipation, we applied 10% cyclic compression for porous hydrogels (instead of 15% for conventional hydrogel) over 10% pre-strain at 1 Hz.

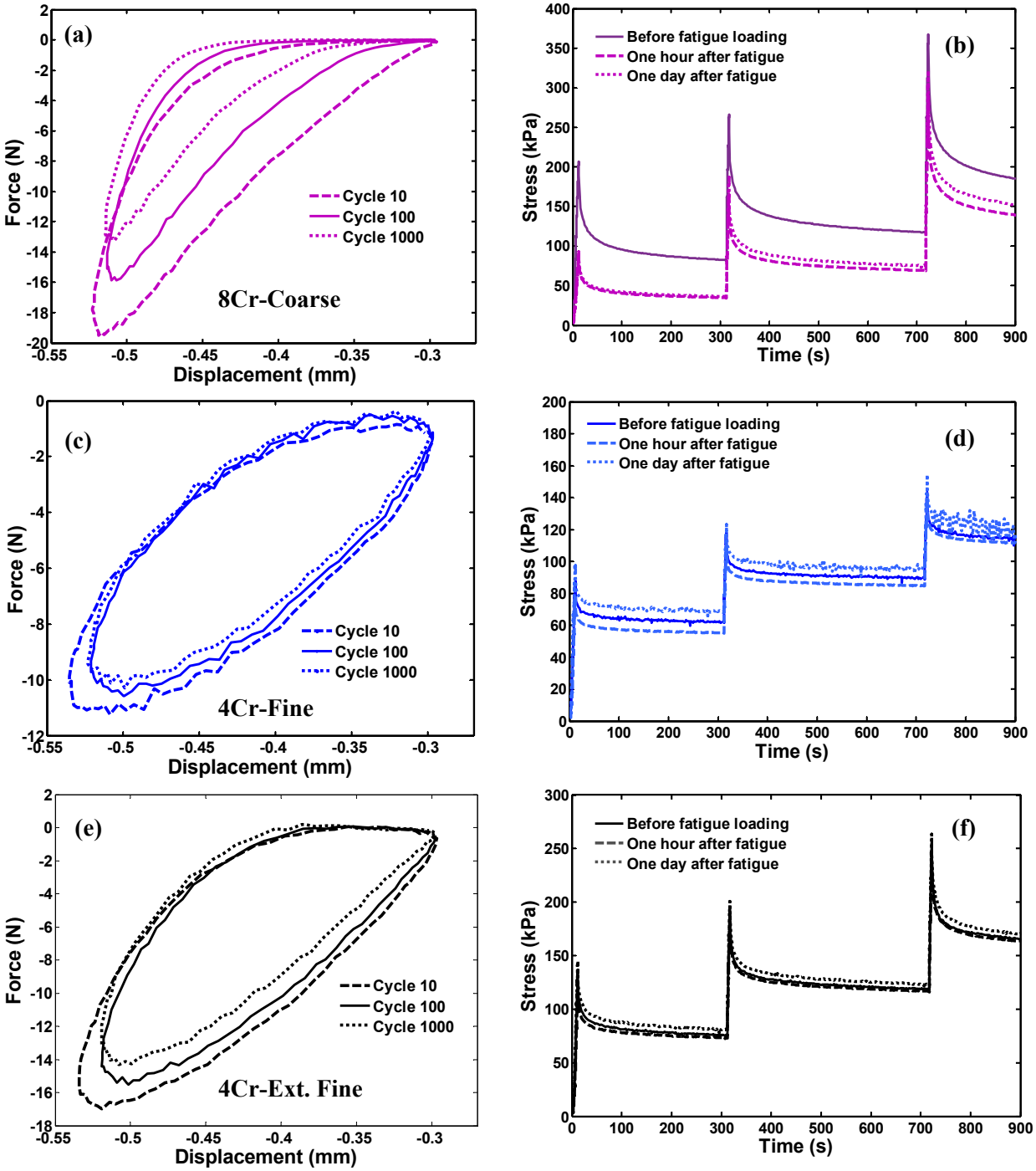

Figure S4. Heteroporous pHEMA based hydrogels mechanical behavior. (a,c & e) Representative hysteresis loop evolution for 8Cr-Coarse (purple), 4Cr-Fine (blue) and 4Cr-Extra Fine (black) during cyclic loading. (b,d & f) Representative time dependent load support of 8Cr-Coarse (purple), 4Cr-Fine (blue) and 4Cr-Extra Fine (black) in sequential stress relaxation (ramp and hold strain) tests before and after fatigue load of 3600 cycles (10% static strain+10% dynamic strain at 1Hz).

Load support capacity in porous hydrogels

We applied 20% strain at a 500 µm/s loading rate and then hold it (stress relaxation) to evaluate the load support capacity of three representative porous hydrogels (8Cr-Coarse, 4Cr-

Fine, and 4Cr-Ext. Fine) under a physiological loading condition (Figure S5). It can be observed that different levels of load support are achievable by varying the morphological architectures or network rigidity of the porous hydrogels. Indeed, the solid phase participation to load support is due to the polymeric network rigidity, while the fluid phase contribution is based on the development of hydrostatic fluid pressure, which can be amplified by reducing the permeability of the porous hydrogel.

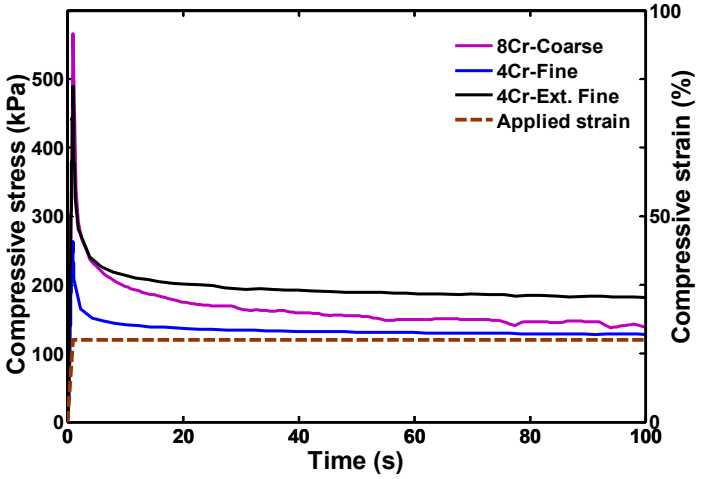

Figure S5. Typical time dependent load support of representative porous hydrogels during stress relaxation test (the load support capacity of 4Cr-Ext. Fine hydrogel at maximum stress is comparable to 8Cr-Coarse hydrogel).

Effect of the fluidic phase viscosity on energy dissipation

To validate the inverse correlation of the flow-dependent dissipation source to the permeability, we increased the viscosity of the fluidic phase of the hydrogel by using glycerol instead of water for the ED evaluation.

As shown in Figure S6, the ED level was further amplified with glycerol compared to water for the 4Cr-Fine hydrogel having a lower permeability ($k \sim 10^{-14}$) than 8Cr-Coarse hydrogel ($k \sim 10^{-12}$). This increase is much more significant in early cycles when the pores still contain considerable amount of glycerol. Due to lower permeability of 4Cr-Fine hydrogels, the glycerol with higher viscosity, cannot refill the pores during unloading time following an applied compression, which enforces fluid seepage. Therefore, the ED is being decreased during cyclic loading.

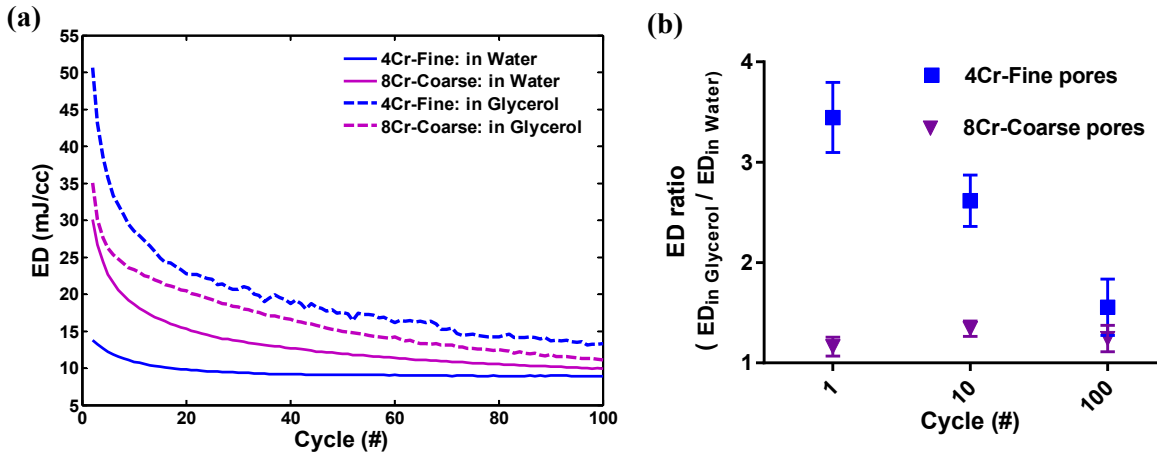

Figure S6. Effect of the fluidic phase viscosity on dissipative behavior of different porous hydrogels. (a) Typical trends of ED level with different fluid viscosities over the applied loading cycles for 4Cr-Fine and 8Cr-Coarse hydrogels. (b) Comparison of ED ratio in cycles 1, 10 and 100 in two groups (mean and SD, n=4).

Separation of solid and fluid phases contribution to load support

We combined experimental characterization and computational optimization to separate the flow-dependent and the flow-independent part of the load support by developing a poro-viscoelastic (PVE) model [4-6]. The solid and the fluid phases were coupled based on theory of poroelsticity [7] and a linear visco-elastic behavior for the solid part was assumed according to Maxwell–Wiechert model [8]. In the model, the 2D axisymmetric cross section of cylindrical samples having 2.5 mm thickness and 4 mm radius was divided to finite elements (Figure S7-a). We then defined an estimation routine using particle swarm optimization (PSO) [9] in MATLAB (see appendix 1 for detail), and run the COMSOL model iteratively to find the optimum set (Figure S7-b). The objective function (OF) for PSO was defined according to equation S4, in which we covered peak and equilibrium stresses (σ) along with stress decay rates ($\frac{d\sigma}{dt}$) at critical time points of relaxation curve. It is worth mentioning that the PSO technique converged to an optimal set much faster than Genetic Algorithm (see appendix 1).

$$OF = \sum w_i \ (\sigma^{exp} - \sigma^m)^2 + \sum u_i \ (\frac{d\sigma^{exp}}{dt} - \frac{d\sigma^m}{dt})^2 \qquad (S4)$$

In equation S4, σ^{exp} is the nominal stress obtained from experiment ($\sigma^{exp}(t) = \frac{F(t)}{A_{initial}}$), σ^m is the total stress obtained from the PVE model which consists of solid phase stress and fluid pressure ($\sigma^m = \sigma_{soild} + p_{fluid}$). Additionally, w_i and u_i are weighting coefficients and assigned based on the importance of the employed time points.

Table S3. Optimized relaxation time (τ_i) and modulus (G_i) of the PVE model relaxation function for the representative porous p(HEMA-co-EGDMA) hydrogels.

Porous hydrogel	G_1 (kPa)	τ_1 (s)	G_2 (kPa)	τ_2 (s)	G_3 (kPa)	τ_3 (s)	G_4 (kPa)	τ_4 (s)
8%Cr-Coarse	295e4	0.002	100	0.1	105	7.26	335	225
4%Cr-Fine	200	0.42	58	5.82	215	1600	-[a]	-[a]

a: It was not necessary to employ the fourth viscoelastic branch in Maxwell–Wiechert model (G_4 and τ_4) for the 4Cr-Fine hydrogel as we obtained good enough precision with n=3 on Prony Series for relaxation function.

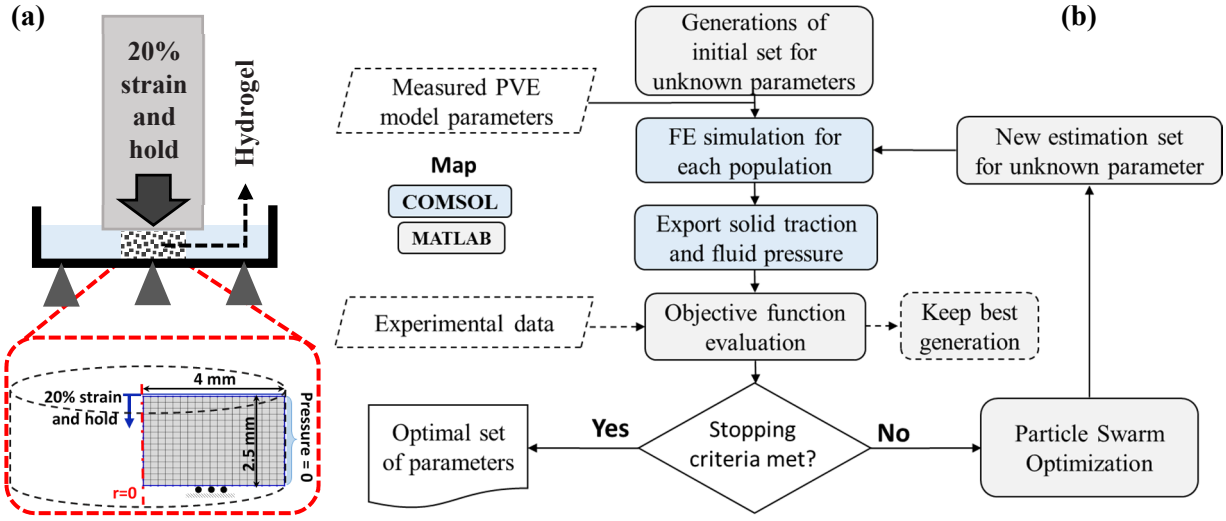

Figure S7. Emplyed method to separate flow-dependent and flow-independent load support via a poro-viscoelastic (PVE) model. (a) Schematic of experimental setup and corresponding model in COMSOL. (b) Flowchart of the combined experimental and computational methods for estimation of relaxation function parameters.

As can be observed in Figure S8-a and b, the optimized poro-viscoelastic model properly predicts experimental data and consequently separates solid and fluid phases contribution (Figure S8-c and d). The obtained values to estimate the relaxation function by using the experiments, performed at a 500 µm/s loading rate, were validated by comparing the model predication for another loading rate (e.g., 50 µm/s) with corresponding experimental data (Figure S8-e and f). Our simulation results revealed that the relaxation moduli (G_i) are directly correlated to crosslinking density of the hydrogels, while there is an inverse correlation between relaxation times (τ_i) and crosslinking density of the polymeric network (Table S3). Moreover, the release of compression-induced fluid pressure takes a longer time in hydrogels with lower permeability contrary to the instantaneous relief in highly permeable hydrogels. In this latter case, the total stress is sustained by the solid matrix (Figure S8-d) and this can be destructive for sample at maximum stress. On the other hand, the load is partly carried by the

solid matrix at the maximum stress in the 4Cr-Fine hydrogel (Figure S8-c) owing to its lower permeability letting fluid pressurization to be established.

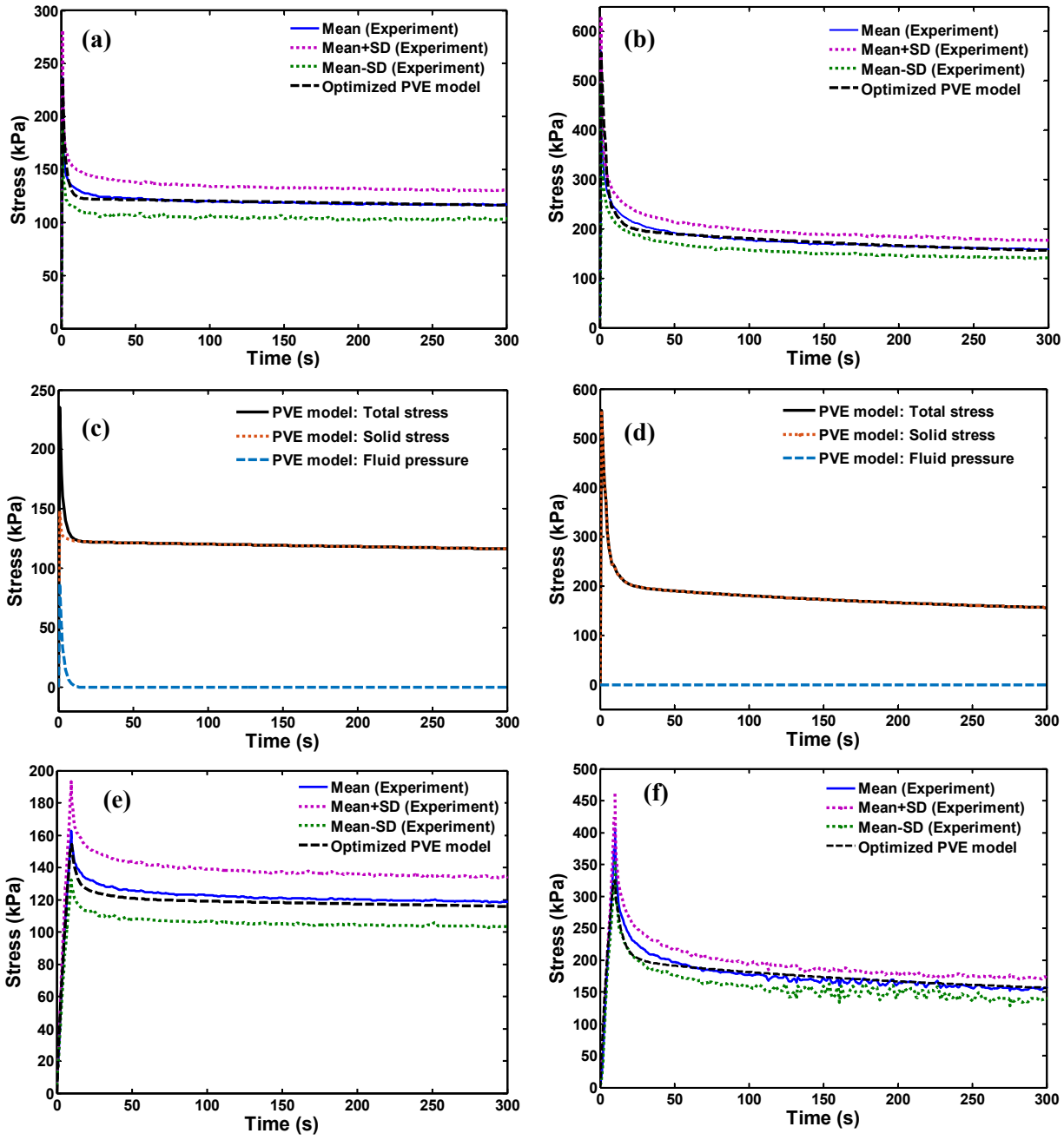

Figure S8. Separating flow-dependent and flow-independent load support by an optimized poro-viscoelastic model. (a, c) 4Cr-Fine hydrogel experimental and simulation results for 500 μm/s loading rate. (b, d) 8Cr-Coarse hydrogel experimental and simulation results for 500 μm/s loading rates. (e, f) Validation of the developed poro-viscoelastic model in 50 μm/s loading for 4Cr-Fine (left) and 8Cr-Coarse (right) hydrogels.

Recoverability of hysteresis loop in porous hydrogels

The destructive and non-destructive processes contribution to the evolution of the porous hydrogels hysteresis loop was evaluated. In this regard, the level of energy dissipation over 100 cycles was compared between two loading sessions (10% static strain+10% dynamic strain at 1 Hz) performed with an overnight interval between them (Figure S9).

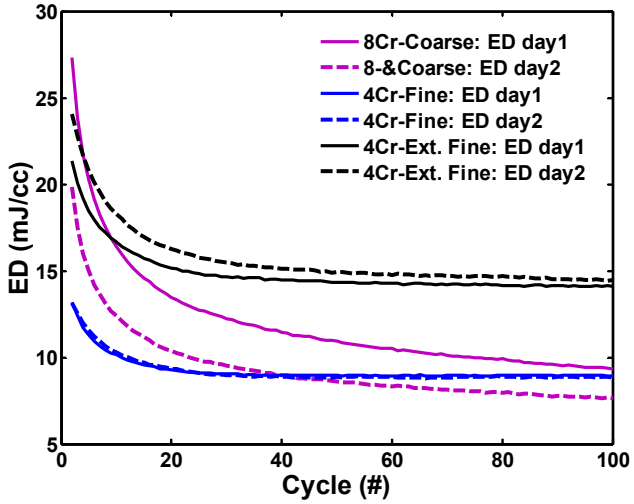

Figure S9. Typical hysteresis loop area (ED) variation for 8Cr-Coarse (purple), 4Cr-Fine (blue) and 4Cr-Extra Fine (black) during two cyclic loading tests performed with an overnight recovery time (the dissipation source in 8Cr-Coarse hydrogel is not recoverable indicating a destructive process).

The dramatic drop of ED in highly crosslinked sample (8Cr-Coarse) over loading cycles is partly due to the destructive sources of the energy dissipation (e.g., chains fracture or bond rupture during loading). However, after overnight resting, there is a partial recovery and the ED level (first cycle) for day 2 starts from a higher value than last cycle of the ED for day 1, but still lower than the first cycle of ED for day 1 (intact condition). In contrast, the combination of reversible solid intrinsic and frictional drag dissipations is fully recoverable in hybridly crosslinked and poorly permeable hydrogels (4Cr-Fine and Ext. Fine).

Cells distribution and viability in porous hydrogels

Human epiphyseal chondro-progenitors (ECP) cells were expanded on T75 culture flasks to increase their population. The consumed Proliferation Medium (PM) for cells was DMEM containing L-Glutamine, 4,5 g/l D-Glucose and Sodium pyruvate, (Life Technologies) which was supplemented with 10% FBS (Sigma) and 1% L-Glutamine and Penicillin (Life Technologies). Cells were grown in standard incubator (37 °C and 5% CO2) to 90%

confluence, trypsinized and redistributed again in 2D culture up to passaged 5. Porous hydrogels were sterilized and coated with fibronectin before cell seeding step for the sake of bioactivity and providing similar cell-hydrogel interface [3, 10]. The optimized compression released induced suction (CRIS) seeding technique was employed to infuse cells (1 and 1.5 million for 8Cr-Coarse and 4Cr-Fine, respectively) inside porous hydrogel discs (2.2 mm thickness and 8 mm diameter) as described in our previous work [3].

The 3-(4,5-dimethylthiazol-2-yl)-2,5-diphenyltetrazolium bromide (MTT) cell proliferation Kit I (Roche Corporation, Indianapolis, USA) was used to observe ECP cells distribution inside porous hydrogels. After cell seeding, infiltration and distribution of cells were evaluated at day 2 by using a Stereomicroscope (LEICA MZ 16 1FA) following MTT labeling as shown in Figure S10. Briefly, the cell-laden hydrogels were cut in half and immersed in 300 ml DMEM medium (without phenol red) inside a 48 well plate. Then, 30 µl of MTT dye was added to each well and samples were incubated (37 °C and 5% CO2) for 4 hours to let formazan formation. The insoluble purple formazan is produced due to cells metabolic activity and therefore demonstrates viable cells distribution within the hydrogels.

We also assessed viability of cells inside porous hydrogels (Figure S11) at different time points (day 5 & 10) by performing live and dead staining using Viability/Cytotoxicity Assay Kit (Biotium, Fremont, CA) following manufacturer protocol. Before staining, the cell-hydrogel constructs were incubated in 500 µl DMEM medium without phenol red inside a 48 well plate for 3 hours to diminish reddish color of the hydrogels due to phenol red in proliferation medium. Then, the samples were stained by 500 µl of the mixed live/dead working solution (1 µl Calcein and 2 µl Eht in 5 ml PBS) for 30 min at room temperature (RT) in dark. Finally, the samples were rinsed twice with PBS, and the images were taken by an invert LSM 700 confocal microscope (Carl Zeiss, Jena, Germany) using a 10X objective and subsequently explored with open source FIJI platform.

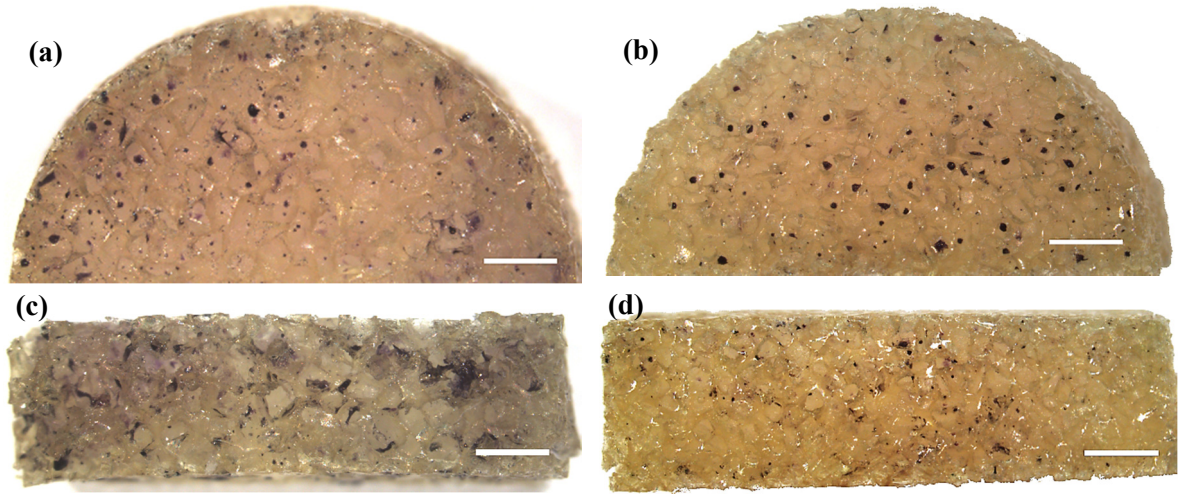

Figure S10. MTT stained cells distribution on surface and cross section of the porous hydrogels after 2 days. (a,c) 8Cr-Coarse porous hydrogel. (b,d) 4Cr-Fine porous hydrogel. The cells are fairly uniform and penetrate inside the hydrogels by employing customized CRIS seeding method (scale bar: 1 mm).

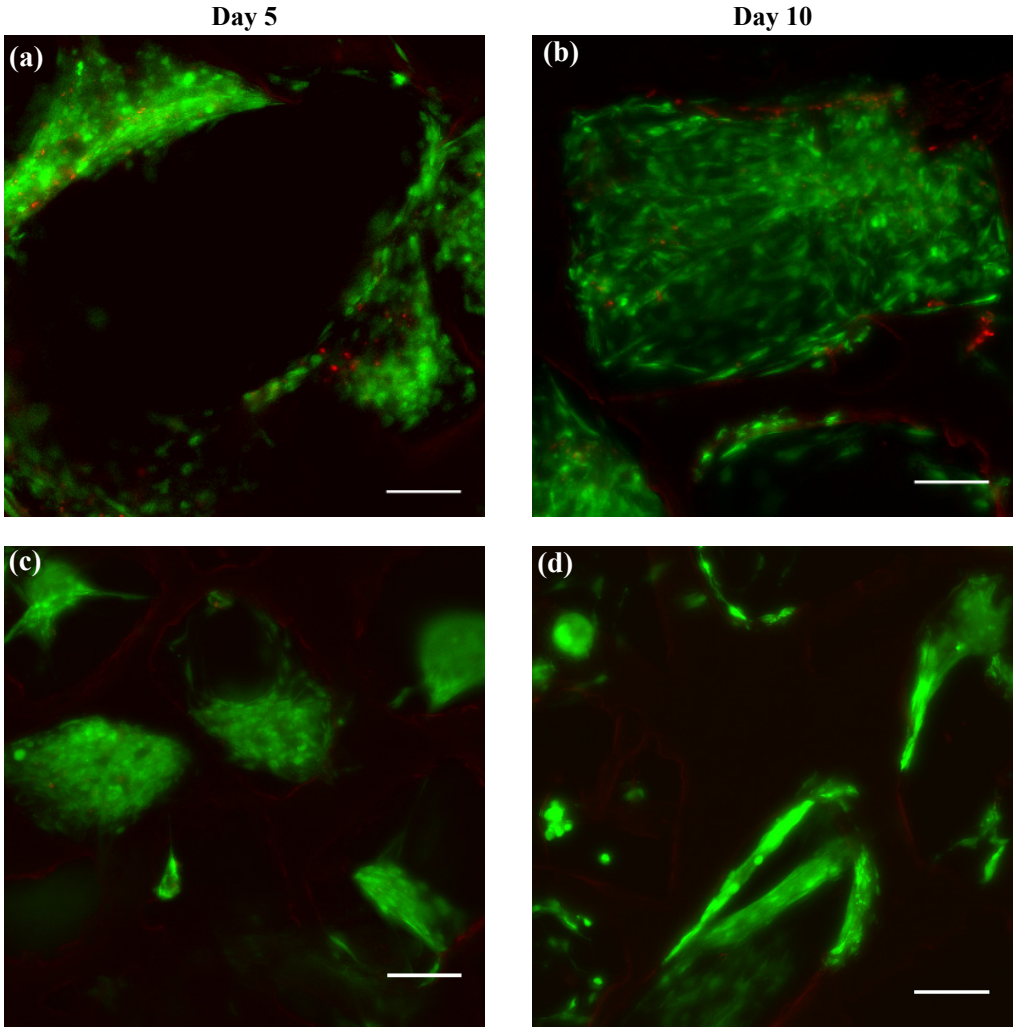

Figure S11. Live/dead staining of cells seeded porous hydrogels at different time points showing a stable cells viability up to 10 days of culture (scale bar: 100 µm). (a, b) 8Cr-Coarse. (c, d) 4Cr-Fine. Green stain illustrates live cells and red stain shows dead cells.

Mechanical stimulation of cell-laden hydrogels in cyclic compression mode

With the developed dissipative porous hydrogels, we investigated the cells response to cyclic compression in a standard loading regime (10% cyclic strain over 10% static strain at 1 Hz). In the beginning of 3D culture, the seeded hydrogels were pre-cultured for 3 days in proliferation medium (PM) inside a standard incubator (37°C, 5% CO_2). After this step, a differentiation medium (DM) was used and the mechanical stimulation was applied on the different groups of dissipative hydrogels (Figure S12-a). Differentiation medium was PM without FBS but having 10% ITS IV (Life Technologies) and 1% Vitamin C. The stimulation time was 2 hours per day for a period of 4 days, while the corresponding control group was preserved in free swelling condition. Finally, we compared the expression of chondrogenic genes between the stimulated and non-stimulated groups of cell-seeded hydrogels. We selected, Aggrecan (Acan), Sex-determining region Y box 9 (SOX9) and Collagen type II (COL2A) genes for comparing cells response as they are important markers for chondrogenesis [11].

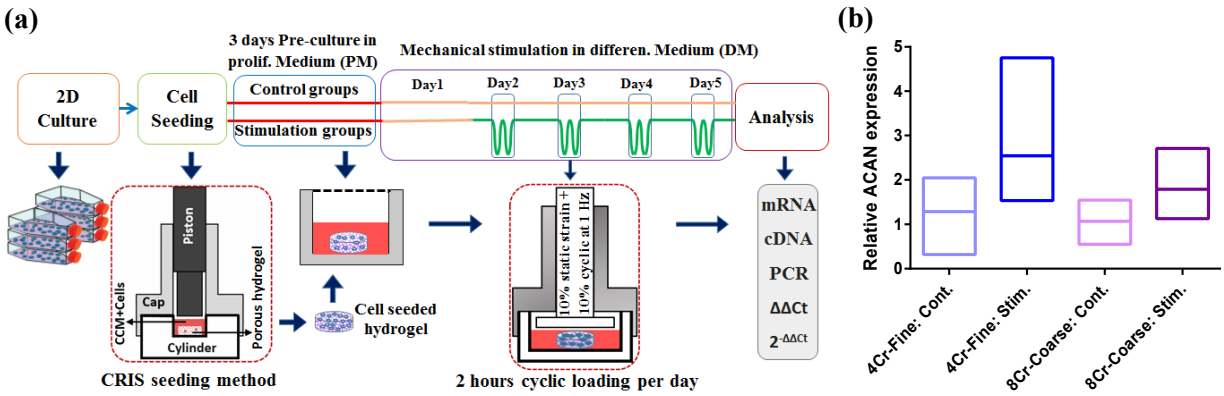

Figure S12. Performed *in vitro* mechanobiological experiment. (a) Schematic plan of the study. (b) Aggrecan(ACAN) gene expression shown as mean value with minimum and maximum ranges. Relative ACAN expressions are shown for two groups of dissipative hydrogel following free-swelling (control group) or mechanical stimulation (treatment group).

RNA extraction and gene expression

After the last period of stimulation in the mechanobiological experiment, each sample was put in a 2 ml Eppendorf tube containing 300 µl Trizol. Total RNA was extracted using the NucleoSpin® RNA (Macherey-Nagel) after a few steps of preparation [10]. Briefly, hydrogels were smashed by the polytron (Kinematica AG, Switzerland), while keeping the tube cold on dried ice. Then, 100 µl chloroform was added and centrifuged for 4 minutes at 12000 rpm at 4°C. The aqueous phase was transferred to 2 ml phase lock tubes and centrifuged for an

additional 6 minutes at 12000 rpm 4°C. The aqueous phase was carefully transferred to 1.5 ml Eppendorf tubes and the extraction was completed by adding a RNA carrier and following the XS kit protocol. The RNA was quantified using the Nanodrop Lite Spectrophotometer (Thermo Scientific) and reverse transcription of 500 ng RNA was carried out for real time PCR analysis. Taqman® Reverse Transcription Reagents (Applied Biosystems) were utilized for cDNA synthesis in reaction volume of 50 µl containing master mix, random hexamer and RNA template.

Fast SYBR® Green Master Mix (Applied Biosystems) was used for PCR amplification in a final volume of 20 µl containing 1 µl of synthesized cDNA. Primers were synthesized by Microsynth (Balgach, Switzerland) according to reported sequences in Table S4. Different annealing temperature and concentration were used for primers to optimize the process resulting in efficiency range of 91 to 110%. The PCR amplification was carried out in duplicate for each sample by StepOnePlus Real-Time PCR platform (Applied Biosystems). The thermal cycling condition was defined as an initial 95°C step for 2 min followed by 40 cycles of 95°C for 5s and corresponding annealing temperature of gene (60 to 65°C, Table S4) for 30s. Gene expression data were analyzed using the comparative ΔΔCt method [12] with B2M as the reference gene [10]. Corresponding free swelling hydrogels in each group were used as the biological reference for the stimulated hydrogels (n=4).

Table S4. Primers data used for qRT-PCR.

Gene	Anealing temp. (°C)	Primer concent. (nM)	Efficeny (%)	Sequence
COL2A	60	250	110	F: 5'- GGCAATAGCAGGTTCACGTACA-3' R: 5'- GATAACAGTCTTGCCCCACTTACC-3'
ACAN	62.5	280	91	F: 5'- GGTACCAGTGCACAGAGGGGTT-3' R: 5'- TGCAGGTGATCTGAGGCTCCTC-3'
SOX9	65	200	108	F: 5'-TGGAAACTTCAGTGGCGCGGA-3' R: 5'-AGAGCAAAAGTGGGGGCGCTT-3'
B2M	60	250	100	F: 5'- TATCCAGCGTACTCCAAAGATTCA-3' R: 5'- TGAAACCCAGACACATAGCAATTC-3'

Mechanical robustness of porous hydrogels subjected to large deformation

The structural stability of 4Cr-Fine versus 8Cr-Coarse porous hydrogels in large deformation was compared following the application of 70% compressive strain twice (Figure S13).

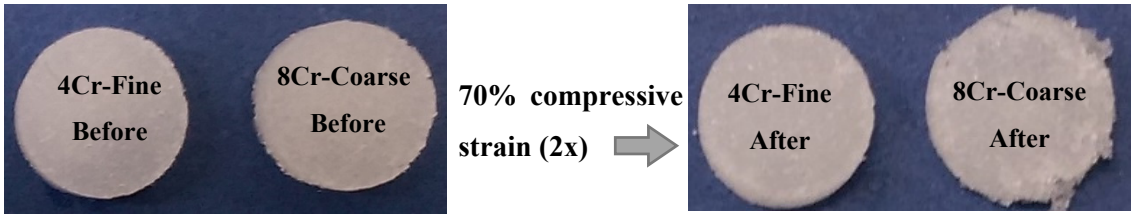

Figure S13. Structural stability of the 4Cr-Fine versus the 8Cr-Coarse porous hydrogels in large deformation. A plastic deformation and defects were observed in the 8Cr-Coarse hydrogel after 70% compressive strain, while the 4Cr-Fine hydrogel appropriately sustained the large deformation.

Supplemental References

[1] Peppas NA, Hilt JZ, Khademhosseini A, Langer R. Hydrogels in biology and medicine: from molecular principles to bionanotechnology. Adv Mater 2006;18:1345-60.

[2] Nasrollahzadeh N, Pioletti DP. Experimental method to characterize the strain dependent permeability of tissue engineering scaffolds. J Biomech 2016;49:3749-52.

[3] Nasrollahzadeh N, Applegate LA, Pioletti DP. Development of an Effective Cell Seeding Technique: Simulation, Implementation, and Analysis of Contributing Factors. Tissue Eng,Part C 2017;23:485-96.

[4] Suh J-K, DiSilvestro M. Biphasic poroviscoelastic behavior of hydrated biological soft tissue. Journal of Applied Mechanics 1999;66:528-35.

[5] Strange DG, Fletcher TL, Tonsomboon K, Brawn H, Zhao X, Oyen ML. Separating poroviscoelastic deformation mechanisms in hydrogels. Appl Phys Lett 2013;102:031913.

[6] Zahedmanesh H, Stoddart M, Lezuo P, Forkmann C, Wimmmer MA, Alini M, et al. Deciphering Mechanical Regulation of Chondrogenesis in Fibrin–Polyurethane Composite Scaffolds Enriched with Human Mesenchymal Stem Cells: A Dual Computational and Experimental Approach. Tissue Eng,Part A 2014;20:1197-212

[7] Biot MA. Mechanics of deformation and acoustic propagation in porous media. J Appl Phys 1962;33:1482-98.

[8] Roylance D. Mechanics of Materials. New York: John Wiley & Sons; 1996.

[9] Marini F, Walczak B. Particle swarm optimization (PSO). A tutorial. Chemometrics Intellig Lab Syst 2015;149:153-65.

[10] Abdel-Sayed P, Darwiche SE, Kettenberger U, Pioletti DP. The role of energy dissipation of polymeric scaffolds in the mechanobiological modulation of chondrogenic expression. Biomaterials 2014;35:1890-7.

[11] Huang AH, Farrell MJ, Mauck RL. Mechanics and mechanobiology of mesenchymal stem cell-based engineered cartilage. J Biomech 2010;43:128-36.

[12] Livak KJ, Schmittgen TD. Analysis of relative gene expression data using real-time quantitative PCR and the 2− ΔΔCT method. methods 2001;25:402-8.

Chapter 5: A Customized *In Vitro* Platform for Cartilage Thermo-Mechanobiology

5-1 Introduction

Structural organization and mechanical properties similar to the articular cartilage could be the eventual outcome of an engineered construct *in vitro* [1]. However, more effort is still required for such achievement and a corresponding clinical translation. To facilitate this process, versatile and biomimetic platforms can be employed to optimize cells response with respect to biological or biomechanical manipulations [2]. Apart from the influence of biological mediators like growth factors, scaffold intrinsic characteristics (surface chemistry, topography) and material properties (permeability, viscoelasticity) act in synergy with physical cues (culture temperature, mechanical stimulation) to orchestrate chondrogenesis. Therefore, careful design of biomaterials properties, cell-scaffold interaction and *in vivo* like stimulation are required to biophysically guide chondrocytes differentiation [2-4].

One mechanism by which cells may sense the surrounding microenvironment is through their integrin interaction with anchored ligands within the extra cellular matrix (ECM) [5]. ECM-mimetic functionalization of synthetic hydrogels can therefore be adopted to enhance integrin mediated mechano-sensing. It is well known that Arginine, Glycine and Aspartate (RGD) sequence in ECM proteins such as fibronectin provides attachment sites for integrin receptors [6, 7]. Physical adsorption of ECM proteins (mostly fibronectin) and ligand containing monomer (mainly RGD) copolymerization are common, relatively easy and fast methods for functionalization of inert biomaterials [7-9]. Despite controversial role of ECM-mimetic elements in chondrogenic differentiation of cells in free swelling hydrogels [10-14], a

chondro-inductive influence was observed for cell-laden hydrogels containing RGD in presence of dynamic loading [15, 16].

The lack of control on ligands availability on the interface to provide exposed attachment sites for cells and deterioration of bulk mechanical properties are the main issues of functionalization approaches [7, 17]. In addition, the inadequate binding strength of non-specific adsorption process is not reliable to provide cell-interface interaction for an entire culture time in case of simple coating. Alternatively, covalent bio-conjugation of ECM analog motifs such as RGD on the exposed surfaces of a pre-formed scaffold can overcome these limitations [18]. In this context, successful immobilization of biological ligands were reported for pHEMA based materials thanks to its reactive hydroxyl elements [19-21]. However, the influence of this post-polymerization process on mechanical properties of a cross-linked pHEMA structure should be carefully minimized. Only in this condition the developed fatigue resistant visco-porous hydrogel (see chapter 4) can be biologically functionalized while preserving its biomechanical characteristics.

Temperature increase due to dissipated energy following cyclic loading is an established observation for viscoelastic materials [22, 23]. Since articular cartilage is a poro-viscoelastic tissue with high dissipative capacity, temperature increase following joint loading could occur. Self-heating phenomenon in cartilage tissue following dynamic loading has been evaluated both numerically and experimentally. With a finite element analysis, Moghadam *et al* have shown that the power of heat generation in articular cartilage submitted to cyclic compression (15% strain at 1.5 Hz) can gradually increase the tissue temperature [24]. In addition to this *in silico* result, the *in vivo* measurements inside intra-articular region of knee joint have shown a temperature rise from 32°C to 38°C following one hour of jogging [25]. A temperature evolution of about 4°C after one hour of walking was also predicted by a simplified heat transfer model for cartilage [26].

Despite existing evidence that chondrocytes can experience different thermal environments subsequent to joint loading, *in vitro* mechanobiological experiments usually consider a constant culture temperature (37°C) during mechanical stimulation. In particular, the measured temperature of knee cartilage at rest has been reported to be around 32-33°C [25, 27], which is 4-5°C lower than conventional culture temperature. In this context, only a few studies have shown the influence of culture temperature on chondrocytes biological response in 2D or 3D pellet conditions without any external loading. In a recent study by Ito *et al* for

monolayer and pellet culture conditions [28], it was observed that culture at 41°C significantly decreases cells metabolic activity and chondrogenesis compared to both 32 and 37°C temperatures. In addition, higher metabolic activity for 32°C condition was observed contrary to a better chondrogenic differentiation at 37°C. Similar conclusions were drawn for human chondro-progenitor cells cultured at 33 and 37°C in 2D culture condition [29]. Yet, to the best of our knowledge, it is not clear how the dynamics of temperature increase may contribute to the chondrogenesis in cell-laden hydrogels either in free swelling or in synergy with cyclic loading. As self-heating links the temperature increase to cyclic deformation, studying cartilage thermo-mechanobiology opens the opportunity to identify different aspects of the energy dissipation (mechanical, thermal or their combination) on chondrocytes behavior.

The aim of this chapter is to present the development of a customized biomimetic *in vitro* platform to study cartilage thermo-mechanobiology. To induce a stable cell-scaffold interaction, we firstly functionalized previously developed fatigue resistant porous hydrogels via bio-conjugation of RGD peptides. This ligand grafting technique was realized in two steps for functional group activation and peptide binding while maintaining the desired mechanical properties of the hydrogels. In addition, a modular home-made compression bioreactor was designed to control the applied stress/strain and temperature scheme during culture of cell-laden hydrogels. By employing this customized *in vitro* system, we could emulate the *in vivo* knee cartilage thermo-mechanical environment and for the first time investigate synergetic or decomposed effects of temperature and loading on cells biophysical response.

5-2 Materials and Methods

5-2-1 Functionalization of dissipative hydrogels by grafting RGD peptides

A previously reported method for functionalization of pHEMA brushes [19, 21] was modified to maintain the structural integrity of crosslinked pHEMA based hydrogels during RGD peptides conjugation. Briefly, the pendant hydroxyl groups of pHEMA hydrogels were firstly activated by using 4-nitrophenyl chloroformate (NPC). For this purpose, lyophilized hydrogels were vacuum-swelled in the freshly prepared activation mixture of 1.41 g NPC in 15 ml acetone and 1 ml distillated triethylamine. The samples were shacked in the solution for 1 hours at room temperature to fulfill activation process. The samples were then extensively rinsed with acetone and methanol several times to remove excess NPC. After the washing steps, the NPC-activated samples were transferred to the methanol solution containing 1 mM

RGD peptides and 2 mM 4-dimethylamino-pyridine. To complete the functionalization process, the samples were incubated overnight at room temperature under gentle shaking in the reactor covered with an aluminum foil. The RGD functionalized samples were then rinsed three times with pure methanol for 2 minutes. To ensure removal of any non-reacted NPC group, the samples were incubated in 0.5 M solution of ethanolamine in methanol for 20 minutes under gentle shaking. The samples were finally rinsed several times with methanol and bi-distillated water to wash non-specifically adsorbed peptides and entrapped NPC molecules inside the porous hydrogels.

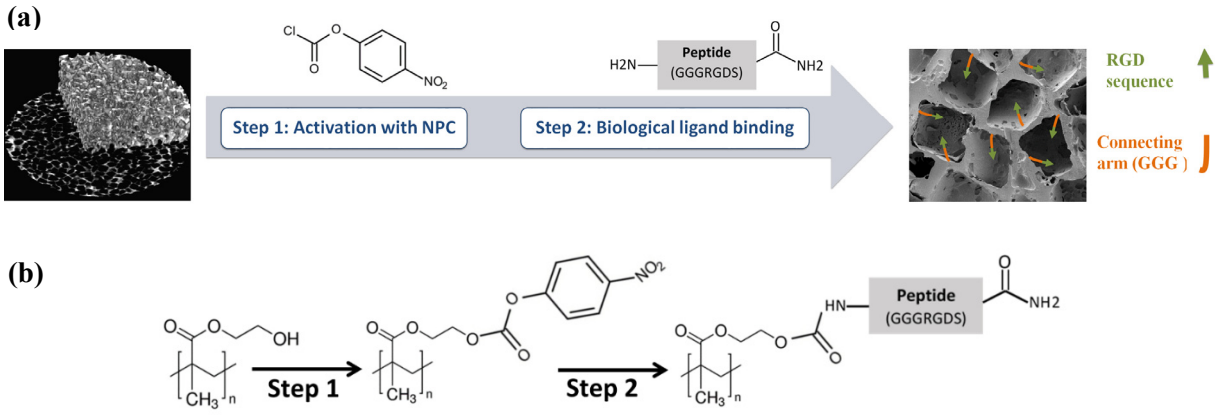

Figure 1. Bio-conjugation process for functionalization of pHEMA based hydrogels. (a) Schematic of RGD binding on pores surface of dissipative hydrogels. (b) Chemical representation of the applied two-step process of hydroxyl (OH) group activation and peptide immobilization.

5-2-2 Development of a customized bioreactor for thermo-mechanobiological study

The bioreactor chamber was custom designed as shown in Figure 2 and supplemented with commercial and off-the-shelf modules for controlling the different environmental signals (Figure 3). Briefly, a thermo-foil heater is embedded below an aluminum conductive plate (Figure 2-d) containing 12 stainless-steel wells (Figure 2-c) for hydrogels culture. The control signal for heater is provided by a microprocessor (Minco-CT16A, Minnesota, USA) based on a closed loop approach [30] while measuring culture temperature by a miniature RTD sensor (Minco-S308). The set-up is compatible with an Instron uniaxial loading machine (Instron-E3000, Massachusetts, USA) to apply the mechanical loading. The bioreactor is fixed to the Instron apparatus at its base by a support, and is stimulated from above by a set of pistons attached to the actuator through an adaptor with adjustable embedded screws (Figure 2-b). Additionally, the CO_2/O_2 concentration and humidity inside the chamber are regulated by an external gas mixer (ibidi-Gas Incubation System, Martinsried, Germany) injecting humidified gas into the bioreactor. To maintain sterility, the wells are isolated with perforated solid caps

covered with filters (OpSite Flexigrid, Smith &Nephew, Hull, UK) from the outside environment to protect the samples from contamination while still allowing gas exchange. A flexible silicon support is also employed to keep the sample in the central region of the well during cyclic compression (Figure 2-c).

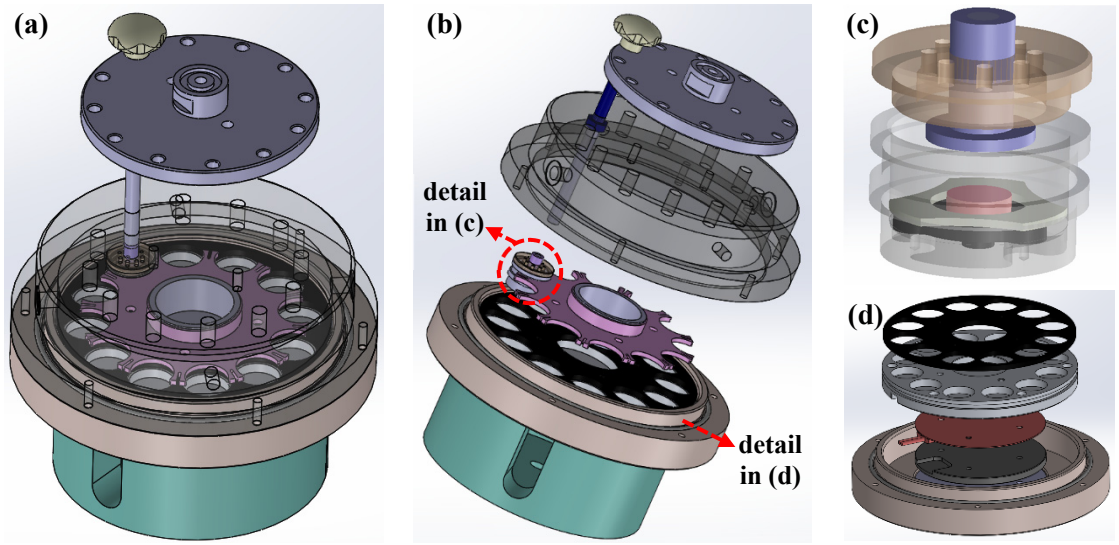

Figure 2. Custom-designed bioreactor chamber containing 12 wells for culture. (a) Assembled chamber compatible with Instron E3000 loading device to apply cyclic compression and desired heat supply while maintaining sterility and predefined gas concentration. (b) Different parts of the bioreactor chamber including adjustable loading system with an embedded screw, chamber cap with different inlets, wells holder/carrier, water bath, chamber base and support. (c) Elements of a well inside the bioreactor chamber. The sample (colored rose) is placed on a thermoplastic base (black part) allowing convection of heated fluid from the bottom of the well (transparent gray part). The sample is kept in the central region by a silicon support (shown in white) during the cyclic loading by a piston (colored blue). The filter-containing perforated cap (transparent brown part) of the well, guids the piston while avoiding contamination of the culture medium. (d) Elements inside the base chamber including heat isolator (colored black), aluminum conductive plate (silver), thermo-foil heater (orange) and its clamper (gray).

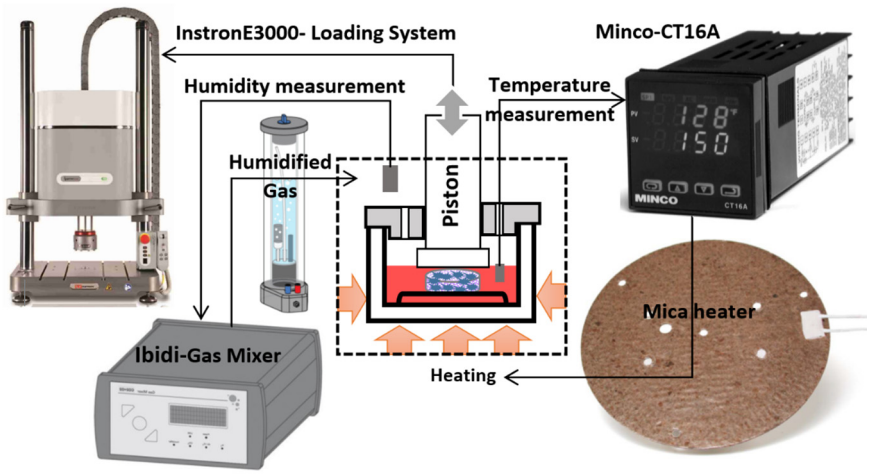

Figure 3. Conceptual design of the modular bioreactor for thermo-mechanical stimulation of cell-laden hydrogels. The different modules were employed to control the mechanical loading, the culture temperature, humidity and the CO_2/O_2 concentration.

The Minco-CT16A device is equipped with a proportional–integral–derivative (PID) controller that enables the system for static or dynamic regulation of the temperature within the wells. In the developed system, the error signal between the measured medium temperature (T_f) and desired temperatures (T_d) is continuously scaled by the PID coefficients (K_p, K_i & K_d) and generates the control signal for the Mica heater (Minco-HM6975). The parameters of the PID controller can be tuned experimentally based on the standard Ziegler-Nichols method [30]. The controller is capable of programming up to 16 independent ramp segments to emulate the desired temperature profile. To minimize the temperature gradient within the sample from bottom to top due to conduction, an Acetal based thermoplastic (POM-C) was incorporated as the seat of samples within the wells while allowing convection of heated fluid (Figure 2-c).

5-2-3 *In vitro* culture and biological evaluations

Human epiphyseal chondro-progenitor cells were expanded in 2D culture according to standard cell culture protocols [31] before seeding them into porous hydrogels. Hydrogels were sterilized in methanol for 2 hours and cells (1.5 million per sample) were infused into them by an optimized compression released induced suction method [32]. MTT staining Kit I (Roche) was used to control the cell distribution and Viability Assay Kit (Biotium) was applied for live/dead evaluation according to the manufacturer protocols. By using the MTT reagent, the purple formazan is produced due to the cells metabolic activity and therefore reveals cells distribution within the hydrogels. Viability assay was performed via a cell-permeable dye (calcine) for staining of live cells and a cell-impermeable dye (ethidium homodimer) for staining of dead cells having a damaged cell membrane.

The Hoechst 33258 dye (ThermoFisher Scientific) was employed for DNA quantification to evaluate the impact of hydrogels functionalization on cells attachment. Briefly, the pure and RGD-modified hydrogels (with and without cells) were cut in small pieces and incubated overnight inside 600 ml papain digestion buffer at 65°C. Then, by dilution of 10 µl of digested solution in 140 µl of the dye (0.2 µg/ml), the emission signal of samples was measured at 460 nm by a Wallac microplate reader after excitation at 355 nm. The DNA content of the samples was finally determined by using a standard curve extracted from sequential dilutions of Calf Thymus DNA (ThermoFisher Scientific) as calibrators. Prestoblue viability kit (ThermoFisher Scientific) was also used to monitor the cells proliferation inside the hydrogels during culture period. To this end, the reagent was 10 times diluted in culture medium and samples were

incubated for 100 minutes inside 1 ml of Prestoblue measurement solution. The fluorescent signal was then measured in triplicates with Wallac microplate reader for excitation/emission wavelengths of 544/590 nm, respectively.

The effect of the different static temperatures on cell-hydrogel constructs were evaluated by culturing identically prepared samples in two incubators (i.e., 37°C or 33°C and 5% CO_2 for both) in free swelling condition for a period of 8 days. In parallel, the effect of dynamic temperature increase was also studied for free swelling and mechanically stimulated cell-laden hydrogels by using the custom-developed bioreactor. For this purpose, after the seeding step, all samples were pre-cultured for 3 days in proliferation medium inside one incubator (32°C and 5% CO_2). After this step, a differentiation medium was used and the thermal (32 to 39°C), mechanical (10% pre-strain, 10% amplitude at 1 Hz) or thermo-mechanical (their combination) stimulation were applied on samples starting from day 4. Three intermittent stimulations in alternate days were applied on the treated groups for 2 hours inside the bioreactor. The gradual temperature increase was obtained by extrapolation of the measured data inside intra-articular region of the knee during jogging obtained from a previous study [25].

Total RNA was extracted using the NucleoSpin® RNA (Macherey-Nagel) after a few steps of preparation [33]. Briefly, samples were put in a 2 ml Eppendorf tube containing 300 µl Trizol. Hydrogels were smashed by the polytron (Kinematica AG, Switzerland), while keeping them cold on dried ice. Then, 100 µl chloroform was added and centrifuged for 5 minutes at 12000 rpm at 4°C. The aqueous phase was transferred to 2 ml phase lock tubes and centrifuged for an additional 5 minutes at 12000 rpm at 4°C. The aqueous phase was carefully transferred to 1.5 ml Eppendorf tubes and the extraction was completed by adding a RNA carrier and following the XS kit protocol. The RNA was quantified using the Nanodrop Lite Spectrophotometer (Thermo Scientific) and reverse transcription of 750 ng RNA was carried out using Taqman® Reverse Transcription Reagents (Applied Biosystems, Massachusetts, USA). Fast SYBR® Green Master Mix (Applied Biosystems) was used for PCR amplification in a final volume of 20 µl containing 10 ng of synthesized cDNA. The PCR amplification was performed for each sample by StepOnePlus Real-Time PCR device (Applied Biosystems) using specific primers for different genes (Table 1). The cycling steps were defined as an initial 95°C for 2 min followed by 40 cycles of amplification. Gene expression data were analyzed using the comparative ΔΔCt method [34] with RLP13a as the reference gene [33].

Table 1. Primers data used for qRT-PCR.

Gene	Primer concent. (nM)	Efficeny (%)	Sequence
RLP13a	175	104	F: 5'- AAGTACCAGGCAGTGACAG -3' R: 5'-CCTGTTTCCGTAGCCTCATG -3'
SOX9	275	108	F: 5'-TGGAAACTTCAGTGGCGCGGA-3' R: 5'-AGAGCAAAAGTGGGGGCGCTT-3'
TWIST1	250	91	F: 5'- AGCAGGGCCGGAGACCTAGATGTCA-3' R: 5'- ACGGGCCTGTCTCGCTTTCTCT-3'
COL2A	250	110	F: 5'- GGCAATAGCAGGTTCACGTACA-3' R: 5'- GATAACAGTCTTGCCCCACTTACC-3'
COL1A	200	97	F: 5'- CAGCCGCTTCACCTACAGC -3' R: 5'- TTTTGTATTCAATCACTGTCGCC -3'

5-3 Results and Discussion

5-3-1 RGD functionalization of porous hydrogels

5-3-1-1 Influence of the conjugation process on hydrogel mechanical properties

Different activation buffers and radical molecules can be used in a bio-conjugation process for synthetic scaffolds functionalization. However, to preserve their biomechanical functionality for load-bearing application, the micro structure of the polymeric network should be minimally altered. By employing acetone and methanol solvents for activation and peptide anchoring steps, the reduction of equilibrium elastic modulus and dissipative capacity of the fatigue-resistant hydrogels (see chapter 4) were minimized to around 15% as shown in Figure 4. We compensated this slight reduction by increasing the initial stiffness of the polymeric network (applying 4.75% crosslinking density instead of 4%) to reach the desired value after the functionalization process. It is worth mentioning that we firstly employed an established functionalization protocol developed for pHEMA brushes [19, 21] for our crosslinked hydrogels. This protocol, however, significantly altered the integrity of the hydrogels structure and substantially reduced the stiffness and dissipative capacity by more than 50%. Evidently, the increased swelling ratio of the hydrogels in the activation (tetrahydrofuran) and anchoring (dimethylformamide) buffers of the standard protocol destroyed the micro structure of the crosslinked polymeric network. Acetone and methanol in turn did not significantly change the swelling ratio of the crosslinked pHEMA hydrogels and their structural integrity was therefore sufficiently preserved.

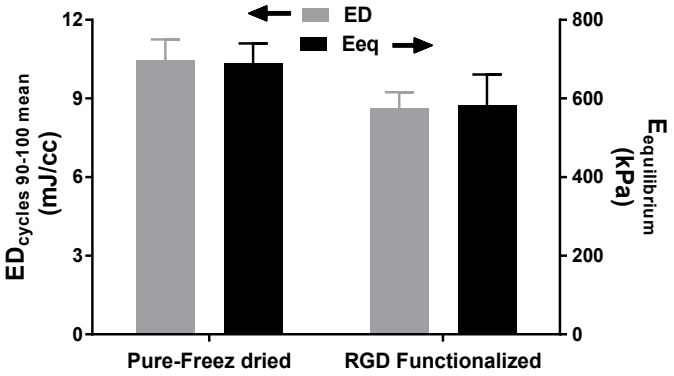

Figure 4. The influence of the functionalization processes on mechanical properties of 4.75Cr-Fine hydrogels (n=3). By minimizing the influence of destructive factors (e.g., increased swelling) during the functionalization process, the risk of losing the required degree of stiffness and dissipation of load-bearing hydrogels can be managed.

5-3-1-2 Effect of functionalization on cells adhesion and growth

Effectiveness of RGD modification process on hydrogels was determined by X-ray photoelectron spectroscopy (XPS) analysis of samples and DNA quantification of cell-seeded hydrogels. The appearance of an N1s peak at 400 eV in the XPS spectra (Figure 5-a) for functionalized samples is the evidence for a successful binding of RGD peptide complex with an amide nitrogen atom in its chemical formulation (see Figure 1). As the pure pHEMA hydrogel does not contain any nitrogen atom in its molecular structure, no signal was observed around 400 eV for non-modified samples. However, the general signal shape and specifically carbon and oxygen atom peaks were similar in both groups. In addition, the RGD peptides grafting effectively contributed to cell attachment capability of pHEMA hydrogels. As shown in Figure 5-b, the DNA content of the functionalized hydrogels after cell seeding was significantly higher than the pure control group without RGD motifs.

To control the efficacy of the sterilization method by ethanol and reconfirm the biocompatibility of the hydrogels after using reactive chemical reagents during the functionalization process, the cell-laden hydrogels were cultured for 10 days at 32ºC and 5% CO_2 level. The cell proliferation was indirectly assessed by PrestoBlue reagent to qualitatively monitor the cells population growth inside the functionalized hydrogels. This resazurin-based assay is not toxic and can be employed intermittently to compare the cells proliferation for the same samples at different time points [35]. In addition, the live/dead assay was employed for cell viability and MTT staining for cell distribution. Indeed, the number of viable cells increased over culture period from day 1 (Figure 6-a, d) to day 10 (Figure 6-b, e) indicating a

firm attachment and a typical proliferation (Figure 6-c) of distributed cells within the functionalized hydrogels.

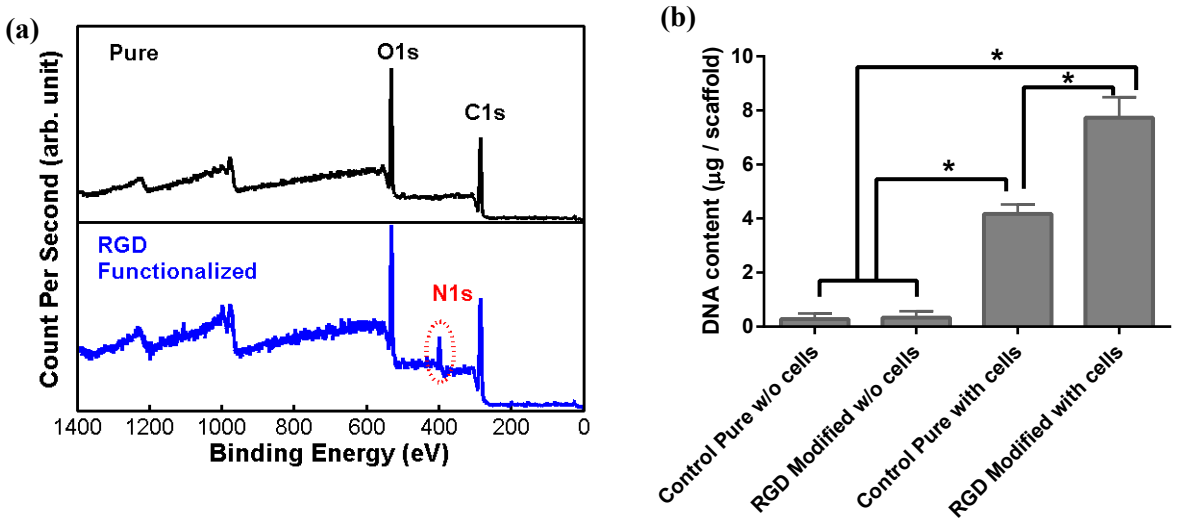

Figure 5. Functionalization evaluation of pHEMA based hydrogel. (a) XPS survey spectra show the Nitrogen pick appearing only for samples with RGD peptides containing NH group. (b) DNA content assay for cell-seeded hydrogels demonstrated significantly higher cells attachment in RGD functionalized scaffolds compared to pure cell-seeded hydrogels (p=0.01, Student t-test, n=3).

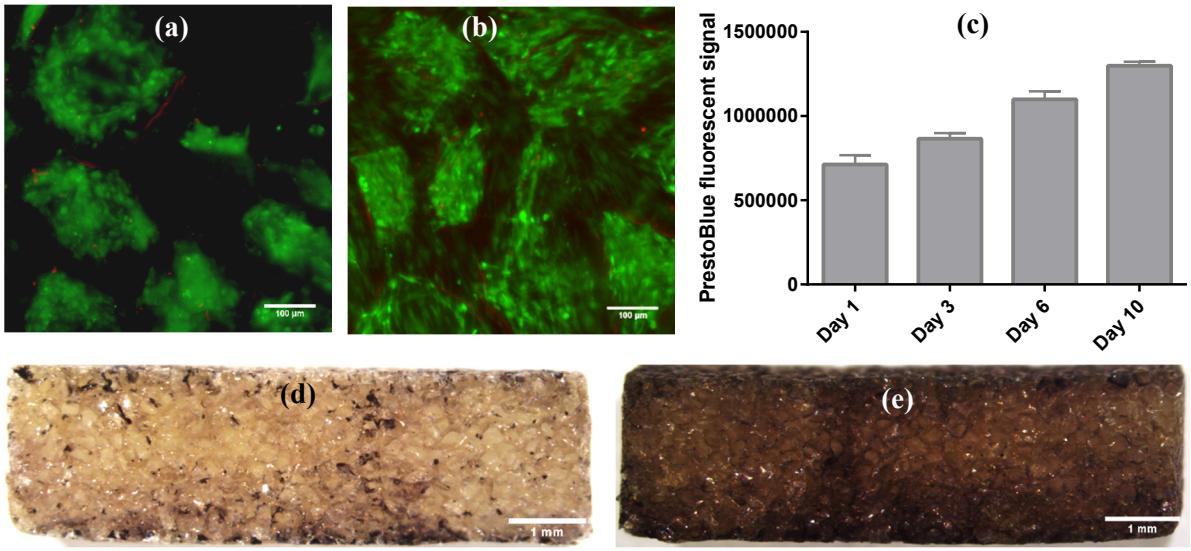

Figure 6. Cells viability inside RGD functionalized hydrogels over 10 days of culture at 32°C and 5% CO_2 condition. (a & b) Live/dead staining of cells-laden porous hydrogels at day 1 and day 10 after seeding (green stain demonstrates live cells and red stain shows dead cells). (c) PrestoBlue assay with increased signals from viable cells during the culture time indicates a typical proliferation for the cell-scaffold constructs (n=4). (d & e) Cells distribution on central cross section of the hydrogel disks after 1 and 10 days, respectively. By using an optimized compression released induced suction seeding method, the cells can penetrate inside porous hydrogels having low permeability.

5-3-2 Thermo-mechanical stimulation of cell-laden hydrogels

5-3-2-1 Influence of static culture temperature

To merely elucidate the influence of temperature on human chondro-progenitor cells behavior inside porous hydrogels, cells proliferation, total RNA and gene expression of samples in different culture temperatures were compared. Our results revealed that cells growth (Figure 7-a) and the amount of extracted RNA (Figure 7-b) were higher when cultured in a condition corresponding to knee intra-articular temperature at rest (32-33^{o}C) compared to core body temperature (37^{o}C). This indicates that a lower temperature is favorable for cells proliferation and metabolism. On the other hand, the expression of chondrogenic markers were significantly upregulated for the 37°C condition compared to the 33°C one. Our results for the effect of culture temperature on progenitor cell-laden hydrogels are similar to previous works focusing on the effect of temperature on human chondrocytes response in monolayer and pellet cultures [28].

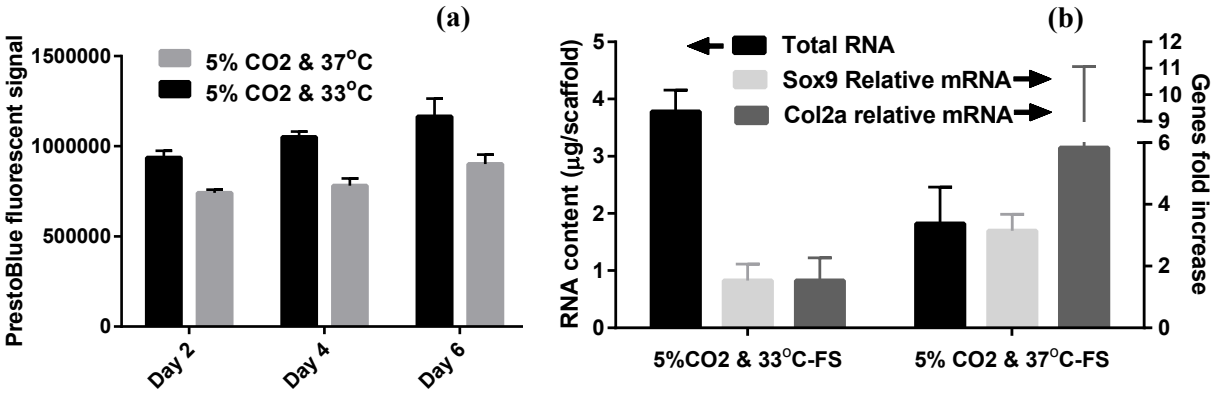

Figure 7. Cells response inside free swelling (FS) RGD functionalized hydrogels at two different temperatures (n=3). (a) PrestoBlue assay during 6 days of culture with identical initial condition shows that cartilage temperature at rest (33^{o}C) is better for cells proliferation. (b) Total RNA and expression of Sox9 and Col2a genes after 8 days of culture with identical initial condition. While amount of extracted RNA as an indicator for cells metabolism confirmed PrestoBlue results, the expression of chondrogenic markers is higher at 37°C than 33°C demonstrating that a moderately higher temperature is more chondro-inductive.

5-3-2-2 Simulating temperature increase during cyclic compression

The scheme of the temperature increase following cyclic compression was modeled by equation 1 and its parameters were estimated by a curve-fitting on reported *in vivo* data during jogging (Figure 8-a) [25].

$$T = A + B(1 - e^{-ct}) \quad (1)$$

The temperature evolution model predicted around 7^{o}C rise after two hours of physical activity with a good correlation coefficient (R=0.95) when using A= 31.62°C, B=7.99°C and

$c=0.023s^{-1}$ in equation 1. The heater controller was tuned to regulate the culture temperature defined by sequential ramps with different slops according to the model prediction. The error between desired and realized temperatures was less than 0.5°C when the PID coefficients were set as $K_P=15$, $K_I=53.9$, $P_D=4.04$. After transferring the samples into the bioreactor chamber once they were prepared under the laminar hood, a preconditioning phase is applied for 25 minutes (Figure 8-b) to reach the steady-state culture condition of 32°C and 5%CO_2. Following this step, the treated group is mechanically stimulated while the control group rests under free swelling condition. During the stimulation phase, the temperature was kept constant at 32°C for one batch and evolved to 39°C in the other batch. Figure 8-c shows the implementation of thermo-mechanical stimulation with the developed tailor-made bioreactor.

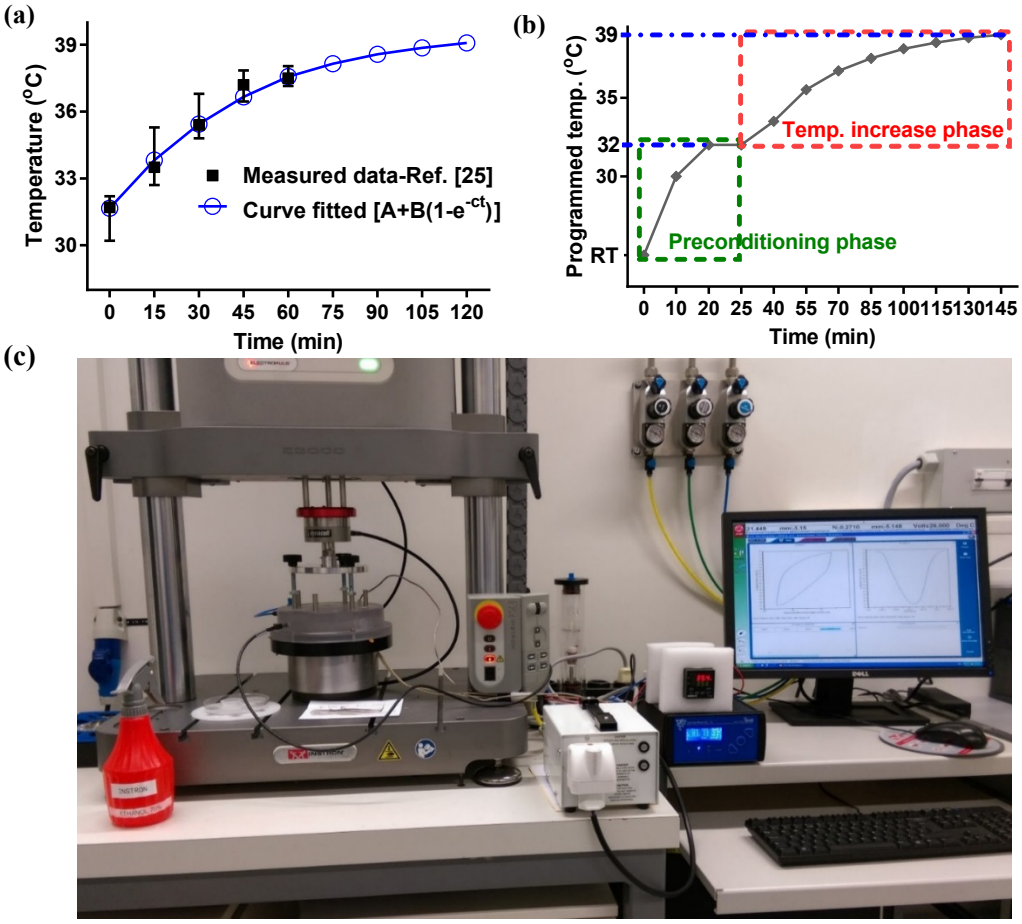

Figure 8. Prediction and implementation of the temperature increase according to experimental data. **(**a) The measured intra-articular temperature following jogging activity as reported in [25] and exponential fitted curve to predict the temperature evolution during 2 hours of cyclic compression. (b) Simulation of the temperature increase during cyclic compression with the developed bioreactor after a preconditioning phase. During the preconditioning, the temperature of the medium inside the culture wells reaches 32°C after 20 minutes to emulate the cartilage temperature at rest. Meanwhile, the humidified gas injection provides a stable 5% CO_2 and 80% humidity inside the chamber. After 25 minutes, the mechanical stimulation starts and the temperature can either be evolved according to the prediction of the curve fitted data or be kept constant during the cyclic compression period. (c) Implementation of thermo-mechanical stimulation by the custom-made bioreactor.

5-3-2-3 Evaluation of cells viability during the thermo-mechanical stimulation

To control how cells react to dynamic temperature increase and cyclic loading, the viability of cells were assessed before and after the two hours thermal and thermo-mechanical stimulation. Our results showed that the cells viability within the hydrogels is preserved after the applied stimulations. However, some cells detached from the hydrogel following a 7°C temperature increase in both non-functionalized (Figure 9-b) and functionalized (Figure 9-e) samples compared to their control groups at 32°C (Figure 9-a and d). Interestingly, when cyclic compression was combined to the temperature rise, the cells were noticeably detached in pure hydrogels without RGD motifs (Figure 9-c). The hydrogels with grafted RGD ligands, on the other hand, maintained cells attachment during thermo-mechanical stimulation (Figure 9-f). Therefore, ECM-mimetic hydrogels not only increased cells attachment in static culture (Figure 9-d vs. 9-a, and Figure S1) but also better preserved the cells-hydrogel interaction following an applied stimulation.

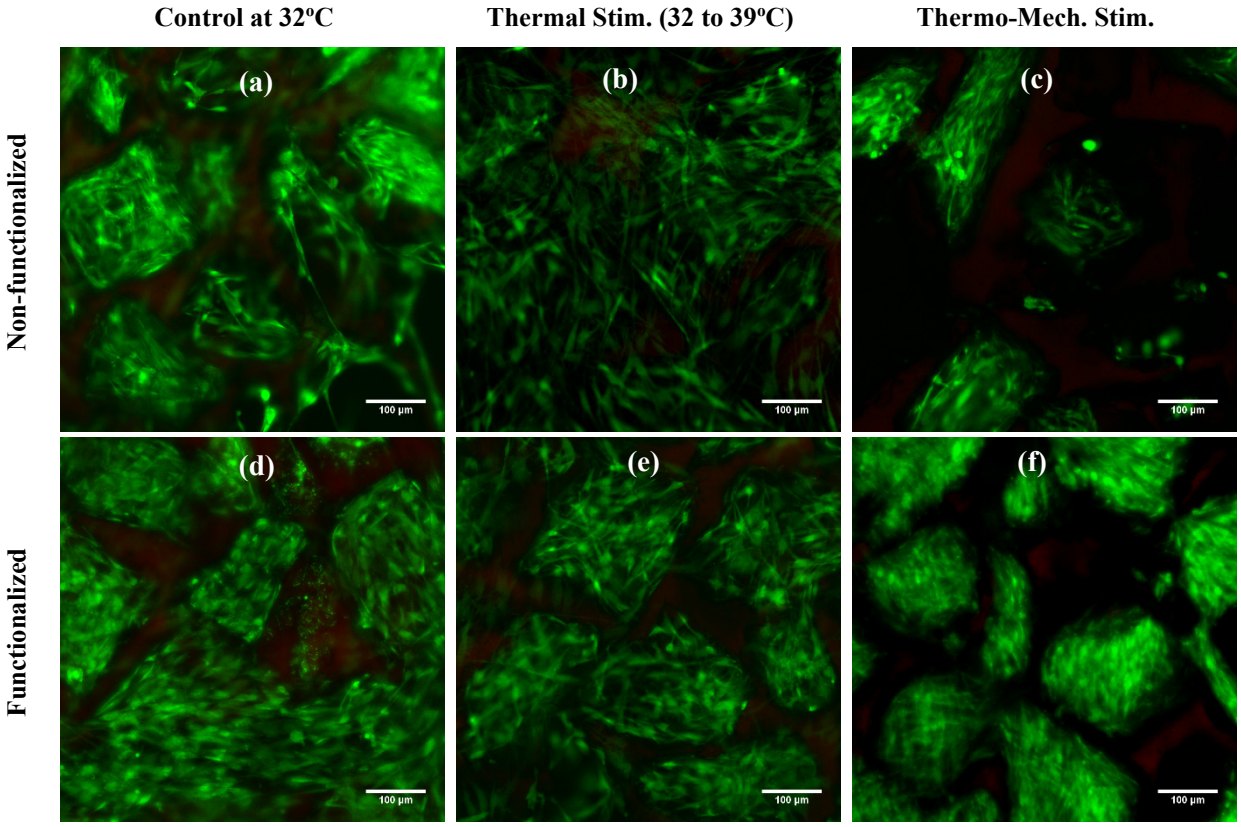

Figure 9. Cells viability and attachment before and after thermo-mechanical stimulation inside bioreactor for non-functionalized (top) and RGD functionalized (bottom) porous hydrogels. (a , d) Cells viability for free-swelling samples at 32°C. (b , e) Cells viability for free-swelling samples subjected to thermal stimulation with temperature increase from 32 to 39°C during 2 hours. (c , f) Cells viability after thermo-mechanical stimulation during 2 hours of 10 % cyclic compression at 1 Hz over 10% pre-strain along with temperature increase from 32 to 39°C.

5-3-2-4 Synergetic effect of thermo-mechanical stimulation on cells behavior

In general, the expression of chondrogenic markers was enhanced by the applied intermittent biophysical stimulus in all groups as shown in Figure 10-a,b and c. In particular, a positive synergetic effect following thermo-mechanical stimulation was observed through an increased expression for Sox9 as the master regulator of chondrogenic differentiation process [36, 37]. In parallel, Twist1, which is known as chondrogenesis inhibitor [38, 39], had its expression significantly downregulated following the thermo-mechanical stimulation (Figure 10-b) compared to mechanical and thermal stimulus alone. While still a promoter, synergetic condition was not as effective as individual mechanical or thermal stimuli for Collagen type 2 (Col2a1) transcription (Figure 10-c). The obtained results indicated that pure mechanical stimulation is a better promoter for Col2a1 gene expression compared to thermal or thermo-mechanical stimulus. However, the large variation of Col2a1 expression made it difficult to draw a firm conclusion from the performed experiment. In addition, it seems that the mechanical stimulation could slightly improve the chondrogenic phenotype as evaluated by the Col2a1/Col1a1 differentiation index [15, 40] contrary to the negative impact of the thermal stimulation (Figure 10-c). These two opposing effects almost compensated each other in case of thermo-mechanical stimulation. Interestingly, even intermittent temperature rises for a short duration (2 hours) had a positive impact on cells chondrogenic expression (Figure 10-a, b & c) similar to a continuous culture of free-swelling samples in higher temperature (c.f. Figure 8). Collectively, the synergetic effect of thermo-mechanical stimulation on chondrogenesis was more complex than simply additive. Given the transient nature of the chondrogenic markers to an applied stimulation [41], analysis of results at different time points could help to better evaluate the gene expression profile. Additionally, the experiment with more replicates (e.g., n=6 instead of n=3) for each group is necessary to reduce the observed variability.

As shown in Figure 10-d, cyclic compression seems to favor cells metabolism as the total RNA is slightly higher in mechanically stimulated groups than corresponding free-swelling samples. Nevertheless, the extracted RNA values (Figure 10-d) and evaluation of cells metabolic activity by PrestoBlue assay (Figure S2) showed low variation among studied groups of intermittent stimuli. Importantly, the total RNA from the samples submitted to intermittent thermo-mechanical stimulation presented similar value to free-swelling control group at 32°C. This was in contrast to substantial reduction in synthesized RNA and cells

proliferation for the conventional culture of samples at 37°C condition compared to 33°C (c.f. Figure 8). These findings demonstrate that adjusting the culture temperature at 32-33°C suits human chondro-progenitor cells metabolism which is in agreement with the results obtained for human and porcine chondrocytes in previous works [28, 42]. In parallel, the chondrogenic differentiation can be promoted by intermittent thermo-mechanical stimulation.

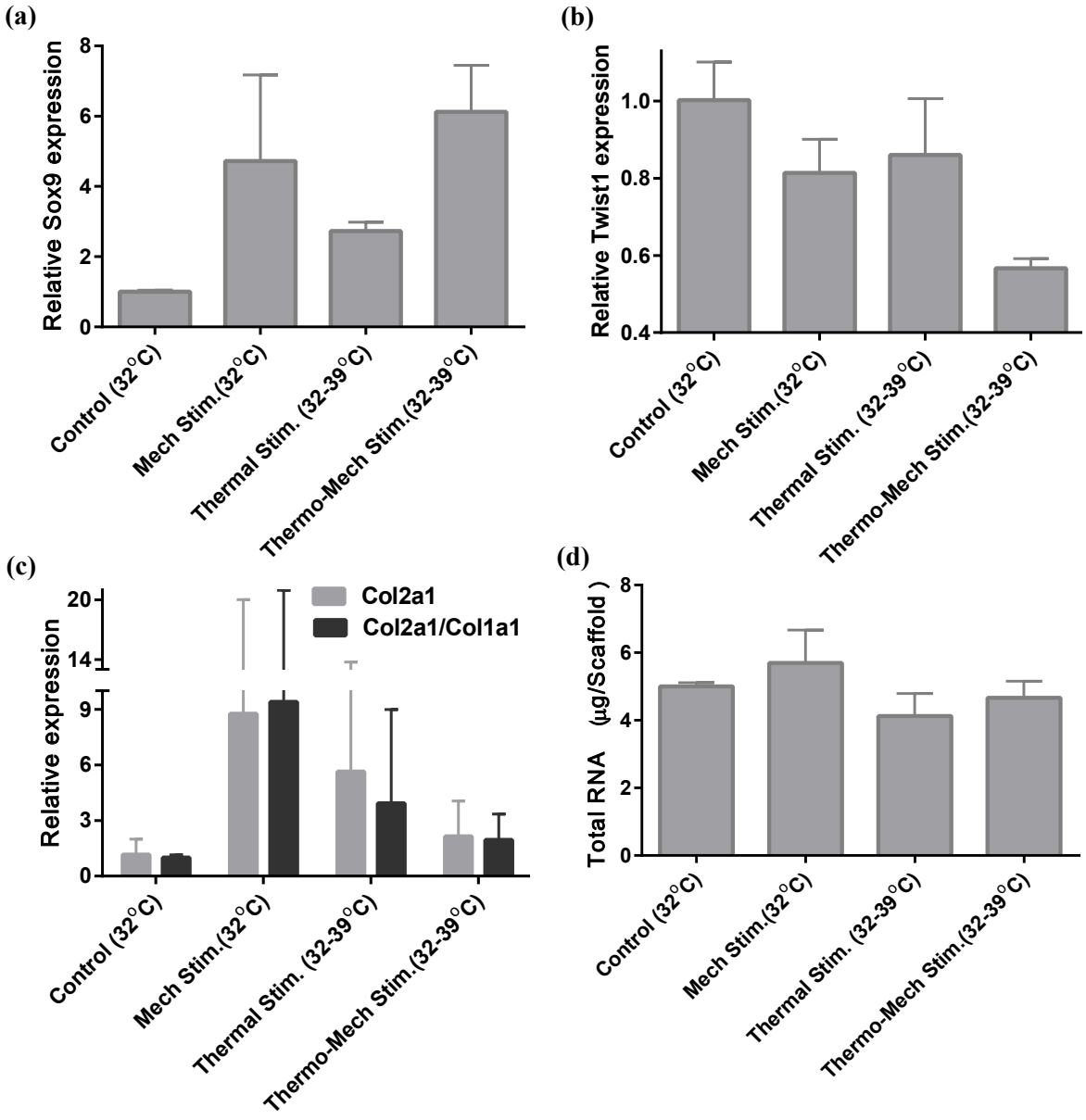

Figure 10. The effect of thermo-mechanical stimulation on cells biophysical response. (a-c) The expression of chondrogenic markers in different experimental groups (n=3). While a synergetic effect of thermo-mechanical stimulation can be observed for Sox9 and Twist1 gene expression, pure mechanical stimulation is a better promoter for Col2a1 gene expression. In addition, it seems that the mechanical stimulation can slightly increase the Col2a1/Col1a1 index contrary to thermal stimulation. (d) Total extracted RNA in different experimental conditions showed a slight difference between studied groups.

5-4 Conclusion

Considering the self-heating phenomenon in knee cartilage following a physical activity, a customized biomimetic *in vitro* platform was developed to study the cartilage thermo-mechanobiology. To enhance cells-scaffold interaction, a method was developed to graft RGD motifs onto the pores of dissipative hydrogels with minimal alteration of their structural integrity. It was shown that the required range of mechanical properties for load-bearing applications can be met following the bio-activation of the inert synthetic hydrogels. Not only cells adhesion was improved within the developed functionalized hydrogels, but also the cells-hydrogel interaction was better preserved following the mechanical stimulation. A modular bioreactor was also designed to independently control the applied stress/strain and temperature profile on cell seeded-hydrogels to emulate *in vivo* like stimulation. The influence of dynamic mechanical, thermal and thermo-mechanical stimuli was then evaluated using this tailored bioreactor. Most importantly, expression of the transcription factor Sox9 as an early chondrogenic marker was increased and complementarily the expression of Twist1 as inhibitor of chondrogenesis was reduced by means of synergy in mechanical and thermal stimuli. In addition, total RNA as an indicator for cells metabolism was minimally varied by intermittent thermo-mechanical stimulation when culture baseline temperature was set at 32°C (knee temperature at rest) contrary to significant decrease of total RNA for continuous incubation of cells at 37°C (core body temperature). While the aspect of temperature increase due to energy dissipation could have opposite influences on cells metabolism and differentiation, the mechanical effect seems to enhance both. Collectively, intermittent thermo-mechanical stimulation as simulation of self-heating phenomenon following joints exercise can enhance chondrogenesis while maintaining cells metabolic activity.

Supporting Information

Corresponding supplementary data can be found at the end of this chapter.

5-5 Acknowledgments

We appreciate the contribution of the Polymers Laboratory of EPFL and in particular Jian Wang for functionalization of pHEMA hydrogels. We also thank EPFL mechanics workshop and in particular Marc Jeanneret for his precious technical support in design of the bioreactor chamber. This work was supported by the Swiss National Science Foundation (#310030_149969/1 and #CR23I3_159301).

5-6 References

[1] Guilak F, Butler DL, Goldstein SA. Functional tissue engineering: the role of biomechanics in articular cartilage repair. Clinical Orthopaedics and Related Research® 2001;391:S295-S305.

[2] Goetzke R, Sechi A, De Laporte L, Neuss S, Wagner W. Why the impact of mechanical stimuli on stem cells remains a challenge. Cell Mol Life Sci 2018:1-16.

[3] Panadero J, Lanceros-Mendez S, Ribelles JG. Differentiation of mesenchymal stem cells for cartilage tissue engineering: Individual and synergetic effects of three-dimensional environment and mechanical loading. Acta Biomater 2016;33:1-12.

[4] Tan AR, Hung CT. Concise review: Mesenchymal stem cells for functional cartilage tissue engineering: Taking cues from chondrocyte-based constructs. Stem cells translational medicine 2017;6:1295-303.

[5] Humphrey JD, Dufresne ER, Schwartz MA. Mechanotransduction and extracellular matrix homeostasis. Nature reviews Molecular cell biology 2014;15:802-12.

[6] D'Souza SE, Ginsberg MH, Plow EF. Arginyl-glycyl-aspartic acid (RGD): a cell adhesion motif. Trends Biochem Sci 1991;16:246-50.

[7] Shin H, Jo S, Mikos AG. Biomimetic materials for tissue engineering. Biomaterials 2003;24:4353-64.

[8] Chung HJ, Park TG. Surface engineered and drug releasing pre-fabricated scaffolds for tissue engineering. Adv Drug Del Rev 2007;59:249-62.

[9] Paterson SM, Shadforth AM, Shaw JA, Brown DH, Chirila TV, Baker MV. Improving the cellular invasion into PHEMA sponges by incorporation of the RGD peptide ligand: the use of copolymerization as a means to functionalize PHEMA sponges. Materials Science and Engineering: C 2013;33:4917-22.

[10] Jeschke B, Meyer J, Jonczyk A, Kessler H, Adamietz P, Meenen NM, et al. RGD-peptides for tissue engineering of articular cartilage. Biomaterials 2002;23:3455-63.

[11] Connelly JT, García AJ, Levenston ME. Inhibition of in vitro chondrogenesis in RGD-modified three-dimensional alginate gels. Biomaterials 2007;28:1071-83.

[12] Connelly J, Petrie T, García A, Levenston M. Fibronectin-and Collagen-Mimetic Ligands Regulate BMSC Chondrogenesis in 3D Hydrogels. European cells & materials 2011;22:168.

[13] Callahan LAS, Childers EP, Bernard SL, Weiner SD, Becker ML. Maximizing phenotype constraint and extracellular matrix production in primary human chondrocytes using arginine–glycine–aspartate concentration gradient hydrogels. Acta Biomater 2013;9:7420-8.

[14] Zhang J, Mujeeb A, Du Y, Lin J, Ge Z. Probing cell–matrix interactions in RGD-decorated macroporous poly (ethylene glycol) hydrogels for 3D chondrocyte culture. Biomedical Materials 2015;10:035016.

[15] Villanueva I, Weigel CA, Bryant SJ. Cell–matrix interactions and dynamic mechanical loading influence chondrocyte gene expression and bioactivity in PEG-RGD hydrogels. Acta Biomater 2009;5:2832-46.

[16] Aisenbrey E, Bryant S. Mechanical loading inhibits hypertrophy in chondrogenically differentiating hMSCs within a biomimetic hydrogel. Journal of Materials Chemistry B 2016;4:3562-74.

[17] Ma PX. Biomimetic materials for tissue engineering. Adv Drug Del Rev 2008;60:184-98.

[18] Hermanson GT. Bioconjugate techniques: Academic press; 2013.

[19] Tugulu S, Silacci P, Stergiopulos N, Klok H-A. RGD—Functionalized polymer brushes as substrates for the integrin specific adhesion of human umbilical vein endothelial cells. Biomaterials 2007;28:2536-46.

[20] Le Droumaguet B, Lacombe R, Ly H-B, Guerrouache M, Carbonnier B, Grande D. Engineering functional doubly porous PHEMA-based materials. Polymer 2014;55:373-9.

[21] Desseaux S, Klok H-A. Fibroblast adhesion on ECM-derived peptide modified poly (2-hydroxyethyl methacrylate) brushes: Ligand co-presentation and 3D-localization. Biomaterials 2015;44:24-35.

[22] Roylance D. Mechanics of Materials. New York: John Wiley & Sons; 1996.

[23] Moghadam MN, Kolesov V, Vogel A, Klok H-A, Pioletti DP. Controlled release from a mechanically-stimulated thermosensitive self-heating composite hydrogel. Biomaterials 2014;35:450-5.

[24] Moghadam MN, Abdel-Sayed P, Camine VM, Pioletti DP. Impact of synovial fluid flow on temperature regulation in knee cartilage. J Biomech 2015;48:370-4.

[25] Becher C, Springer J, Feil S, Cerulli G, Paessler HH. Intra-articular temperatures of the knee in sports–An in-vivo study of jogging and alpine skiing. BMC Musculoskel Disord 2008;9:46.

[26] Abdel-Sayed P, Moghadam MN, Salomir R, Tchernin D, Pioletti DP. Intrinsic viscoelasticity increases temperature in knee cartilage under physiological loading. J Mech Behav Biomed Mater 2014;30:123-30.

[27] Haimovici N. Three years experience in direct intraarticular temperature measurement. Progress in clinical and biological research 1982;107:453-61.

[28] Ito A, Nagai M, Tajino J, Yamaguchi S, Iijima H, Zhang X, et al. Culture temperature affects human chondrocyte messenger RNA expression in monolayer and pellet culture systems. PloS one 2015;10:e0128082.

[29] Abdel-Sayed P, Vogel A, Nassajian Moghadam M, Pioletti D. Cartilage self-heating contributes to chondrogenic expression. European Cells and Materials 2013;26:171-8.

[30] Bequette BW. Process control: modeling, design, and simulation: Prentice Hall Professional; 2003.

[31] Darwiche S, Scaletta C, Raffoul W, Pioletti DP, Applegate LA. Epiphyseal chondroprogenitors provide a stable cell source for cartilage cell therapy. Cell Medicine 2012;4:23-32.

[32] Nasrollahzadeh N, Applegate LA, Pioletti DP. Development of an Effective Cell Seeding Technique: Simulation, Implementation, and Analysis of Contributing Factors. Tissue Eng,Part C 2017;23:485-96.

[33] Abdel-Sayed P, Darwiche SE, Kettenberger U, Pioletti DP. The role of energy dissipation of polymeric scaffolds in the mechanobiological modulation of chondrogenic expression. Biomaterials 2014;35:1890-7.

[34] Livak KJ, Schmittgen TD. Analysis of relative gene expression data using real-time quantitative PCR and the 2− ΔΔCT method. methods 2001;25:402-8.

[35] Sonnaert M, Papantoniou I, Luyten FP, Schrooten J. Quantitative Validation of the Presto Blue™ Metabolic Assay for Online Monitoring of Cell Proliferation in a 3D Perfusion Bioreactor System. Tissue Eng,Part C 2015;21:519-29.

[36] Bi W, Huang W, Whitworth DJ, Deng JM, Zhang Z, Behringer RR, et al. Haploinsufficiency of Sox9 results in defective cartilage primordia and premature skeletal mineralization. Proceedings of the National Academy of Sciences 2001;98:6698-703.

[37] Akiyama H, Chaboissier M-C, Martin JF, Schedl A, de Crombrugghe B. The transcription factor Sox9 has essential roles in successive steps of the chondrocyte differentiation pathway and is required for expression of Sox5 and Sox6. Genes Dev 2002;16:2813-28.

[38] Gu S, Boyer TG, Naski MC. Basic helix-loop-helix transcription factor Twist1 inhibits transactivator function of master chondrogenic regulator Sox9. J Biol Chem 2012;287:21082-92.

[39] Reinhold MI, Kapadia RM, Liao Z, Naski MC. The Wnt-inducible transcription factor Twist1 inhibits chondrogenesis. J Biol Chem 2006;281:1381-8.

[40] Martin I, Jakob M, Schäfer D, Dick W, Spagnoli G, Heberer M. Quantitative analysis of gene expression in human articular cartilage from normal and osteoarthritic joints. Osteoarthritis and Cartilage 2001;9:112-8.

[41] Scholtes S, Krämer E, Weisser M, Roth W, Luginbühl R, Grossner T, et al. Global chondrocyte gene expression after a single anabolic loading period: Time evolution and re-inducibility of mechano-responses. Journal of cellular physiology 2018;233:699-711.

[42] Kocaoglu B, Martin J, Wolf B, Karahan M, Amendola A. The effect of irrigation solution at different temperatures on articular cartilage metabolism. Arthroscopy: The Journal of Arthroscopic & Related Surgery 2011;27:526-31.

Supplemental Data for Chapter 5

Comparison of cells attachment and growth on non-functionalized and functionalized hydrogels in static culture

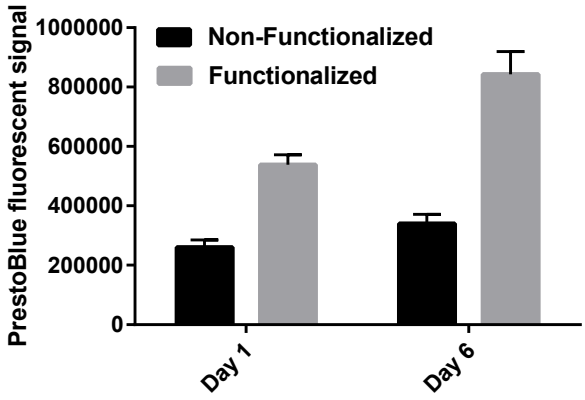

Figure S1. Cells adhesion and proliferation were significantly higher in RGD functionalized hydrogels over the static culture period compared to non-functionalized samples.

Metabolic activity of cells seeded into functionalized hydrogels before and after applying intermittent stimuli

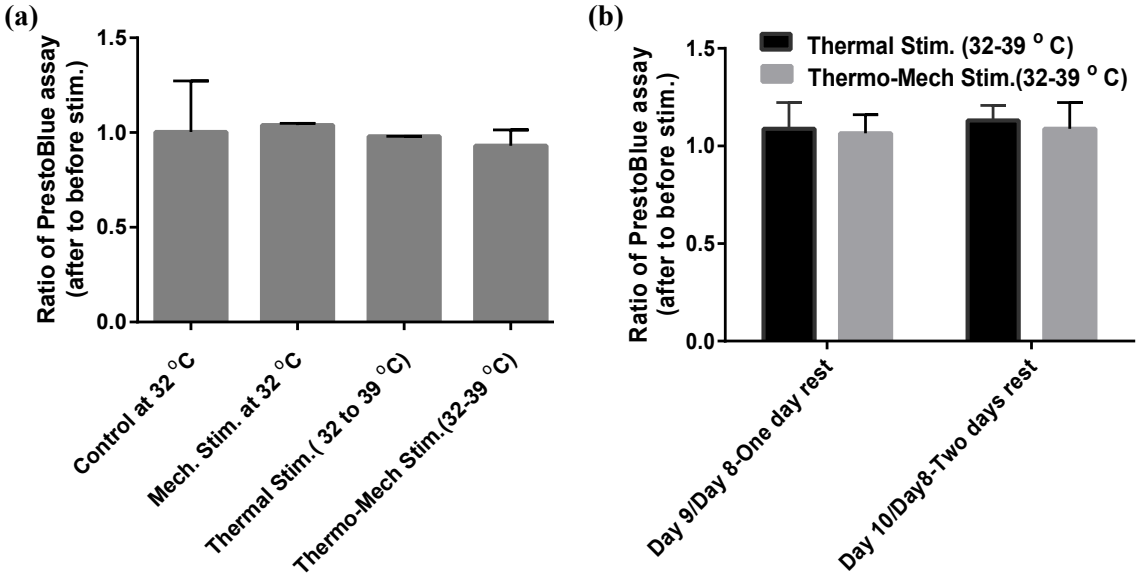

Figure S2. Comparision of metabolic activity of cells inside functionalized hydrogels submitted to different biophysical stimuli. (a) Rtaio of PrestoBlue signal at day 7 corresponding to one day after stimulus to day 6 corresponding to just before applied stimulus. (b) Follow up of the intermittent thermal and thermo-mechanical stimuli effects over two days after the applied stimulus at day 8.

Chapter 6: Conclusions and Perspectives

6-1 Summary of the thesis and major findings

From a material standpoint, dissipative capacity is an essential viscoelastic property for a load-bearing biomaterial to damp the input energy and avoid failure. From a biological point of view, evidence is now growing that cells fate can be regulated by viscoelasticity of its surrounding microenvironment. Therefore, an interesting potential exists to capitalize on dissipation for these two complementary aspects, material and biological, to develop functional scaffolds for load-bearing applications.

With this perspective in view and inspired from cartilage dissipative features, we proposed a novel design strategy based on the combination of flow-dependent and flow-independent dissipation sources to develop relatively stiff, hysteretic and fatigue-resistant hydrogels. In particular, by combining weak physical bonds with strong covalent bonds in hydrogels network, different sources of flow-independent dissipation could be incorporated. In parallel, fluidic frictional drag dissipation could be applied to the hydrogel system by controlling the morphological attributes of its structure. Interestingly, we found that the mechanism of dissipation could also play an important role in the chondrogenic differentiation of progenitor cells. To further gain insight on the contribution of mechanical hysteresis on cells behavior, synergetic influence of temperature and loading on chondrogenesis were studied by means of a custom-developed platform as the dissipated energy within the loaded cartilage leads to temperature rise.

We therefore divided the thesis in four successive steps, where in the two first steps we developed practical methods for permeability characterization and effective cells seeding as

they were contributing to reliably evaluate mechanical and biological aspects in the two following steps of this thesis regarding energy dissipation and thermo-mechanobiology. The four steps are briefly described in the following paragraphs.

In the first step, a straightforward method was proposed to directly measure the strain-dependent permeability of stiff and viscoelastic porous hydrogels. This characterization was necessary for two different aspects before proceeding to our next steps. Firstly, permeability as an overarching morphological determinant for porous structures can be correlated to hydrogels flow-dependent viscoelasticity. Secondly, the strain dependent permeability is a key input for numerical modeling of biphasic material to perform a valid simulation. Direct permeability measurements demonstrated significant decrease in the permeability of the scaffolds with finer pores while the total porosity was maintained. Applied compressive strain also considerably decreased the permeability compared to strain-free condition. It was shown that the trend of the permeability decrease with compressive strains could be different depending on the range of pores size within the scaffolds. This observation confirmed the importance of direct characterization rather than relying on indirect evaluations (e.g. using exponential function proposed for cartilage based on void volume fraction). The release of compression-induced fluid pressure was also correlated to permeability in the stress relaxation experiment.

As a second step, we developed a practical cell seeding protocol leading to uniform distribution of cells inside dissipative scaffolds presenting different morphological features. This step was an a *priori* requirement for our *in vitro* studies to ensure the cell-seeding process effectiveness and reproducibility. For this purpose, the compression release-induced suction (CRIS) technique was optimized by employing a poroelastic model and supplemented by a slow rotation after seeding treatment. This dynamic incubation, after optimized CRIS, enhanced cells penetration and distribution, especially for scaffolds showing low permeability. An experimental design was then performed to identify the relative importance of the contributing factors to the outcome of the developed cell-seeding technique. This systematic analysis indicated that the scaffold's permeability is the most significant factor for both cell seeding efficiency and cells distribution compared to coating and thickness. Since scaffold permeability directly influences cells distribution and infusion depth, it can constrain the design of cells-penetrable hydrogels with major flow-dependent dissipation source.

In the third and central step of the thesis, the intrinsic hydrogel dissipation was supplemented with a flow-induced drag dissipation to develop fatigue-resistant heteroporous hydrogels presenting similar range of compressive stiffness, dissipation and water content to cartilage. Permeability of the hydrogel was introduced as an agent for flow-dependent dissipation and hydrogel's material composition for intrinsic network dissipation. We discovered that stiffness and dissipative capacity of a heteroporous hydrogel with a water content similar to the cartilage (~70%) are significantly higher than corresponding conventional hydrogels. While hydrogels having a dissipation mainly originating from non-destructive processes presented a preserved hysteresis with a robust load support performance, the hysteresis loop in hydrogels with destructive dissipation source was shrinking over the fatigue loading cycles resulting in a reduced load support capability. By employing an iterative optimization process, a reliable poro-viscoelastic model was then developed for two types of hydrogels having the same level of energy dissipation while arising from different sources. It was shown that the release of the pressurized fluid is effectively contributing to the transient stress in the visco-porous hydrogels with low permeability, while flow-dependent viscoelasticity has no influence on decaying stress for highly permeable hydrogels. When these dually porous (heteroporous) hydrogels were seeded with chondro-progenitors cells and were mechanically stimulated under cyclic loading, we observed that the flow-dependent dissipation process favored chondrogenesis. These findings indicate that chondrocytes differentiation can be enhanced by biophysical cues which mimic more similarly the cartilage extracellular characteristics (poor permeability and high fluid pressure).

In the fourth and last step, a customized biomimetic *in vitro* platform was developed to study the cartilage thermo-mechanobiology. This final step was performed to investigate combined and decoupled effects of loading and temperature. In fact, the cartilage hysteresis may indirectly influence chondrocytes behavior by rising the tissue temperature following conversion of the lost energy to heat. To enhance cell-scaffold interaction, a method was developed to graft RGD motifs onto the pores of hybridly crosslinked hydrogels with minimal alteration of the structure integrity. It was shown that cell adhesion was improved and cells-hydrogel interaction following biophysical stimulus was better preserved within the RGD functionalized hydrogels. In addition, a modular and tailor-made bioreactor was designed to apply compressive load and desired temperature scheme during culture of cell-laden hydrogels while CO_2/O_2 and humidity levels could be controlled. A synergetic effect following thermo-

mechanical stimulation was observed for increasing Sox9 expression, one of the main regulators of chondrogenic differentiation process, compared to thermal and mechanical stimulation alone. In parallel, Twist1 which is known as chondrogenesis inhibitor was significantly downregulated following thermo-mechanical stimulation. In addition, total RNA as an indicator for cells metabolism was minimally varied by intermittent thermo-mechanical stimulation when culture baseline temperature was set at 32°C (knee temperature at rest). This was in contrast to the situation of a thermal stimulation alone where a significant decrease of total RNA was observed for a continuous incubation of cells at 37°C (core body temperature) compared to a 32°C culture temperature. Therefore, adjusting *in vitro* culture temperature at 32°C and applying a proper thermo-mechanical stimulus can enhance the development of engineered cartilage products, contrary to conventional culture of cell-scaffolds constructs at 37°C.

6-2 General discussion

Permeability of 3D biomaterials has considerable effect on solutes transport, and developed hydrostatic pressure or velocity fields upon loading [1]. Indeed, different extent of solid-fluid interaction can be induced by modulation of the permeability to influence the mechanical and biological features of biomaterials. Indirect estimation of permeability by using biphasic theory [2, 3] could not be reliable as this method neglects the effect of solid network viscoelasticity and tends to follow the time-dependent data by merely optimizing the permeability. Similarly, in a poro-viscoelastic model, different combinations of strain dependent permeability and intrinsic viscoelasticity can generate the same time-dependent behavior which are not necessarily reflecting the real contribution of poroelastic and viscoelastic attributes [4, 5]. We showed that the flow-dependent and flow-independent mechanical behavior of visco-porous material under loading can be reliably separated thanks to a direct characterization of the strain dependent permeability.

Controlling cell seeding in scaffolds is important in developing tissue engineering products which have to be compliant with regulatory aspects necessitating reproducible and consistent procedures. There is a growing evidence that sophisticated seeding methods for different biomaterials should be employed to optimize the cells infiltration during the seeding process [6, 7]. In this context, we showed that numerical simulations and systematic experimental design help to identify the key parameters affecting cells infusion inside pre-formed scaffolds.

Dissipative capacity is indeed a key attribute for toughness of hydrogels under mechanical loading [8, 9]. In load bearing applications, there is a supplemental complexity as the dissipation sources must be carefully designed for a robust fatigue performance. Already revealed by its name, a hydrogel presents a biphasic composition. The mechanical energy dissipation of hydrogels can then be due to flow-dependent and flow-independent processes. While frictional drag is critical for biomechanical performances of cartilage tissue [10, 11], this flow-dependent source of dissipation is usually overlooked in dissipative hydrogels with intrinsic dissipation sources [8, 12, 13]. We therefore designed hybridly crosslinked heteroporous hydrogels with nano-meshes and meso-pores to combine reversible dissipation sources, either dependent or not on the flow, to simultaneously enhance stiffness, dissipation and fatigue performance. With this approach, the total applied stress to the biomaterial is non-destructively sustained by the flexible solid network of the hydrogel and the pressurized fluid entrapped within its poorly permeable structure.

As already established, the biophysical cues significantly influence the cells response [14, 15]. In particular, the function of the chondrocytes within the tissue is controlled through a set of fluid and solid related physical cues such as interstitial fluid pressure and transmitted strain [11, 16]. The energy dissipation capability of the cartilage tissue originates from intrinsic matrix viscoelasticity and interstitial fluid flow [4, 17] and therefore encompass all mechanical cues that might regulate cells behavior. Accordingly, dissipation can be considered as a relevant functional property to address the mechanobiology of cartilage under physiological loading [17]. Matching the dissipative capacity of cell-scaffold construct with cartilage could therefore be an overarching feature to simulate a mechano-mimetic niche. While fundamentally different processes can generate equal dissipation level, we showed that chondrogenesis is favored by preserved sources of dissipation with effective contribution of frictional drag force.

Since articular cartilage is a viscoelastic tissue with high dissipative capacity, temperature increase following joint loading could occur [18]. The self-heating phenomenon, therefore, links the temperature increase to cyclic deformation. By elucidating thermo-mechanobiological aspects thanks to the custom-developed bioreactor, different facets of the pertinent physical cues (mechanical, thermal or their combination) on chondrocytes behavior could be identified. While *in vitro* studies typically consider a constant culture temperature of 37°C, our findings in agreement with similar studies [19] suggest that core body temperature

(37°C) does not induce proliferation as cartilage temperature at rest (32°C) for cells with chondrogenic lineage. In addition, our preliminary results indicated that by intermittent thermo-mechanical stimulation, we can still profit from the positive influence of higher temperature on chondrogenic differentiation process [19, 20] and simultaneously preserve cells metabolism.

6-3 Perspectives

Collectively, dissipative capacity of biomaterials is of great importance for their robust mechanical performance, and it can generate different physical cues to influence cells behavior. Translating the functional role of cartilage mechanical hysteresis in tissue engineering scaffolds can therefore open new opportunities to enhance the outcome of engineered cartilage and can contribute to the field of regenerative medicine.

Homogenous fluid phase distribution may lead to isolated chains within the water-rich network of conventional hydrogels and can deteriorate their mechanical properties. In contrast, the presence of heterogeneous water compartments of different length scales (pore and bound water) within constituents of load-bearing tissues such as bones and cartilage ensures their mechanical performance (e.g. intra fibrillar and extra fibrillar fluid phases in cartilage tissue). There is thus an interesting potential to employ emerging fabrication technologies (e.g. additive manufacturing) for manipulating architecture of hydrogels structure across multiple length scales for the sake of biomechanical functionality similar to the presented concept of a heteroporous structure.

As shown for the first time in this work, the temperature synergy with mechanical loading could be influential on cells behavior. However, identifying the optimal thermo-mechanical environment remains to be established. Additionally, the developed bioreactor provides a new system to better study the cartilage hemostasis as temperature and loading conditions as well as CO_2 and O_2 levels can be independently controlled. It is known that applying hypoxia condition on cells (similar to cartilage tissue) has significant impact on their phenotype and biosynthetic activity. Controlling the oxygen tension in conjunction with thermo-mechanical stimulation could therefore shed more light on the *in vivo* chondrogenesis process.

6-4 References

[1] Pennella F, Cerino G, Massai D, Gallo D, Labate GFDU, Schiavi A, et al. A survey of methods for the evaluation of tissue engineering scaffold permeability. Ann Biomed Eng 2013;41:2027-41.

[2] Ateshian G, Warden W, Kim J, Grelsamer R, Mow V. Finite deformation biphasic material properties of bovine articular cartilage from confined compression experiments. J Biomech 1997;30:1157-64.

[3] Mow VC, Kuei S, Lai WM, Armstrong CG. Biphasic creep and stress relaxation of articular cartilage in compression: theory and experiments. J Biomech Eng 1980;102:73-84.

[4] Mak A. The apparent viscoelastic behavior of articular cartilage—the contributions from the intrinsic matrix viscoelasticity and interstitial fluid flows. J Biomech Eng 1986;108:123-30.

[5] Suh J-K, DiSilvestro M. Biphasic poroviscoelastic behavior of hydrated biological soft tissue. Journal of Applied Mechanics 1999;66:528-35.

[6] Nasrollahzadeh N, Applegate LA, Pioletti DP. Development of an Effective Cell Seeding Technique: Simulation, Implementation, and Analysis of Contributing Factors. Tissue Eng,Part C 2017;23:485-96.

[7] Levin A, Sharma V, Hook L, García-Gareta E. The importance of factorial design in tissue engineering and biomaterials science: Optimisation of cell seeding efficiency on dermal scaffolds as a case study. Journal of tissue engineering 2018;9:2041731418781696.

[8] Zhao X. Multi-scale multi-mechanism design of tough hydrogels: building dissipation into stretchy networks. Soft Matter 2014;10:672-87.

[9] Long R, Hui C-Y. Fracture toughness of hydrogels: measurement and interpretation. Soft Matter 2016;12:8069-86.

[10] Mow VC, Ratcliffe A, Poole AR. Cartilage and diarthrodial joints as paradigms for hierarchical materials and structures. Biomaterials 1992;13:67-97.

[11] Mow VC, Wang CC, Hung CT. The extracellular matrix, interstitial fluid and ions as a mechanical signal transducer in articular cartilage. Osteoarthritis and Cartilage 1999;7:41-58.

[12] Zhang YS, Khademhosseini A. Advances in engineering hydrogels. Science 2017;356:eaaf3627.

[13] Gong JP. Materials both tough and soft. Science 2014;344:161-2.

[14] Jaalouk DE, Lammerding J. Mechanotransduction gone awry. Nature reviews Molecular cell biology 2009;10:63-73.

[15] Humphrey JD, Dufresne ER, Schwartz MA. Mechanotransduction and extracellular matrix homeostasis. Nature reviews Molecular cell biology 2014;15:802-12.

[16] O'Conor CJ, Case N, Guilak F. Mechanical regulation of chondrogenesis. Stem Cell Res Ther 2013;4:61.

[17] Abdel-Sayed P, Darwiche SE, Kettenberger U, Pioletti DP. The role of energy dissipation of polymeric scaffolds in the mechanobiological modulation of chondrogenic expression. Biomaterials 2014;35:1890-7.

[18] Abdel-Sayed P, Moghadam MN, Salomir R, Tchernin D, Pioletti DP. Intrinsic viscoelasticity increases temperature in knee cartilage under physiological loading. J Mech Behav Biomed Mater 2014;30:123-30.

[19] Ito A, Nagai M, Tajino J, Yamaguchi S, Iijima H, Zhang X, et al. Culture temperature affects human chondrocyte messenger RNA expression in monolayer and pellet culture systems. PloS one 2015;10:e0128082.

[20] Abdel-Sayed P, Vogel A, Nassajian Moghadam M, Pioletti D. Cartilage self-heating contributes to chondrogenic expression. European Cells and Materials 2013;26:171-8.

Appendix: Optimization Method

Particle swarm optimization

The particle swarm optimization (PSO) technique was firstly developed by Eberhart and Kennedy [1] based on an inspiration from the fishes and birds social behavior [2]. Accordingly, population of particles update their position within the searching space, to find the optimum spot, according to an individual-social compromise between what a particle conceives and what society estimates as shown in Figure A1 based on equations 1 to 3.

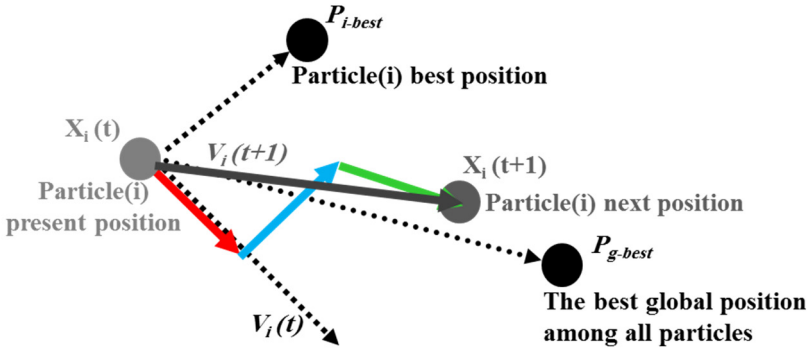

Figure A1. The mechanism of searching to find the optimum condition on PSO. The next position of a particle is influenced by its present direction (Red arrow), its best history (blue arrow) and the group best history (green arrow).

$$X_i(t+1) = X_i(t) + V_i(t+1) \quad (1)$$

$$V_i(t+1) = W(t+1)V_i(t) + C_1 \times randfunc \times \left(P_{i-best} - X_i(t)\right) + C_2 \times randfunc \times (P_{g-best} - X_i(t)) \quad (2)$$

$$W(t+1) = w_{max} - \frac{w_{max} - w_{min}}{Max_t} * t \quad (3)$$

where:

X_i represents the position of an particle.

V_i is the velocity of an particle.

i is the particle's number in a predefined population size with N particles (we set it to 20).

t is the iteration number.

Max_t is a predefined number for maximum iterations to finish the process (we set it to 50), if stoping criteria (90% of particles find the same best optimium) was not met .

$W(t+1)$ is the inertia coefficient (reflects influence of current velocity).

w_{max} and w_{min} are constant coefficnts to define particles range of wights (we set them to 1 and 0.3, respectively).

C_1 is the constant coefficient for cognitive memory as importance of particle's best (we set is to 1).

C_2 is the constant coefficient for social memory as importance of group's best (we set is to 1.5) .

Performance of PSO technique compared to Genetic algorithm (GA)

As shown in Figure A2, the PSO searching method converged to an optimal set after 37 generation with much more better results than the best set of GA routine [3] after 100 generation while same population number was assigned for both (N=20).

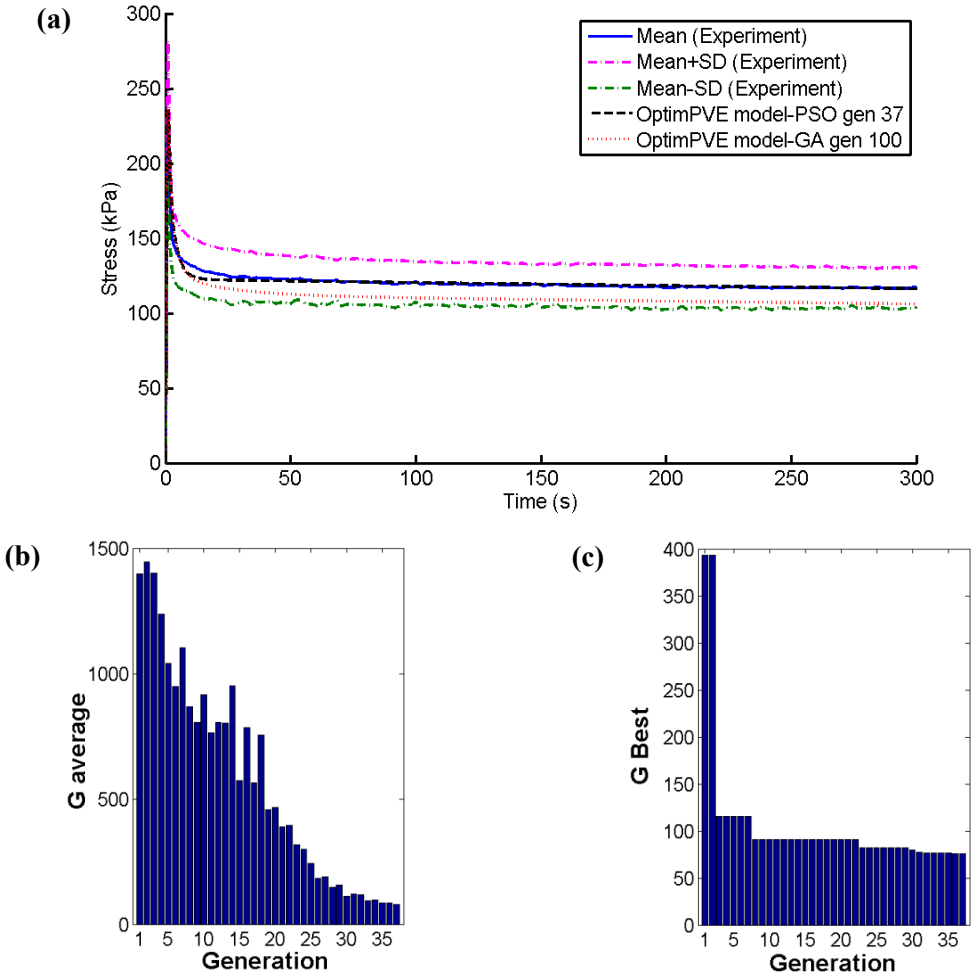

Figure A2. Comparison of PSO and GA performance to find the optimal set for 4Cr-Fine hydrogel's stress relaxation test at 500 μm/s loading rate. (a) The model prediction for PSO and GA optimal sets after 37 and 100 generations, respectively. (b) The average of objective function valus for all particles (G average) is minimized and converges to the optimal set after 30 generations meaning that most of the particels find one optimal set in the searching field. (c) The objective function value for the best agent (G best) in pupolation over different generations.

References for Appendix

[1] Eberhart R, Kennedy J. A new optimizer using particle swarm theory. Micro Machine and Human Science, 1995 MHS'95, Proceedings of the Sixth International Symposium on: IEEE; 1995. p. 39-43.

[2] Marini F, Walczak B. Particle swarm optimization (PSO). A tutorial. Chemometrics Intellig Lab Syst 2015;149:153-65.

[3] Goldberg DE, Holland JH. Genetic algorithms and machine learning. Machine learning 1988;3:95-9.

Curriculum Vitae

Naser Nasrollahzadeh

27.08.1983 - Tehran, Iran

Education

PhD Candidate (2014-now) - EPFL, Switzerland

Major: Bioengineering, **Minor:** Biomechanics.

Thesis: The role of mechanical hysteresis source in mechanical and mechanobiological performances of biomaterials.

Master of Science (2009-2012) - University of Tehran, Iran

Major: Mechanical Engineering, **Minor:** Structural dynamics and vibration control.

Thesis: CAE-NVH characterization and optimization of the automotive BIW and seat structure.

Professional Experience

Research assistant (2014-present) - EPFL, STI-IBI, LBO

Data analysis, biomaterials development, cartilage mechanobiology, functional tissue engineering, customized test rigs design.

Research assistant (2011-2013) - University of Tehran, NVA Lab

Vibration control, noise mitigation, viscoelasticity and optimal parameters estimation.

R&D Engineer (2012-2014) - Turbotec. Co., Dynamical Analysis Division

Development of a remote monitoring and fault diagnosis package for 25 Mw gas turbine.

Internship (2005-2006) - Sadid Group-Saba Niroo Co., Design and Technology Division

Wind turbine nacelle assembly, 3D modeling and Non conformity reports analysis.

Selected Publications

Naser Nasrollahzadeh, Peyman Karami, Dominique P. Pioletti, *Hydrogels preserving hysteresis for enhanced mechanical and mechanobiological performances*. Under review in Advenced Functional Materials journal.

Nasrollahzadeh N, Applegate LA, Pioletti DP. *Development of an Effective Cell Seeding Technique: Simulation, Implementation, and Analysis of Contributing Factors*. Tissue Eng,Part C 2017;23:485-96.

Nasrollahzadeh, N., and D. P. Pioletti. *Experimental method to characterize the strain dependent permeability of tissue engineering scaffolds*. J. Biomech. 49: 3749, 2016.

Allahverdizadeh A, Mahjoob MJ, Nasrollahzadeh N, Eshraghi I. *Optimal parameters estimation and vibration control of a viscoelastic adaptive sandwich beam incorporating an electrorheological fluid layer*. J Vibrat Control 2014;20:1855-68.

Allahverdizadeh A, Mahjoob M, Eshraghi I, Nasrollahzadeh N. *On the vibration behavior of functionally graded electrorheological sandwich beams*. International Journal of Mechanical Sciences 2013;70:130-9.

Nasrolahzadeh N, Fard M, Tatari M, Mahjoob M. *Automotive concept modelling: Optimization of the vehicle NVH performance*. Proceedings of the FISITA 2012 World Automotive Congress: Springer; 2013. p. 365-76.

Conference Contributions

N. Nasrollahzadeh, L. A. Applegate, and D. P. Pioletti. *A customized in vitro platform for cartilage thermo-mechanobiology*. TERMIS EU, 2019, Rhodes-Greece.

N. Nasrollahzadeh, P. Karami, and D. P. Pioletti. *Mechanical properties of pHEMA based hydrogels with heteroporous design outperform corresponding homoporous structure in physiological water content*. Multifunctional, Hybrid and Nanomaterials, 2019, Sitges-Spain.

N. Nasrollahzadeh, P. Karami, and D. P. Pioletti. E*nhanced mechanical and mechanobiological properties of hydrogels by controlling their dissipation sources*. Advances in Functional Materials, 2019, Los Angeles-USA.

N. Nasrollahzadeh, P. Karami, and Dominique P. Pioletti. *The role of dissipation in developing hydrogels for functional tissue engineering*. MRS Fall Meeting, 2018, Boston, USA.

N. Nasrollahzadeh, L. A. Applegate, and Dominique P. Pioletti. *Frictional drag dissipation promotes chondrogenesis in mechanically stimulated cell-seeded scaffolds*. TERMIS WC, 2018, Kyoto-Japan.

N. Nasrollahzadeh, J. Wang, H. A. Klok, and D. P. Pioletti. *How may bio-conjugation influence synthetic biomaterials mechanical properties?* WCB, 2018, Dubline-Ireland.

N. Nasrollahzadeh and D. P. Pioletti. *Role of flow dependent and flow independent viscoelasticity on time dependent behaviour of visco-porous scaffolds*. CMBBE, 2018, Lisbon-Portugal.

N. Nasrollahzadeh and D. P. Pioletti. *The importance of after seeding treatment following compression release-induced suction seeding*. TERMIS EU, 2017, Davos-Switzerland.

N. Nasrollahzadeh and D. P. Pioletti. *Significance of permeability and crosslinking density on viscoelastic behavior of tissue engineering scaffolds*. ORS 2017. California-USA, March 2017. Poster presentation.

N. Nasrollahzadeh and D. P. Pioletti. *A practical cell seeding technique*, ESB, 2016, Lyon-France.

N. Nasrollahzadeh and D. P. Pioletti. *Development of dissipative scaffolds with different mechanisms of dissipation*. Mechanics of Time Dependent Materials, 2016, Paris-France.

**Ce document a été imprimé au Centre d'impression EPFL,
imprimerie climatiquement neutre, certifiée myClimate.**